

**MECHANO-CHEMICAL SYNTHESIS OF ULTRAFINE
PARTICLE Mn-Zn MIXED METALS FERRITES**

A THESIS

SUBMITTED TO THE

GOA UNIVERSITY

For the degree of

DOCTOR OF PHILOSOPHY

in

CHEMISTRY

By

VIKAS J. S. PISSURLEKAR

DEPARTMENT OF CHEMISTRY

GOA UNIVERSITY

Taleigao Plateau

GOA 403206


2011

621.34
PIS/Mec

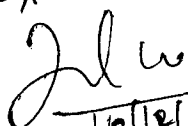
T-545


STATEMENT

I hereby state that this thesis for the Ph.D. degree on "Mechano-Chemical Synthesis of Ultrafine Particle Mn-Zn Mixed Metals Ferrites" is my original work and that it has not previously formed the basis for the award of any degree, diploma, associateship and fellowship or any other similar title to the best of my knowledge and information.


Vikas J. S. Pissurlekar

(Candidate)

Examined on 16/12/2011

16/12/2011
(Ext. Examiner)

EXAMINED
BY

16/12/11
(Int. Examiner)

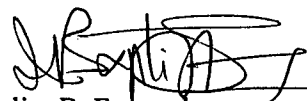
CERTIFICATE

As required under the University Ordinance, we certify that the thesis entitled "Mechano-Chemical Synthesis of Ultrafine Particle Mn-Zn Mixed Metals Ferrites" submitted by Shri. Vikas J. S. Pissurlekar for the award of **Doctor of Philosophy** in Chemistry is a record of research done by the candidate during the period of study under our guidance and that it has not previously formed the basis for the award to the candidate of any degree, diploma, associateship, fellowship or other similar titles.

Date: 12/5/2011



Jayant. S. Budkuley
Professor
Research guide



Julio. B. Fernandes
Professor
Research Co-guide,
Department of Chemistry,
Goa University.

ACKNOWLEDGEMENTS

It is with great pleasure that I express my deep sense of gratitude to thesis supervisor Prof. Jayant. S. Budkuley for his valuable guidance, stimulating discussions and constant encouragement throughout the course of the present study. This work would not have seen the light of this day, if Prof. Budkuley had not motivated me to register for Ph.D. During this entire study, as friend, philosopher and guide he spared no time or efforts in making suggestions and in critically evaluating my work, as also in helping and accompanying me to visit various institutions for gathering and presenting the data. I owe this to the warm and helpful nature of Prof. Budkuley and find no adequate words to express my gratitude to him.

I wish to express my deep sense of gratitude to Prof. Julio B. Fernandes, my research Co-guide, Department of Chemistry for all the help, support and encouragement extended to me, at the various stages during the course of this work.

It is with great pleasure that I express my thanks to,
The Head, Department of Chemistry, Goa University for extending necessary research laboratory facilities,
The Management, P. E. S's College of Arts & Science, Farmagudi, Ponda, Goa for their cooperation,
Dr. Anil. S. Dingu Principal, of the College for his help, constant support and encouragement throughout the study period.

I am also thankful to all my colleagues at P. E. S. College, especially Dr. S. H. P. Keluskar for his help and support, and to the Chemistry laboratory

staff Ranganath, Eknath, Raju, Prakash, Nitin and Sangeeta, for their assistance during this work.

I am also thankful to the U. G. C. New Delhi for sanctioning me two years study leave as Teacher Fellow under the Faculty Improvement Programme during this study.

My thanks are also due to Shri Anand Samant of I. I. T., Mumbai, Shri Girish Prabhu and Shri Vijay Khedekar of N. I. O., Goa, and Miss Shahin of N. C. A. O. R. Goa.

I thank the authorities of I. I. T. Mumbai, N. I. O. Goa, N. C. A. O. R. Goa and Shivaji University Kolhapur, for permitting me to collect the instrumental data of samples.

I thank faculty members of the Department of Chemistry, Goa University for their help and support; I also express my thanks to the non teaching members of the department, for their cooperation.

My thanks are also due to my research colleagues, Guirish, Satish, Priyanka, Lectina, Rohan, Shrikant, Manoj and Kiran for making my working time in the laboratories useful and comfortable. I also thank Mr. Jaiprakash Kamat and Mr. Agnel Lopes, of U. S. I. C., Goa University, for their help.

My sincere thanks are also due to my brothers, sister and other family members, for their continuous moral support and especially, to my nieces Priyanka and Prajakta, who were constantly with me for every type of work connected with this thesis.

CONTENTS

CHAPTER ONE

1.1.	General introduction	1
1.2.	Compounds of iron	3
1.2.1.	Oxides of iron	4
1.2.2.	Naturally occurring oxides of iron	4
1.2.3.	Mixed oxides of iron	4
1.3.	History of ferrites	5
1.4.	The ferrite structure	6
1.4.1.	The spinel structure	7
1.4.1.1.	The normal ferrites	8
1.4.1.2.	The inverse ferrites	8
1.4.1.3.	The random or mixed ferrites	8
1.4.2.	The garnet structure	9
1.4.3.	The hexagonal structure	10
1.4.4.	The orthoferrites structure	10
1.5.	Synthetic methods of ferrites	10
1.5.1.	The ceramic method	12
1.5.2.	The decomposition method	13
1.5.3.	The co-precipitation method	13
1.5.4.	The precursor method	15
1.5.5.	The hydrothermal method	15

1.5.6.	The vapour phase method	16
1.5.7.	The sol-gel method	16
1.5.8.	The chimie-douce method	17
1.5.9.	The combustion synthesis method	18
1.5.10.	The plasma synthesis method	19
1.5.11.	The reverse micelle method	19
1.5.12.	The CTAB method	20
1.5.13.	Other methods	21
1.6.	Properties of ferrites	22
1.6.1.	Magnetic properties	22
1.6.1.1.	Saturation magnetization	22
1.6.1.2.	Magnetic hysteresis	23
1.6.1.3.	Permeability	23
1.6.1.4.	A. C. susceptibility	24
1.6.2.	Electrical properties	24
1.6.2.1.	Resistivity	25
1.6.2.2.	Thermo-electric power	25
1.6.2.3.	Dielectric behavior	27
1.7.	Applications of ferrites	27
1.8.	Scope of present work	29

CHAPTER TWO

2.1.	Introduction	39
2.2.	Ball-mill technique in mechano-chemical synthesis	40
2.3.	Instrumental techniques used for characterization	40
2.3.1.	Atomic absorption spectroscopy (AAS)	40
2.3.2.	Infrared (IR) spectroscopy	43
2.3.3.	Simultaneous thermal analyzer (TGA-DTA)	47
2.3.4.	X-ray diffraction spectroscopy (XRD)	50
2.3.4.1.	Line broadening analysis for crystallite dimension	53
2.3.5.	Scanning electron microscopy (SEM)	54
2.3.6.	Energy dispersive x-ray analysis (EDS)	56
2.3.7.	Transmission electron microscopy (TEM)	59
2.4.	Magnetic and electrical properties	63
2.4.1.	Magnetic properties	64
2.4.1.1	Saturation magnetization	65
2.4.1.2.	A. C. Susceptibility	66
2.4.1.3.	Magnetic permeability	67
2.4.2.	Electrical properties	68
2.4.2.1.	Resistivity	69
2.4.2.2.	Thermo electric power (TEP)	70
2.4.2.3.	Dielectric constant	71

CHAPTER THREE

3.1.	Introduction	75
3.2.	Synthesis of $Mn_{(x)}Zn_{(1-x)}Fe_2O_4$ mixed metal ferrite	75
3.2.1.	Mechano-chemical method	76
3.2.2.	Wet chemical method	77
3.3.	Characterization	78
3.3.1.	Characterization using percentage yield method	79
3.3.2.	Atomic absorption spectroscopy (AAS)	80
3.3.3.	Infrared spectroscopy (IR)	81
3.3.4.	Simultaneous thermal analyzer (TGD-DTA)	82
3.3.5.	X-ray diffraction spectroscopy	83
3.3.6.	Energy dispersive X-ray analysis (EDS)	83
3.3.7.	Transmission electron microscopy (TEM)	84
3.4.	Physical properties	84
3.4.1.	Lattice constant from X-ray diffraction data	85
3.4.2.	X-ray density	86
3.4.3.	Mass or bulk density	86
3.4.4.	Porosity measurement	86
3.5.	Results and discussion	87
3.5.1.	Percentage yield method	87
3.5.1.1.	Mechano-chemical method	87
3.5.1.2.	Wet chemical method	88
3.5.2.	Atomic absorption spectroscopy	90

3.5.3. Infrared spectroscopy	91
3.5.4. Thermal analysis of precursors	93
3.5.5. X-ray diffraction analysis	96
3.5.6. EDS data	98
3.5.7. Transmission electron microscopy (TEM)	100
3.5.8. Lattice constant 'a' from X-ray diffraction data	100
3.5.9. Particle size using X-ray analysis	102
3.5.10. X-ray density	104
3.5.11. Mass or bulk density	105
3.5.12. Porosity measurement	107

CHAPTER FOUR

4.1. Introduction	112
4.1.1. Diamagnetism	113
4.1.2. Paramagnetism	113
4.1.3. Ferromagnetism	114
4.1.4. Antiferromagnetism	115
4.1.5. Ferrimagnetism	115
4.1.6. Soft and hard ferrites	116
4.2. Characteristics of soft ferrites	116
4.2.1. Magnetic domains	117
4.2.2. Magnetostriction	118
4.2.3. Anisotropy	118

4.2.4. Hysteresis	118
4.2.5. A. C. Susceptibility	121
4.2.6. Permeability	121
4.2.6.1. Models of permeability	122
4.2.6.2. Dependence of initial permeability	125
4.3. Experimental measurement	127
4.3.1. Saturation magnetization	127
4.3.2. A. C. susceptibility	129
4.3.3. Initial permeability	130
4.4. Results and discussion	131
4.4.1. Saturation magnetization	131
4.4.2. A. C. susceptibility	141
4.4.3. Permeability	146
4.4.4. Relative loss factor	154

CHAPTER FIVE

5.1. Introduction	160
5.2. Resistivity	162
5.2.1. Models for the electrical properties	166
5.2.1.1. Hopping electron model	166
5.2.1.2. Small polaron model	167
5.2.1.3. Phonon induced tunneling	168
5.3. Thermo-electric power	168

5.4.	Dielectric constant	170
5.5.	Experimental measurement	173
5.5.1.	Resistivity	173
5.5.2.	Thermo-electric power	174
5.5.3.	Dielectric constant	174
5.6.	Results and discussion	175
5.6.1.	Resistivity	175
5.6.2.	Thermo-electric power	186
5.6.3.	Dielectric constant	192
5.6.3.1	Frequency dependence of dielectric constant	192
5.6.3.2.	Temperature dependence of dielectric constant	199
5.6.3.3.	Dielectric loss factor	204

CHAPTER SIX

6.1.	Conclusions	211
6.2.	Scope for the future work	217

LIST OF FIGURES

CHAPTER ONE

- Fig: 1.1. Crystal structure of ferrites exhibiting (a) the spinel structure, (b) tetrahedral, and (c) octahedral coordination.

CHAPTER TWO

- Fig.2.1. Reflection of X-rays from two different crystal planes.
- Fig.2.2.(a). Scanning Electron Microscope JEOL Model 840(SEM).
- Fig.2.2.(b). Line diagram of typical Scanning Electron Microscope.
- Fig.2.3.(a). Transmission Electron Microscope- Philips model CM200.
- Fig.2.3.(b). Sketch of radiation path in TEM.

CHAPTER THREE

- Fig.3.1. IR Spectra of various Mn-Zn ferrite samples obtained by the mechano-chemical method.
- Fig.3.2. IR Spectra of various Mn-Zn ferrite samples obtained by the wet chemical method.
- Fig.3.3. TG – DTA thermogram of precursors obtained from the mechano – chemical method for (a) $\text{Mn}_{0.5}\text{Zn}_{0.5}\text{Fe}_2\text{O}_4$
(b) $\text{Mn}_{0.6}\text{Zn}_{0.4}\text{Fe}_2\text{O}_4$.

- Fig.3.4. TG – DTA thermogram of precursors obtained from the wet chemical method for (a) $Mn_{0.5}Zn_{0.5}Fe_2O_4$
(b) $Mn_{0.65}Zn_{0.35}Fe_2O_4$.
- Fig.3.5.(a). X-ray diffraction patterns of mixture of oxides after ball-milling.
- Fig.3.5.(b). X-ray diffraction patterns of final products, after decomposition, obtained by the mechano-chemical method.
- Fig.3.5.(c). X-ray diffraction patterns of Mn-Zn ferrite samples obtained by the wet chemical method.
- Fig.3.6. EDS spectrum of (a) $Mn_{0.5}Zn_{0.5}Fe_2O_4$, (b) $Mn_{0.6}Zn_{0.4}Fe_2O_4$.
- Fig.3.7. TEM micrographs of (a) $Mn_{0.5}Zn_{0.5}Fe_2O_4$ (b) $Mn_{0.6}Zn_{0.4}Fe_2O_4$
- Fig 3.8. Variation of lattice value 'a' with concentration of Mn for samples prepared by (a) the mechano-chemical (b) the wet chemical method.
- Fig 3.9. Variation of X- ray density with concentration of Mn for samples prepared by (a) the mechano-chemical method (b) the wet chemical method.
- Fig. 3.10. Variation of mass density with concentration of Mn in ferrite samples obtained by (a) the mechano-chemical method (b) the wet chemical method.
- Fig.3.11. Variation of porosity with the concentration of Mn in samples prepared by (a) the mechano-chemical method (b) the wet chemical method.

CHAPTER FOUR

- Fig. 4.1. Alignment of magnetic moments.
- Fig.4.2. Plot of magnetization (M) versus magnetic field strength (H).
- Fig.4.3. Variation of saturation magnetisation value of Mn-Zn ferrite unsintered samples with Mn contents, prepared by the mechano-chemical method
- Fig.4.4. Variation of saturation magnetisation of Mn-Zn ferrite samples, with Mn contents sintered at (a)1100⁰C (b) 1200⁰C and (c) 1300⁰C.
- Fig.4.5. Variation of saturation magnetisation of Mn-Zn ferrite unsintered samples, with Mn contents, prepared by the wet chemical method.
- Fig.4.6. Variation of saturation magnetisation of Mn-Zn ferrite samples, with Mn contents sintered at (a) 1200⁰C and (b)1300⁰C.
- Fig 4.7. Magnetic hysteresis curves obtained by VSM at room temperature for unsintered samples (a) $Mn_{0.5}Zn_{0.5}Fe_2O_4$ and (b) $Mn_{0.6}Zn_{0.4}Fe_2O_4$, for the mechano-chemical method.
- Fig 4.8. Magnetic hysteresis curves obtained by VSM at room temperature for (c) $Mn_{0.625}Zn_{0.375}Fe_2O_4$ sintered at 1200⁰C and (d) $Mn_{0.675}Zn_{0.325}Fe_2O_4$ sintered at 1300⁰C for the wet chemical method.

- Fig.4.9. Curie temperature for various unsintered Mn-Zn ferrites samples with different Mn content, prepared by the mechano-chemical method.
- Fig.4.10. Curie temperature for various Mn-Zn ferrite samples with different Mn content sintered at 1300⁰C, prepared by the mechano - chemical method.
- Fig.4.11. Curie temperature for various unsintered Mn-Zn ferrite samples with different Mn content, prepared by the wet chemical method.
- Fig.4.12.(a). Variation of magnetic permeability of Mn-Zn ferrite with temperature for sintered (1000⁰C) samples obtained by the mechano- chemical method.
- Fig.4.12.(b). Variation of magnetic permeability of Mn-Zn ferrites with temperature for sintered (1100⁰C) sample obtained by the mechano- chemical method.
- Fig.4.12.(c). Variation of magnetic permeability of Mn-Zn ferrites with temperature for sintered (1200⁰C) sample obtained by the mechano-chemical method.
- Fig.4.12.(d). Variation of magnetic permeability of Mn-Zn ferrites with temperature for sintered (1300⁰C) sample obtained by the mechano-chemical method.
- Fig. 4.13. SEM micrographs of Mn_{0.6}Zn_{0.4}Fe₂O₄ ferrite (a) unsintered sample, and sintered at (b)1000⁰C, (c)1100⁰C, (d)1200⁰C, (e)1300⁰C.

Fig.4.14. SEM micrographs of $Mn_{0.5}Zn_{0.5}Fe_2O_4$ ferrite (a) unsintered sample, and sintered at (b)1000⁰C, (c)1100⁰C, (d)1200⁰C, (e)1300⁰C.

Fig.4.15. Variation of relative loss factor with log f for various Mn-Zn ferrites sintered at (a)1000⁰C and (b)1200⁰C, obtained by the mechano-chemical method.

CHAPTER FIVE

Fig.5.1.(a). Variation of resistivity ($\log\rho$) with 1000/T (K) for different unsintered Mn-Zn ferrite samples obtained by the mechano – chemical method.

Fig.5.1.(b). Variation of resistivity ($\log\rho$) with 1000/T (K) for different sintered Mn-Zn ferrite (1000⁰C) samples obtained by the mechano - chemical method.

Fig.5.1.(c). Variation of resistivity ($\log\rho$) with 1000/T (K) for different sintered Mn – Zn ferrite (1200⁰C) samples obtained by the mechano - chemical method.

Fig.5.1.(d). Variation of resistivity ($\log\rho$) with 1000/T (K) for different sintered Mn-Zn ferrite (1300⁰C) samples, obtained by the mechano - chemical method.

Fig.5.2. SEM micrographs of $Mn_{0.6}Zn_{0.4}Fe_2O_4$ ferrite (a) unsintered sample, and sintered, at (b)1000⁰C, (c)1100⁰C, (d)1200⁰C, (e) 1300⁰C by the mechano-chemical method.

- Fig.5.3. SEM micrographs of $Mn_{0.5}Zn_{0.5}Fe_2O_4$ ferrite (a) unsintered sample, and sintered, at (b) $1000^{\circ}C$, (c) $1100^{\circ}C$, (d) $1200^{\circ}C$, (e) $1300^{\circ}C$ by the mechano-chemical method.
- Fig. 5.4. Variation of resistivity ($\log\rho$) with $1000/T$ (K) for various Mn-Zn ferrite (a) unsintered samples, and sintered, at (b) $1200^{\circ}C$ and (c) $1300^{\circ}C$ samples obtained by the wet chemical method.
- Fig. 5.5. SEM micrographs of $Mn_{0.6}Zn_{0.4}Fe_2O_4$ ferrite (a) unsintered sample, and sintered at (b) $1000^{\circ}C$, (c) $1100^{\circ}C$, (d) $1200^{\circ}C$, (e) $1300^{\circ}C$ obtain by wet chemical method.
- Fig.5.6. Variation of Seebeck coefficient with Temperature (K) for various Mn-Zn ferrite unsintered samples obtained by the mechano-chemical method.
- Fig.5.7. Variation of Seebeck coefficient with Temperature (K) for various Mn-Zn ferrite unsintered samples obtained by the wet chemical method.
- Fig.5.8. Variation of dielectric constant with $\log f$ for various Mn-Zn ferrites (a) unsintered samples, and sintered, at (b) $1100^{\circ}C$ and; (c) $1300^{\circ}C$ samples prepared by the mechano-chemical method.
- Fig.5.9. Variation of dielectric constant with $\log f$ for various Mn-Zn ferrites (a) unsintered samples, and sintered, at (b) $1100^{\circ}C$ and, (c) $1300^{\circ}C$ samples prepared by the wet chemical method.

- Fig.5.10. Variation of dielectric constant with temperature for various Mn-Zn ferrite (a) unsintered samples, sintered, at (b) 1100⁰C and (c) 1300⁰C obtained by the mechano-chemical method.
- Fig.5.11. Variation of dielectric constant with temperature for various Mn-Zn ferrite (a) unsintered samples, sintered, at (b) 1100⁰C and (c) 1300⁰C obtained by the wet chemical method.
- Fig.5.12. Variation of relative loss factor with log f for Mn-Zn ferrites (a) unsintered (b) sintered at 1300⁰C samples, obtained by the mechano- chemical method.
- Fig.5.13. Variation of relative loss Factor with log f for various Mn-Zn ferrite (a) unsintered (b) sintered at 1200⁰C samples, obtained by the wet chemical method.

LIST OF TABLES

CHAPTER THREE

- Table 3.1. Amount of oxides taken for the mechano-chemical synthesis of Mn-Zn ferrites.
- Table 3.2. Amount of metal salts taken for the wet chemical synthesis of Mn-Zn ferrite.
- Table 3.3. Percentage yield for various compositions of $Mn_xZn_{(1-x)}Fe_2O_4$ ferrites obtained by the mechano-chemical method.
- Table 3.4. Percentage yield for various compositions of $Mn_xZn_{(1-x)}Fe_2O_4$ ferrites obtained by the wet chemical method.
- Table 3.5. AAS analysis data for ferrite samples obtained by the mechano-chemical method.
- Table 3.6. AAS analysis data for ferrite samples obtained by the wet chemical method.
- Table 3.7. EDS analysis of (a) $Mn_{0.5}Zn_{0.5}Fe_2O_4$ (b) $Mn_{0.6}Zn_{0.4}Fe_2O_4$
- Table 3.8. Calculated lattice constant for Mn-Zn ferrites obtained by (a) the mechano-chemical method, and (b) the wet chemical method.
- Table 3.9. Particle size of Mn- Zn ferrites obtained by (a) the mechano-chemical method, and (b) the wet chemical method.
- Table 3.10. X-Ray Densities for ferrite samples obtained by (a) the mechano-chemical method, and (b) the wet chemical method.

Table 3.11. Mass Densities of the ferrite samples obtained by (a) the mechano-chemical method, and (b) the wet chemical method.

Table 3.12. Porosity for Mn-Zn ferrite samples obtained by (a) the mechano-chemical method, and (b) wet chemical method

CHAPTER FOUR

Table 4.1. Saturation magnetization values of unsintered and sintered Mn-Zn ferrite samples, of various compositions, obtained by the mechano-chemical method.

Table 4.2. Saturation magnetization values of unsintered and sintered Mn-Zn ferrite samples, of various compositions, obtained by the wet chemical method.

Table 4.3. Curie temperature of unsintered and sintered Mn-Zn ferrite samples obtained by the mechano-chemical method.

Table 4.4. Curie temperature of Mn-Zn ferrite sample of various composition, obtained by the wet chemical method.

CHAPTER ONE

LITERATURE SURVEY

1.1. GENERAL INTRODUCTION:

Iron is the 26th element in the periodic table believed to have been introduced on Earth by meteors. Iron was found in Egyptian tombs dating from 3500 B.C.. Elemental iron, whose atomic weight is 55.847 a.m.u., is the fourth most abundant element in the earth crust after oxygen, silicon and aluminium. The percentage of iron in the earth crust is roughly estimated to be about 6.2% by weight. In the crust, iron is found mainly as the oxide minerals: α -Fe₂O₃ (Hematite), γ -Fe₂O₃ (Maghemite), Fe₃O₄ (Magnetite), and various forms of FeO(OH) (Limonite) also as FeCO₃ (Siderite) and FeS₂ (Pyrites).

Iron is an essential element in almost all living organisms. In the human body, its concentration ranges between 3 and 380 parts per million (ppm) in bone, 380–450 ppm in blood, and 20–1,400 ppm in tissue. It is also present in plants as cytochrome and Ferredoxins. Iron has a very stable nucleus and has fourteen known isotopes. Four isotopes, ⁵⁴Fe (5.9%), ⁵⁶Fe (91.72%), ⁵⁷Fe (2.1%), and ⁵⁸Fe (0.28%) make up essentially 100 percent of naturally occurring iron. Pure iron is a soft, white, lustrous metal. The melting point of iron is 1535⁰C, the boiling point is 2750⁰C and the specific gravity is 7.874 (20⁰C). Elemental iron oxidizes in moist air but is stable in dry air.

Finely divided elemental iron is pyrophoric. Four allotropic forms, or ferrites, are known as: 'a', 'b', 'g' and 'd', with transition points at 770, 928, and 1530°C respectively. The 'a' form is magnetic, but when iron is transformed into the 'b' form, the magnetism disappears, although the lattice remains unchanged.

Pure iron is chemically reactive and corrodes rapidly, especially in moist air or at elevated temperatures. Iron dissolves in dilute mineral acid and in hot sodium hydroxide solution. Iron has seven oxidation states (2-, 0, 1+, 2+, 3+, 4+ and 6+) with the 2+, ferrous or Fe(II), and 3+, ferric or Fe(III), state being the most common. With mild heating, iron reacts with the halogens and with sulfur, phosphorus, boron, carbon, and silicon to form a variety of compounds, with a valence of 2, 3, 4, or 6.

Iron, with electronic configuration of $1s^2 2s^2 2p^6 3s^2 3p^6 3d^6 4s^2$, has unfilled "3d" orbitals thus showing the properties of transition metal. Standard electrode potential value of Fe/Fe^{2+} is -0.440 V and Fe^{2+}/Fe^{3+} is +0.771V and therefore iron is present in nature not as pure free metal but as oxides. Most common method of extracting iron on large scale from its ore is by using blast furnace for reduction.

Pure iron is chemically reactive and forms oxides in the presence of water and oxygen which is called rusting. The economic importance of rusting is such that it has been estimated that the loss due to corrosion is over 1% of the world's economy. Rusting of iron consists of the formation

of hydrated oxide, $\text{Fe}(\text{OH})_3$ or $\text{FeO}(\text{OH})$, and is an electrochemical process which requires the presence of water, oxygen and an electrolyte. In the absence of any one of these, rusting does not occur to any significant extent. In air, a relative humidity of over 50% provides the necessary amount of water and at 80%, the corrosion is severe [1-3].

1.2. COMPOUNDS OF IRON:

Iron mostly has compounds with two oxidation states namely 2+ and 3+. Fe^{2+} is one of the most important oxidation states. The compounds are crystalline in nature and are mostly pale yellowish green or grey in color, examples are FeF_2 , $\text{FeCl}_2 \cdot 6\text{H}_2\text{O}$, FeBr_2 , FeI_2 , $\text{FeSO}_4 \cdot 7\text{H}_2\text{O}$, $\text{Fe}(\text{ClO}_4) \cdot 6\text{H}_2\text{O}$. Similarly, Fe^{3+} which is another important oxidation state of iron have large number of compounds obtained by oxidation of corresponding salts of Fe^{2+} state. Ferric ions form compounds with all anions except iodine (I^-). Many salts of Fe^{3+} exists both in anhydrous as well as hydrous forms. The compounds in ferric state exhibit different colors and are crystalline in nature. FeF_3 and $\text{FeBr}_3 \cdot 6\text{H}_2\text{O}$ are green, $\text{Fe}(\text{NO}_3)_3 \cdot 6\text{H}_2\text{O}$ is colorless, $\text{Fe}(\text{NO}_3)_3 \cdot 9\text{H}_2\text{O}$ is purple while $\text{FeCl}_3 \cdot 6\text{H}_2\text{O}$ and $\text{Fe}_2(\text{SO}_4)_3 \cdot 9\text{H}_2\text{O}$ are yellow in color. Iron also forms a variety of complexes with various ligands. Most important class of compounds of iron is its oxides.

1.2.1. OXIDES OF IRON:

Iron forms three different types of oxides namely FeO, Fe₂O₃ and Fe₃O₄. These are non-stoichiometric (the ratio of cations and anions may vary from the one given in the formula) and are easily oxidized or reduced into each other. These aspects can be explained on the basis of their crystal structure.

1.2.2. NATURALLY OCCURRING OXIDES OF IRON:

In nature, iron is mostly present in three oxide forms as α -Fe₂O₃ known as hematite, γ -Fe₂O₃ as maghemite and Fe₃O₄ or FeOFe₂O₃ as magnetite. Maghemite and magnetite are magnetic in nature.

1.2.3. MIXED OXIDES OF IRON:

When iron oxide is doped with other divalent or trivalent metal ions, then the oxides formed are called mixed oxides of iron. They are also referred as ferrites. Hilpert [4] suggested the basic formula for ferrites as MeFe₂O₄, where Me is a divalent metal ion. It exists in a variety of chemical compositions and represented as MeFe₂O₄, MeFe₁₂O₁₉, (where Me is divalent ion in both cases) and MeFeO₃, Me₃Fe₅O₁₂ (where Me is trivalent ion in both cases).

1.3. HISTORY OF FERRITES:

The first magnetic material to be discovered was magnetite Fe_3O_4 or ferrous ferrite. Du Bios [5] measured its saturation magnetization. P. Weiss [6] studied the magnetic properties of Fe_3O_4 and determined the saturation magnetization and Curie temperature. Hilpert [4], who suggested its basic formula, synthesized many ferrites. Some researchers [7, 8] have made structural studies of ferrite and reported the structure to be spinel. Barth and others [9] carried out X-ray analysis of ferrites and assumed that divalent and trivalent ions interchange their position in crystals thus leading to the discovery of inverted spinel structure for ferrite. Verway [10] reported investigation on divalent and trivalent Fe ions and suggested higher conductivity due to exchange of electrons between the two Fe ions. Neel [11] introduced the idea of presence of magnetic sublattices and also developed the theory of ferrimagnetism with spin-spin interaction in ferrites.

Systematic and detailed studies were carried out by Van-Vleck [12] and Anderson [13] with theory of super exchange interactions. Yafet and Kittel [14] extended the theory of magnetic sublattices by postulating triangular arrangement of these sublattices. Later on, Gorter [15] measured the magnetization of Mg, Fe, Mn, Ni, Co and Cu ferrites mixed with zinc and gave the direct experimental proof of Neel's theory. Gulliaud and co-workers [16] studied the variation of magnetization with temperature for mixed ferrite in ferrimagnetic region. Other researchers [17, 18] further proved Neel's theory by studying some ferrites by neutron diffraction.

Snoek and co workers [19] at the Philips Research Laboratory in Netherlands developed the first soft ferrites for the commercial applications. He [20] along with his co-workers systematically studied the ferrites at high frequency by showing the importance of oxygen and homogeneity. Many investigators [21-23] have developed ferrites by solid state reactions. The correlation between Curie temperature, magnetization and cation distribution was carried out by Gilleo [24]. Koops [25] studied high conductivity associated with high dielectric constant and obtained a formula giving phenomenological theory to explain the conduction behaviour.

As the science and technology has taken the front seat, with rapid pace the work on ferrites is progressing by leaps and bounds. The new sophisticated instruments have made it possible for interpretation of data to almost perfection.

1.4. THE FERRITE STRUCTURE:

Ferrites are mixed metal oxides of magnetic nature in which iron is the main component. Ferrites show four different types of crystal structures:

- 1] Spinel structure,
- 2] Garnet structure,
- 3] Hexagonal structure, and,
- 4] Orthoferrite structure.

1.4.1. THE SPINEL STRUCTURE:

The ferro-spinels have derived their name from non-magnetic mineral MgAl_2O_4 and have a cubic structure as determined by Bragg [26]. The divalent Mg^{2+} ion can be replaced by Fe, Zn, Mn, Ni, Co etc or with the combination of two ions while Al^{3+} is replaced by Fe^{3+} or with other trivalent ions. It is a face centre cube with $O_h^7\text{-fd}3m$ space group. The general formula for it is, $\text{MeO.Fe}_2\text{O}_3$ or MeFe_2O_4 , where Me is a divalent metal ion or a mixture of metal ions having average valence of two. The unit cell is cubic.

The oxygen ions form a nearly close-packed face centered cubic structure and the metal ions in the unit cell occupy the interstitial positions with four fold and six fold oxygen coordinations. The metal ion surrounded by four oxygen ions is called A site which is tetrahedral and that surrounded by six oxygen is called B site which is octahedral. There are 96 interstitial positions with 64 A sites and 32 B sites. However 8 cations occupy A sites and 16 occupy B sites. The occupation of position of metal ions over two sites depends upon the relative site preference and energies of cations present. This governs the intrinsic properties of ferrites.

Depending upon modes of occupation of A and B sites by metal ions and on the basis of cation distribution, Barth and Posnjak [27] have classified spinel into three classes as: Normal ferrites, Inverse ferrites and Random or Mixed ferrites.

1.4.1.1. THE NORMAL FERRITES:

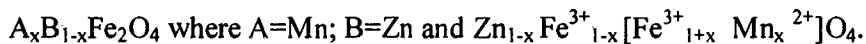
In normal ferrites all divalent metal ions occupy A sites and all the Fe^{3+} occupy B sites- $\text{Me}^{2+}[\text{Fe}_2^{3+}]\text{O}_4$. Ferrites like ZnFe_2O_4 , CdFe_2O_4 etc are normal ferrites and they are non-magnetic in nature.

1.4.1.2. THE INVERSE FERRITES:

In this type of ferrite all the eight divalent metal ions and half the Fe^{3+} ions occupy B sites while remaining half of Fe^{3+} occupy A sites- $\text{Fe}^{3+}[\text{Fe}^{3+} \text{Me}^{2+}]\text{O}_4$. Examples are MgFe_2O_4 , NiFe_2O_4 , CoFe_2O_4 , Fe_3O_4 etc.

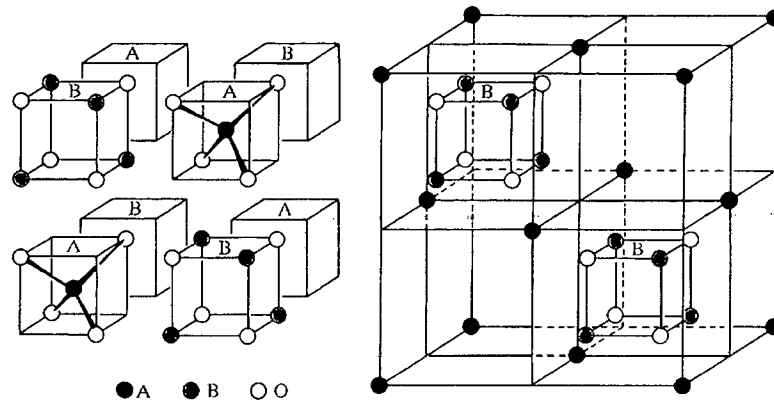
1.4.1.3. THE RANDOM OR MIXED FERRITES:

Random or mixed ferrites are intermediate between normal and inverse ferrite, in which all divalent metal ions and Fe^{3+} ions are uniformly distributed over the tetrahedral and octahedral sites. Mn-Zn ferrite is a mixed spinel ferrite, which has general formulae-

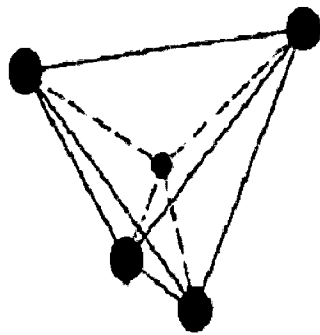


Zn^{2+} ions occupy tetrahedral sites while Mn^{2+} ions occupy octahedral sites, whereas Fe^{3+} ions occupy both octahedral and tetrahedral sites.

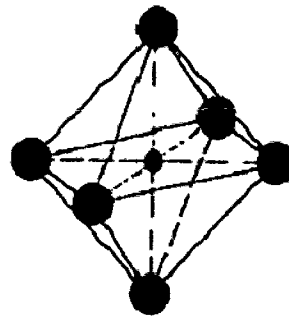
Ferrosinell structure is the most important group of ferrites in which technologically useful oxide magnetic materials are classified.



(a)



(b)



(c)

Fig. 1.1. Crystal structure of ferrite exhibiting (a) the Spinel Structure, (b) tetrahedral, and (c) octahedral coordination.

1.4.2. THE GARNET STRUCTURE:

These ferrites have the general formulae $\text{Me}_3\text{Fe}_5\text{O}_{12}$ where Me is a trivalent ion such as rare-earth. The unit cell is cubic and contains eight molecules of $\text{Me}_3\text{Fe}_5\text{O}_{12}$.

1.4.3. THE HEXAGONAL STRUCTURE:

The general formula of hexagonal ferrites is $\text{MeFe}_{12}\text{O}_{19}$ where Me is a divalent metal ion with large atomic radius. The crystal structure is hexagonal in nature eg. Barium ferrite.

1.4.4. THE ORTHOFERRITES STRUCTURE:

This class of ferrites has MeFeO_3 as their general formula, where Me is a trivalent ion such as rare-earth. These compounds crystallize in a distorted perovskite structure with an orthorhombic unit cell.

1.5. SYNTHETIC METHODS OF FERRITES:

Due to wide variety of applications, ferrites materials are much sought after inorganic compounds. Amongst the ferrites, Mn-Zn ferrites are very useful in electrical and electronic applications. Efforts are on to develop newer methods of synthesis which are cheaper, less time consuming and convenient. Attempts are also made to modify known methods to make them simple without compromising the targeted end product having desired structure and properties. Therefore, preparative technique assumes an important role in any study of solid materials.

There are several well established methods of preparing oxide materials. Most of them are also standardized to obtain tailor-made products. Rational synthesis of materials requires knowledge of crystal

chemistry apart from thermodynamics, phase equilibria and reaction kinetics. Most commonly used method has been the ceramic method which involves mixing and grinding of powders of constituent oxides, carbonates and such other compounds, which yield mostly the gaseous products (along with solid oxide), and heating them at high temperature with intermittent grinding, whenever necessary. However, the products obtained by this method are non-uniform, coarse and non-stoichiometric in most of the cases.

To overcome these disadvantages, therefore, low-temperature chemical routes are employed. These methods are less stringent and avoid higher energy associated with higher temperatures which is essential for better control of structure, stoichiometry and phase purity. Soft chemistry routes such as *Chemie – douce*, therefore, attract more interest since these processes give novel products, in addition to being more convenient. Importantly, some of the oxide products are metastable and cannot be otherwise prepared. Soft chemistry reaction essentially uses simple reactions like intercalation, ion-exchange, hydrolysis, dehydration and reduction that can be carried out at relatively low temperatures.

The various known and standardized methods of synthesis of oxide materials, with special reference to ferrites, are discussed below.

1.5.1. THE CERAMIC METHOD:

The most common method of preparing ferrites and other solid materials is the ceramic method. It essentially involves mixing and grinding of the stoichiometric amounts of oxides, carbonates, oxalates or other compounds containing the relevant metals and heating the mixture at the predetermined temperature. For ferrite synthesis by the ceramic method, usually, iron oxide is thoroughly mixed with (a) other divalent metal oxides taken in calculated amount, or (b) other divalent reactive oxide obtained in situ by decomposing metal salts like nitrates, carbonates, oxalates etc. They are mixed first manually and wet milled (using water, alcohol, acetone) with steel balls for few hours. Wet mixing of these oxides in an attritor can reduce the mixing time significantly.

After milling, the mixture is dried up and pressed into a suitable shape before calcination. The milling, after calcination and sintering, lead to formation of the final product. Organic binders like polyvinyl alcohol (PVA) are often added to the preheated samples and then they are milled and pressed into desired shape and size. The pressed material is then fired in air or oxygen between 1100°C - 1500°C , for the solid state reaction between the metal oxides to give a homogenous ferrite product. The mechanism of formation of ferrite by the solid state reaction between metal oxide and ferric oxide has been well explained by several researchers [28-32].

In spite of having several limitations, the ceramic technique has been often used for the synthesis of various ferrites [33-37] and several other solid state materials.

1.5.2. THE DECOMPOSITION METHOD:

The starting material for this method is mixture of metal salts such as carbonates, nitrates, oxalates, etc. Oxides are mixed in requisite proportions and then preheated in air, usually to form oxides by thermal decomposition. The preparation in situ of oxides makes them to undergo a solid state reaction more readily [38]. Other details of the method are similar to ceramic method. Many oxides are prepared using this simple method [39].

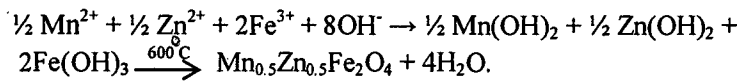
1.5.3. THE CO-PRECIPIATION METHOD:

In this method, the relevant metal cations are taken as soluble salts e.g. chloride, nitrates etc. and they are co-precipitated from a common medium, as hydroxide, carbonates, oxalates or citrates. This method required better understanding of chemistry and was established by Economos [40]. In practice oxides or carbonates of the selected metals are digested with an acid and the metal ions are precipitated by adding precipitating agent. The precipitate after drying is heated to the set temperature in a desired atmosphere to get the final products. The decomposition temperature of the precipitate is generally lower than the

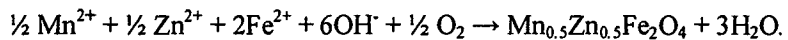
temperatures employed in the ceramic method. Co-precipitation is a simple method for the synthesis of solid powders [41-44].

There are two co-precipitation routes possible for the preparation of Mn-Zn ferrites:

i) *The calcination route*- In this procedure, the co-precipitation of hydroxides of Mn^{2+} , Zn^{2+} and Fe^{3+} in the first stage is followed by calcination of the hydroxide precursors in the second stage to give desired ferrite material:



(ii) *The oxidation of Fe (II) hydroxide before decomposition*- In this procedure, the co-precipitation of hydroxides of Mn^{2+} , Zn^{2+} and Fe^{2+} in the first stage is followed by the oxidation of Fe (II) hydroxide in the second stage, which directly results in the formation of the spinel ferrite (in situ), after decomposition according to Shikorr's reaction [45].



One of the disadvantages of the co-precipitation method is the difficulty of controlling the particle size and morphology. In order to overcome this problem, a microemulsion method is used, which involves co-precipitation in water-in-oil microemulsion [46].

1.5.4. THE PRECURSOR METHOD:

This is comparatively a simple method in which a compound of metal or mixed metals, called as precursor, is prepared which on heating decomposes to produce the desired product. In practice, fine particle product is obtained which is of high purity and homogenous in nature. By using this wet chemical method it is possible to prepare different ferrite materials, with smaller grain size, low porosity and a very high surface area. Different anion-based salts viz. nitrate, oxalate, sulfite, formate etc., have been used Patil et al. [47-49] to prepare many novel hydrazine precursors, which produces fine-particle ferrites at temperatures as low as 125-165⁰c. It is reported that these precursors undergo autocatalytic decomposition, that is, the combustion is self-sustained once ignited. Many precursors, including citrate, are used to synthesize the ferrite material [50-53].

1.5.5. THE HYDROTHERMAL METHOD:

In this method water is used under pressure and temperature at above its boiling point for the synthesis of material by hydrothermal oxidation. The advantage of using water is that it performs two roles: firstly, as liquid or vapor it serves as the pressure transmitting medium, and secondly, almost all the reactants are either wholly or partially soluble in water under high pressure. Hence, the reaction can occur with the help of liquid or vapor phases at fairly lower temperatures. These reactions, otherwise, may take place at high temperature in absence of water.

The method has been successfully used to prepare ferrites [54-56]. The other advantages of the method are recrystallization, single crystal growth monitoring of grain size and shapes etc.

1.5.6. THE VAPOUR PHASE METHOD:

Schaifer developed this method in 1971. It is the method of chemical transport by vapour phase. The method is used for the synthesis of new compounds as also for the growth of single crystals or for the purification of the compounds. Because of higher mobilities and diffusion, gases react much faster compared to solid and liquids. In this method, gas phase besides functioning as transporting agent, also has influence on the rate of reaction. In addition, the gaseous phase is important in normal solid state reactions under isothermal conditions where it may act as a faster means of transporting matter from one crystal to another [57].

1.5.7. THE SOL-GEL METHOD:

Sol – gel method, today, is one of the important techniques for preparing oxide material. It is multi-step wet chemical process involving both chemical and physical processes like hydrolysis, polymerization, drying and densification. The name sol-gel is given to the process because of the distinctive increase in the viscosity that occurs at a particular point in the sequence of steps. Synthesis of inorganic oxides is achieved from inorganic or organometallic precursors. The important features of the

Sol-gel method are better homogeneity, high purity, lower processing temperature and a uniform phase distribution in multicomponent system, as well as better size and morphological control. This method [58-60] makes it possible to prepare new crystalline and non-crystalline materials; and also thin films and coatings with ease.

1.5.8. THE CHIMIE-DOUCE METHOD:

The advantage of precursor methods are that the reaction takes place at much lower temperatures compared to normal solid state reaction procedures. Another advantage of precursor methods is in the synthesis of new, metastable phases which cannot be prepared by other routes. Although these phases are thermodynamically metastable they are often kinetically stable to quite high temperatures and there is a close structural relationship between the precursor phase and final product. Often new phases, therefore, have unusual structures and interesting properties. The French researchers have termed this method as chimie-douce [57].

Crystallite sizes of the powder specimen can be obtained on calcinations at various temperatures. It is observed that the size increases with calcination temperature. For ferrites, as the calcination temperature affects the particle size, all parameters like Curie temperature, permeability, saturation magnetization, resistivity, dielectric properties etc. are also affected by the same way. Ferrites have gained importance due to their microstructures. The magnetic properties of Mn-Zn ferrites depend

on the microstructures. The microstructure of Mn-Zn ferrites is greatly influenced by sintering conditions as well, thus it is extremely important to control the same.

Chemical methods of synthesis play a crucial role in designing and discovering new and novel materials and in providing less cumbersome methods for preparing known materials. Chemical methods also enable the synthesis of metastable materials, which are otherwise difficult to prepare.

1.5.9. THE COMBUSTION SYNTHESIS METHOD:

Combustion synthesis or the self-propagating high temperature synthesis is a useful method for preparation of variety of solid materials. The method makes use of a highly exothermic decomposition reaction which produces a flame due to spontaneous combustion which then yields the desired products or its precursors in finely divided form. Essential requirement in the combustion method is the presence of a fuel and an oxidant in the reacting compounds. During recent times, the combustion method has been successfully tried to synthesize different metal oxides by using nitrate mixture with a fuel like glycine, urea and hydrazine [61, 62] in an atmosphere of air or oxygen.

1.5.10. THE PLASMA SYNTHESIS METHOD:

Plasma synthesis has been successfully used for producing Mn-Zn ferrite nanoparticles [63]. The method uses metallic precursors ball milled into fine powder using high energy ball mill and high energy radio frequency induction thermal plasma system. The fine precursor powder is ejected through the plasma jet stream by Argon as carrier gas. Compressed air is also introduced in the reactor as an oxidizer [64, 65]. This method of preparation is highly complex and involves complex systems.

1.5.11. THE REVERSE MICELLE METHOD:

Reverse micelle technique has been used in recent years by some researchers [66, 67] to synthesize manganese-zinc ferrite nanoparticles. This technique basically uses a surfactant to stabilize varying aqueous droplet sizes in hydrocarbon medium. Metal salt precursors are contained in the aqueous portion and are transformed by a reactant from the hydrocarbon phase. Both the structure of the surfactant and the steric size are able to produce metals having a wide range of grain sizes. In this synthesis, two reverse micellar solutions are prepared, the first using the metal solution and the second one using ammonium hydroxide. Stock solution of 0.5 M. sodium dioctylsulfosuccinate (AOT) micellar is prepared in 2, 2, 4 -trimethylpentane-(isooctane).

It has been observed that precipitation of metals is influenced by pH and electrochemical potential of the solution. Therefore, the initial ratio

of metal precursors is modified to account for the reduction of metals in the precipitate and subsequently fired samples. In this method, the micelle size can be controlled by the molar ratio of water to AOT, which is chosen to yield a fine particle size in nm. The volume of aqueous solution and desired particle sizes are used to determine the amount of the precursor solution to be used. The ammonia solution is then added to the metal-salt solution under constant stirring. The reaction is allowed to proceed for about 2 hrs, until particle flocculation is induced by adding excess methanol.

The particles are then collected using centrifugation and washed using methanol to remove excess surfactant, followed by a methanol: water solution to remove any additional unreacted ions. After final centrifugation, the material is dried overnight under a dynamic vacuum, and subsequently fired at 525⁰C for 5 hours under inert atmosphere to obtain the required product.

1.5.12. THE CTAB METHOD:

Mn-Zn ferrite nanoparticles, with a narrow size distribution, can be prepared in water-CTAB-hexanol microemulsions [68]. In this, ferrite-nanoparticles are synthesized in the water pools of reverse micelles in a microemulsion system consisting of an aqueous phase, n-hexanol as the oil phase and n-hexadecyl trimethylammonium bromide (CTAB) as the surfactant. The synthesis of the magnetic ferrite occurs in situ with the

co-precipitation of hydroxides of Mn^{2+} , Zn^{2+} and Fe^{2+} ions in the first stage, followed by the oxidation of Fe(II) hydroxide in the second stage. The influence of the pH after the precipitation of hydroxides on the nature of the product is determined.

The microemulsion containing an aqueous solution of the corresponding metal ions is mixed with a microemulsion containing an aqueous solution of precipitating agent. By varying the amount of the latter microemulsion, at different pH values, between 4 and 13, can be set. The pH needs to be approximately 8 and above to produce the spinel ferrite product after the oxidation of Fe (II) hydroxide. At lower pH values, FeOOH is obtained as the major product. Although the spinel product is obtained at room temperature, the temperature has a large influence on the particle size [69].

1.5.13. OTHER METHODS:

Apart from the methods mentioned above there are many other methods which are also used for the synthesis ferrites [70 - 74].

It may be seen that many of the methods mentioned above yield nanoparticle ferrites. However, these methods involve sophisticated instrumentation techniques for preparation, require expensive high purity starting materials, constant monitoring of temperature, lengthy preparative condition, and are also time consuming.

1.6. PROPERTIES OF FERRITES:

The properties of ferrites are broadly classified into two types: intrinsic and extrinsic.

Intrinsic properties are saturation magnetization; magnetostriction, anisotropy, permeability and Curie temperature. Where as, hysteresis, resistivity, dielectric constant etc. are extrinsic properties. The extrinsic properties are structure sensitive properties.

1.6.1. MAGNETIC PROPERTIES:

Magnetic properties are the most fundamental properties of any ferrite material. The magnetic properties include saturation magnetization, retentivity, coercivity, permeability, susceptibility and Curie temperature.

1.6.1.1. SATURATION MAGNETIZATION:

Saturation magnetization is one of the intrinsic properties of ferrite and is governed by the chemical composition, cation distribution etc. The saturation magnetization is the maximum induced magnetic moment that can be obtained in a magnetic field; beyond which no further increase in magnetization occurs. The normal spinels are non magnetic at room temperature whereas the inverse spinels are magnetic at that temperature. In the case of inverse spinel the Fe^{3+} ions on A-sites are coupled with their

spins antiparallel to those of Fe^{3+} ions on B-sites. Therefore the net magnetic moment is only due to divalent Me^{2+} metallic ions.

The saturation magnetization of Mn-Zn ferrite is known to depend on method of preparation as well as on the sintering temperature.

1.6.1.2. MAGNETIC HYSTERESIS:

The lagging of magnetic induction to the magnetizing field is referred to as magnetic hysteresis. If an alternating magnetic field is applied to the material; its magnetization will trace out a loop called a hysteresis loop. The lack of retraceability of the magnetization curve is the property called as hysteresis. Hysteresis study of ferrites helps to find out valuable information about saturation magnetization, retentivity, coercivity, permeability etc. Ferrites with low coercive force are called soft ferrites and with high coercive force are called the hard ferrites. The permeability, saturation magnetization, coercive force and remnants magnetization help to decide the nature of application of ferrites.

1.6.1.3. PERMEABILITY:

Magnetic permeability (μ) is the ratio of magnetic flux density (B) to the magnetic field strength (H), given by expression

$$\mu = B/H \quad \text{-----} \quad 1.1.$$

Magnetic permeability is microstructural dependent. The permeability is due to the reversible displacement of domain walls within the material. It increases with temperature and is affected by the grain size, presence of impurities, density etc.

1.6.1.4. A.C. SUSCEPTIBILITY:

Magnetic susceptibility of a material is expressed by relation,

$$\chi = M/H \quad \text{-----} \quad 1.2.$$

where, M is the intensity of magnetization and H is the applied field. The AC susceptibility measurement explores the existence of single domain (SD) or multidomain (MD) or super paramagnetic (SP) particles in the material. Many researchers [75-77] have studied the variations of AC susceptibility with temperature for many ferrimagnetic materials and have given the information about the Curie temperature and the type of domain structure. Bean [78] has reported that for single domain particles, coercive force is large, and it tends to be zero for the super paramagnetic materials.

1.6.2. ELECTRICAL PROPERTIES:

The D.C. electrical properties of ferrites, namely, resistivity and thermo-electric power is commercially important, where as, the most important A.C. electrical property includes dielectric constant and the extent of loss.

where Q is referred as the thermo-electric power or thermo-power, is also known as the Seebeck coefficient while, ΔE is the thermo-e.m.f. produced by the sample due to temperature difference ΔT .

The Seebeck voltage does not depend on the distribution of temperature along the metals between the junctions. This effect is the physical basis for a thermocouple, which is often used for temperature measurement. Hall-effect and thermo-electric properties are widely used in interpretation of the conduction mechanism in semiconductors. The ferrites in general are semiconductors and have low conductivity compared to metals. The interpretation of Hall-effect is more, straight forward and gives precise results. However, in the case of low mobility materials such as ferrites, it is sometimes difficult to measure the Hall-effect. In such cases the thermo-electric power measurement is the only alternative. The sign of the thermo- emf gives vital information about the type of conduction in the semiconductors- whether it is p-type or n-type. Another important significance is that it enables one to calculate the value of carrier concentration. There are two known methods to measure the thermo electric power [82].

Zinc ferrite and lithium ferrite are found to be n-type semiconductors. Murthy et al. [83] have investigated dc conductivity and Seebeck coefficient of some nickel zinc ferrite as a function of temperature- from room temperature to 300°C . The ferrites, with excess

iron, show n-type semiconductor behaviour and those with iron deficiency show p-type conduction.

1.6.2.3. DIELECTRIC BEHAVIOUR:

Ferrites shows high dielectric constant and dispersion of dielectric constant in the frequency range from 20Hz to 1GHz [84]. The dielectric properties of ferrites are dependent upon several factors including the method of preparation, chemical composition, grain-size and sintering temperature. A dielectric substance, when subjected to an alternating electric field, the positive and negative charges within the material gets displaced with respect to one another and the system acquires an electric dipole moment. The dipole moment per unit volume is called polarization. Some researchers have studied the dielectric properties of ferrites [85]. Koops [25] gave a phenomenological theory of dispersion in the dielectric constant.

1.7. APPLICATIONS OF FERRITES:

Mn-Zn ferrites, with grain size in nanometer range, possess interesting micro-magnetic and electrical properties such as magneto-optic, magneto-caloric effect, giant magnetic resistance etc. Their application in different devices like motors, transformers, sensors, inductors, insulators, and in ferrofluids [86] is on the rise. These materials are useful in a variety of applications in the electronic industry due to their high permeability,

high saturation magnetization, high resistivity and low loss as these formed the key impediments in downsizing of transformer cores, deflection yokes, power inductors, antenna rods etc. in the world of miniaturization.

As nanomaterial possesses unique beneficial properties of chemical, physical, and mechanical nature, they can be used in a wide variety of applications. Current research in this area of magnetic nanoparticles is being carried out by focusing on their applications where their unique properties will allow for significant advances in scientific technology. In the electronics field researchers are investigating the design of superstructures comprised of magnetic ordered arrays to enhance sensitivity in magnetic sensors [87].

After going through several research articles in the scientific journals on magnetic materials, and particularly on soft ferrites like Mn-Zn ferrite and Ni-Zn ferrite, as also through the Proceedings of 9th International Conference on Ferrites (San Francisco USA 2004) one realizes the importance of Mn-Zn ferrite due to its fascinating properties. It finds wide applications in many fields. Government of India, through Ministry of Science and Technology and Department of Science and Technology (DST) has given stress to promote research in frontier and emerging areas. such as Neurobiology, Solid State Chemistry, Nanomaterials, Materials Science, Surface Science, Plasma Physics, Macromolecular Crystallography and Ultrafast Processes. To produce

innovative and new materials, DST has launched Nano Science and Technology Initiative (NSTI), and the Nano Mission in the XIth five year plan for the advance research on nanomaterial including nano magnetic materials.

1.8. SCOPE OF PRESENT WORK:

Mn-Zn ferrite is a soft magnetic material and enjoys a large spectrum of applications due to its high performance. Efforts are on to enhance the performance of this material in particular. The performance of this material is dependent on a number of factors. Some of the factors are the method of preparation, the degree of Mn concentration in the sample, the grain size, the sintering temperature and the conditions at sintering etc. As per the study conducted and reported [88, 89] the most important parameter for high performance is the small grain size. The ultra fine grain size materials have gained importance due to developments in the nanoscience and nanotechnology as well as because of the development of newer methods for their synthesis and the fascinating properties exhibited by them.

Soft as well as hard ferrites are extensively used as magnetic materials in different fields from audio video devices to telecommunications to Defence, and in power sector. Mn-Zn ferrite is a soft magnetic material and enjoys a large spectrum of applications due to its high performance. Efforts are on to further enhance the performance of

this material in particular. The performance of this material is dependent on number of factors; important among them is the method of preparation.

Ceramic method of preparation of oxide material has its own importance in certain aspect. However, since this method involves high temperature synthesis, uniform crystalline size, compositional control and homogeneity cannot be guaranteed.

It has been reported that the low temperature synthesis for ferrite materials, in most of the cases, gives ultrafine product with improved crystalline size and desired composition. Importantly, these two factors play crucial role in the performance of the ferrite materials. Hence the development of newer methods of synthesis has drawn lot of attention from the researchers worldwide.

Research in our laboratory has been aimed to develop newer routes of synthesis of oxide material having improved performances. In this direction, we have already reported the low temperature preparation of ferrite using hydrazine based precursor [90].

Literature survey on ferrite materials indicates that there are no reports on the use of partial ceramic procedure in combination with chemical method for the synthesis of ferrites. This method of preparation may draw the additional advantages from the two different procedures

involved. A proper study in this direction will therefore add to the knowledge of ferrites in particular and oxide material in general.

In so doing, it is envisaged to develop a new method namely, mechano-chemical method using an indigenous ball mill to produce a homogenous mixture of oxides and treat it with hydrazine based ligand to produce nano size Mn-Zn ferrite. For comparison, a wet chemical method using the same ligand with soluble salts of manganese, zinc and iron has been also proposed to prepare the Mn-Zn ferrite.

The present work is undertaken to explore these new synthetic routes for the preparation of high performance Mn-Zn ferrite of different compositions. Further, it is also aimed at studying the electrical and magnetic properties of the materials so obtained by using various known instrumental techniques.

The investigations have been carried out in the following sequence.

- (i) The synthesis of ultrafine $\text{Mn}_x\text{Zn}_{(1-x)}\text{Fe}_2\text{O}_4$ samples (where $x = 0.40, 0.50, 0.60, 0.625, 0.65, 0.675, 0.70, 0.80$) by using the mechano-chemical and the wet chemical method,
- (ii) The characterization of powder samples by known methods and determination of the physical properties of these samples,

(iii) The evaluation of the magnetic properties such as saturation magnetization, A. C. susceptibility and permeability to understand the performance of these ferrite materials, and,

(iv) The study of the electrical properties such as resistivity, thermoelectric power and dielectric constant of the powder samples.

REFERENCES:

- [1] J. D. Lee, 'Concise Inorganic Chemistry', 4th Ed. ELBS. Pub., (1994).
- [2] F. A. Cotton, G. Wilkinson, C. A. Murillo, M. Bochmann, 'Advanced Inorganic Chemistry', 6th Ed. Wiley Pub., (1999).
- [3] N. N. Greenwood, A. Earnshaw, 'Chemistry of the Elements', 2nd Ed. Butterworth Heinemann Pub., (1998).
- [4] S. Hilpert, BerDeut. Chem. Ges., 42 (1909) 2247.
- [5] H. E. DuBois, Phil. Mag., 29 (1890) 293.
- [6] P. J. Weiss, J. Phys., 6 (4) (1907) 66.
- [7] Y. Kato, T. Takei, J. Institute of Electrical Engineers Japan, 53 (1953) 408.
- [8] H. Forestier, Ann. Chemie Xe series tome, 9 (1928) 353,
- [9] T. F. Barth, E. Z. Posnjak, Krist., 82 (1952) 325.
- [10] E. J. W. Verwey, P. W. Haayman, G.W. Van Costerhout, Phil. Res. Rep., 173 (1950).
- [11] L. Neel, Proc. Phys. Soc. London, A 65 (1952) 869.
- [12] J. H. Van-Vleck, Phys. Rev., 78 (1950) 266.
- [13] P. W. Anderson, Phys. Rev., 79 (1950) 350.
- [14] Y. Yafet, C. Kittle, Phys. Rev., 87 (1952) 290.
- [15] E. W. Gorter, Philips Res. Rept., 9 (1954) 295.
- [16] C. J. Guillaud, Proc. IEEE, 104 B, (1957) 165.
- [17] C. G. Shull, W. A. Strauser, Phys. Rev., 83 (1951) 121.
- [18] J. M. Hastings, L.M. Corliss, Rev. Mod. Phys., 25 (1953) 114.
- [19] J. L. Snoek, Physica, 3 (1936) 33.

- [20] J. L. Snoek, 'New development in Ferro magnetic materials', Elsevier Press, Inc. New York, (1947).
- [21] J. A. Hedvall, *Ber Deut. Chem.*, 45 (1912) 2095.
- [22] G. Tammann, *Z. Anorg. Ollgem. Chem.*, 111 (1921) 78.
- [23] W. Jander, *Z. Anorg. Ollgem. Chem.*, 117 (1927) 1631.
- [24] M. A. Gilleo, S. Geller, *Acta. Crystal.*, 10 (1957) 239.
- [25] C. G. Koop, *Phys. Rev.*, 83 (1951) 121.
- [26] W. H. Bragg, *Nature* 95 a, (1915) 561.
- [27] T. F. Barth, E. Posnjak, *Z. Krist.*, 82 (1952) 325.
- [28] K. Hauffe, K. Pshera, *Z. Anorg. Chem.*, 262 (1950)147.
- [29] C. Wagner, 'Diffusion and High Temperature Oxidation of Metals, Atom Movements', (A.S.M. monograph, Cleveland, 1951) p.153.
- [30] L. C. F. Blackman, *J. Am. Ceram. Soc.*, 42 (1959)143.
- [31] P. Reijnem, *Sci. Ceram.*, 42 (1959) 143.
- [32] G.C. Kucznski, *Proc. I. C. F. Kyoto, Japan, 1970* (University of Tokyo Press, 1971) p.87.
- [33] S. Solyman, *Ceram. Inter.*, 32 (2006) 755–760.
- [34] H. Aiping, H. Huahui, F. Zekun, W. Shilei, *Mater. Chem.Phys.*, 105 (2007) 303–307.
- [35] P. Mathur, A. Thakur, M. Singh, *Phys. Scr.*, 77 (2008) 025701.
- [36] O. Caltun, I. Dumitru, M. Feder, N. Lupu, H. Chiriac, *J. Magn. Mater.*, 320 (2008) 869–873.
- [37] M. Kaiser, *J. Alloys Compounds*, 468 (2009) 15–21.
- [38] K. J. Standley, 'Oxide Magnetic Materials', chap. 2 p.9 Clearndon Press Oxford, (1972).

- [39] B. R. V. Narasimhan, S. Prabhakar, P. Manohar, F. D. Gnanam, Mater. Lett., 52 (2002) 295–300.
- [40] G. Economos, 'Kinetics of High Temperature processes' (ed. W. D. Kingery, M. I. T. Press, Cambridge, 1959) p.243.
- [41] T. N. Brusentsova, V. D. Kuznetsov, J. Magn. Magn. Mater., 311 (2007) 22–25.
- [42] P. Mathur, A. Thakur, M. Singh, J. Magn. Magn. Mater., 320 (2008) 1364–1369.
- [43] L. Ma, L. Chen, S. Chen, Mater. Chem. Phys., 114 (2009) 692–696.
- [44] E. Calderon-Ortiz, O. Perales-Perez, P. Voyles, G. Gutierrez, M.S. Tomar, Microelectronics Journal, 40 (2009) 677–680.
- [45] G. Schikorr, Z. Allg. Chem., 212 (1938) 33.
- [46] M. P. Pileni, J. Phys. Chem., 97 (1993) 6961.
- [47] K. C. Patil, D. Gajapathy, V. R. Pai Vernekar, Mater. Res. Bull., 17 (1989) 29.
- [48] K. C. Patil, D. Gajapathy, Mater. Chem. Phys., 9 (1983) 423.
- [49] S. S. Manoharan, K. C. Patil, 'Advances in Ferrites', (eds. C. M. Srivastava, M. J. Patani, Oxford and IBH Pub. Co. Pvt. Ltd., New Delhi) 1 (1989) 43.
- [50] A. Thakur, M. Singh, J. Magn. Magn. Mater., 320 (2008) 1364-1369.
- [51] K. G. Kanade, D. P. Amalnerkar, H. S. Potdar, B. B. Kale, Mater. Chem. Phys., 117 (2009) 187–191.
- [52] D. C. Bharti, K. Mukherjee, S. B. Majumder, Mater. Chem. Phys., 120 (2010) 509–517.

- [53] A. Angermann, E. Hartmann, J. Topfer, *J. Magn. Magn. Mater.*, 322 (2010) 3455-3459.
- [54] Y. Xuan, Q. Li, G. Yang, *J. Magn. Magn. Mater.*, 312(2007) 464–469.
- [55] L. Nalbandian, A. Delimitis, V. T. Zaspalis, E. A. Deliyanni, D. N. Bakoyannakis, E. N. Peleka, *Micro. Meso. Mater.*, 114 (2008) 465 – 473.
- [56] K. Praveena, K. Sadhana, S. Bharadwaj, S. R. Murthy, *J. Magn. Magn. Mater.*, 321 (2009) 2433–2437.
- [57] A. R. West, ‘Solid State Chemistry and its Applications’, John Wiley and Sons, (2007).
- [58] S. Zahia, M. Hashima, A.R. Daud, *J. Magn. Magn. Mater.*, 308 (2007) 177–182.
- [59] J. Azadmanjiri, *J. Non-Cryst. Solids*, 353 (2007) 4170–4173.
- [60] N. Rezlescu, E. Rezlescu, F. Tudorache, P. D. Popa, *Romanian Rept. Phys.*, 61, 2 (2009) 223–234.
- [61] Y. P. Fu, K.Y. Pan, C.H. Lin, *Mater. Lett.*, 57 (2002) 291–296.
- [62] S. T. Aruna, A. S. Mukasyan, *Curr. Opinion Solid State Mater. Sci.*, 12 (2008) 44–50.
- [63] S. Son, R. Swaminathan, M. E. McHenry, *J. Appl. Phys.*, 93 (10) (2003) 7495.
- [64] M. I. Boulos, *J. High Temp. Chem. Processes*, 1 (1992) 401.
- [65] S. Son, R. Swaminathan, *J. Appl. Phys.*, 91 (10) (2002) 7589.
- [66] S. Gubbala, H. Nathani, K. Koizol, R.D.K. Misra, *Physica B*, 348 (2004) 317.

- [67] P. Poddar, H. Srikanth, S. A. Morrison, E. E. Carpenter, J. Magn. Mater., 288 (2005) 443.
- [68] D. Makovec, A. Kosak, M. Drofenik, Nanotechnology, IOP Publishing, 15 (2004) S160–S166.
- [69] A. Kosak, D. Makovec, M. Drofenik, J. Metastab. Nanocryst. Mater., 23 (2005) 251–254.
- [70] X. M. Liu, S.Y. Fu, J. Magn. Mater., 308 (2007) 61–64.
- [71] Z. G. Zheng, X.C. Zhong, Y.H. Zhang, H.Y. Yu, D.C. Zeng, J. Alloys Compounds, 466 (2008) 377-382.
- [72] J. Wang, F. Ren, R. Yi, A. Yan, G. Qiu, X. Liu, J. Alloys Compounds, 479 (2009) 791–796.
- [73] M. Jalaly, M.H. Enayati, F. Karimzadeh, J. Alloys Compounds, 480 (2009) 737–740.
- [74] M. A. Gabal, Mater. Lett., 64 (2010) 1887–1890.
- [75] G. J. Baldha, R. G. Kulkarni, Solid Stat. Commun., 53 (1985) 11.
- [76] C. Radhakrishnamurthi, J. Goel, Soc. India, 26(9) [1985] 640.
- [77] R. V. Uphadhyay, G. J. Baldha, R. G. Kulkarni, Mater Res. Bull., 21 (1986) 1015.
- [78] C. P. Bean, J. Appl. Phys., 26 (1955) 1381.
- [79] L. G. Van Uitert, Proc. I.R.E., 44 (1956) 1294.
- [80] A. P. Komar, V. V Klivshin, Bull. Acad. Sci. USSR., 18 (1954) 409.
- [81] E. J. Verway, G. Haayman, F. Romeijen, G. Van Oosterhout, Philips Res. Rept., 5 (1950) 173, J. Chem. Phys., 15 (1947) 81.
- [82] A. Mandal, D. Banerjee, R. N. Bhattacharya, A. A. Ghosh, J. Phys Condens. Matter., 8 (1996) 2865-2868.

- [83] V. R. K. Murthy, J. Sobhanadri, Phys. Stat. Sol.(a), 38, (1976) 647.
- [84] K. Kamiyoshi, Sci. Rept. Res. Ins. Tohoku University, A-3 (1951)
716.
- [85] G. Moltgen. Z. Angew, Phys., 4 (1952) 216.
- [86] P. K. Gallagher, E. M. Gyorgy, D. W. Johnson, W. David,
M. Robbins, E. M. Vogel, J. Am. Ceram. Soc., 66 (7) (1983) C 110.
- [87] D. A. Thompson, J. S. Best, IBM J. Res. Dev., 44 (2000) 311.
- [88] H. Inaba, T. Abe, Y. Kitano, J. Shimomura, Solid State Chem., 121
(1996) 117- 128.
- [89] M. Drogenik, A. Znidarsic, I. Zajc, J. Appl. Phys., 82 (1) (1997)
333- 340.
- [90] R. B. Tangsali, S. H. Keluskar, G. K. Naik, J. S. Budkuley, Int. J.
Nanoscience, 3 (4 & 5) (2004) 1-9.

CHAPTER TWO

EXPERIMENTAL METHODS

2.1. INTRODUCTION:

In the present study, mechano-chemical method as well as wet chemical method has been used for the synthesis of the ferrite materials. Identification and structural determination is necessary once the product has been obtained since it gives insight into the nature and the quality of the product obtained. Secondly, one can visualize the applications of such compounds only after assessing the various properties exhibited by the materials. The products obtained from the synthesis have been characterized by using chemical methods as well as instrumental techniques. The magnetic and the electrical properties of the ferrite materials have been investigated by using common instrumental methods [1-4].

A brief account of the principles and the instrumentation of the different analytical tools used in the investigation has been given in this chapter. The Instrumentations used are Ball-Mill Technique, Atomic Absorption Spectroscopy (AAS), Infrared Spectroscopy (IR), X-Ray Diffraction Spectroscopy (XRD), Scanning Electron Microscopy (SEM), Transmission Electron Microscopy (TEM), among others.

2.2. BALL-MILL TECHNIQUE IN MECHANO-CHEMICAL SYNTHESIS:

Oxides of manganese, zinc and iron were taken in calculated quantities and ball-milled to obtain a homogeneous mixture. The ball-mill has an electromagnetic rotor which moves stainless steel balls in the container at high speed resulting in thorough mixing of the oxides taken in the container. High speed rotation of the stainless steel balls also reduces the particle size of the oxide powders.

An indigenous Ball mill Acmas Technocracy (Model Acm-8203) with a speed of 80 rpm was used in which oxides of the manganese; zinc and iron were ball milled for 10 hours, with balls to material ratio of 10 to obtain a powdered mixture.

2.3. INSTRUMENTAL TECHNIQUES USED FOR CHARACTERIZATION:

A few techniques have been used in the present study to characterize the ferrite material. These methods are selectively used for the specific information required to confirm the formation of the desired product.

2.3.1. ATOMIC ABSORPTION SPECTROSCOPY (AAS):

Atomic absorption spectroscopy is a well known method for elemental analysis, since it is the most powerful instrumental technique for

the quantitative determination of metals in trace quantity. The analysis is done by drawing the metal in solution state (ionic) and is independent of the molecular form of the metal in the sample. The method is accurate and can detect the presence of small quantity of a metal, even in presence of other metals and amount detected can be lower than one ppm. It is simple as it does not require a sample preparation. It has become an important technique for quantitative analysis of metal because of its high sensitivity and comparative ease with which the results are obtained [3, 5].

Experimentally, a solution containing metallic species is introduced into a flame which produces vapors of those metals. When a light of the required wavelength is allowed to pass through a flame having atoms of the metal, part of that light will be absorbed and the absorption will be proportional to the density of the atoms in the flame. Thus by using atomic absorption spectroscopy, it is possible to determine the amount of light absorbed. By knowing the value of this absorption, the concentration of the metallic element is known, as the absorption is directly proportional to the density of the atoms in the flame.

The total amount of the light absorbed is given by an equation:

$$\text{At } \nu \text{ (frequency), the total amount of light absorbed} = \frac{\pi e^2}{mc} Nf \quad \text{-----} \quad 2.1.$$

where 'e' is the charge on the electron of mass 'm', 'c' the speed of the light, 'N' the total number of atoms that can absorb at frequency 'ν' in the light path and 'f' the oscillator strength or ability for each atom to absorb

at frequency, ν . As π , e , m and c are constants, the equation (2.1.) can be simplified to the following expression:

$$\text{Total amount of high absorbed} = (\text{constant}) Nf \quad \text{-----} \quad 2.2.$$

From expression (2.2.), it follows that:

- (a) Firstly, there is no term involving the wavelength (or frequency) of absorption other than the indication of the actual absorption wavelength;
- (b) Secondly, there is no term involving the temperature.

From the above, it follows that absorption by atom is independent of the wavelength of absorption and the temperature of the atoms. These two features provide AAS distinct advantage over flame emission spectroscopy.

It should be pointed out, however, that although the temperature does not affect the process of absorption by atoms, it does affect the efficiency with which atoms are produced from a sample and therefore indirectly affects the signal quite significantly. Furthermore, some atoms, particularly those of the alkali metals, easily ionize at high temperatures. Ions do not absorb at atomic absorption wavelengths. Atoms that become ionized are effectively removed from the absorbing population, resulting in a loss of signal, hence efficiency.

AAS was used to determine the amount of Mn, Zn and Fe in the ultrafine mixed metals oxides prepared by two methods in the present study using atomic absorption spectrophotometer GBC Model 932AA.

2.3.2. INFRARED (IR) SPECTROSCOPY:

Infrared Spectroscopy is one of the most powerful analytical techniques which can be used for chemical and structural identification. This technique, combined with intensity measurements, is also useful for quantitative measurements. The important advantage of infrared spectroscopy over the other methods of structural analysis (XRD, ESR, etc) is that it instantaneously provides useful information about the structure of molecule without the use of much difficult evaluation techniques. IR spectroscopy, therefore, has become a versatile tool for both qualitative and quantitative analysis of molecular species [6].

The technique is based upon a simple fact that a chemical substance shows marked selective absorption in the infrared region. After absorption of IR radiations, the molecules (bonds) of chemical compounds vibrate with different modes of vibration giving rise to close-packed absorption bands called as IR absorption spectrum which may extend over a wide wavelength range. Various bands will occur in IR spectrum which will correspond to the characteristic functional groups and bonds present in the chemical substance. Band intensities in IR spectrum may be expressed either as transmittance (T) or absorbance (A).

IR spectroscopy can be applied at all levels of expertise from simple matching of spectra on one hand, to the theoretical calculations at the other. The instruments are simple, relatively inexpensive and easy to operate.

IR includes a broad region from red end of visible spectrum (12500cm^{-1}) to the microwave (10 cm^{-1}) in the electromagnetic spectrum and based upon application and instrumentation involved it is conveniently divided into Near-IR (12500 to 4000 cm^{-1}), Mid-IR (4000 to 200 cm^{-1}) and Far-IR (200 to 10cm^{-1}). The most fundamental region of interest for the analytical purpose is from 4000 cm^{-1} to 400 cm^{-1} as it provides the information about the different vibrations of molecules, and therefore about the structure of molecules [7].

When IR radiation is passed through a sample, certain frequencies are absorbed by the molecule of the sample and so it gives rise to vibrational changes in the molecule. For such vibrational changes to occur there must be a mode of interaction between the incident radiation and the vibrational energy levels. This mode of interaction is an oscillating electric dipole induced by the vibration, which interacts with the oscillating electric field of the electromagnetic radiation. IR absorption occurs for each vibrational degree of freedom of the molecule provided that a change in the dipole moment of the molecule takes place during the vibration. In many of the normal modes of vibration of a molecule the main participants in the vibrations will be the two atoms held together by a chemical bond. These vibrations have frequencies which depend primarily on the masses of the two vibrating atoms and the force constant of the bond between them. Also, these frequencies are slightly affected by other atoms attached to the two atoms concerned. These vibrational modes are characteristic of the groups in the molecule and are useful in the identification of a

compound. For a large molecule with many vibrational degrees of freedom there may be many IR bands observed. Since each molecule has individual sets of energy levels, the absorption spectrum is characteristic of the fundamental groups that are in the molecule

For example, A carbon-carbon triple bond ($\text{-C} \equiv \text{C-}$) absorbs in the region $2250\text{-}2100\text{ cm}^{-1}$, where as a carbon double bond ($\text{-C} = \text{C-}$) is weaker and absorbs at lower frequency, $1670\text{-}1620\text{ cm}^{-1}$.

The hydrogen-oxygen bond of O-H group gives a characteristic absorption band in the infrared region. The frequencies of peak maxima depend on O-H bond strength. This provides information like, the location of O-H group, whether it belongs to water molecule and whether hydrogen bonding is present or not. Peaks associated with vibrational modes of covalently bonded groups such as oxyanions usually occur at high frequency. At lower frequency in the far region, lattice vibrations give rise to absorption peaks. At temperatures above absolute zero, all the atoms in molecules are in continuous vibration with respect to each other. Each atom has three degrees of freedom, corresponding to motions along any of the three Cartesian coordinate axes (x, y and z). A polyatomic molecule of 'n' atoms has $3n$ total degrees of freedom. However, 3 degrees of freedom are required to describe the translation that is the motion of the entire molecule through space. In addition, 3 degrees of freedom correspond to rotation of the entire molecule, therefore the remaining $(3n - 6)$ degrees of freedom are true, fundamental vibrations for the nonlinear molecules.

Linear molecules possess $(3n - 5)$ fundamental vibrational modes because only two degrees of freedom are sufficient to describe the rotation. Among the $(3n - 6)$ or $(3n - 5)$ fundamental vibrations or normal modes of vibrations, those that produce a net change in the dipole moment may result in an IR activity and those that give polarizability changes may give rise to Raman activity. Therefore, some vibrations can be both IR and Raman-active.

The total numbers of observed absorption bands are different from the total number of fundamental vibrations. It is less because some modes are not IR active and a single frequency can cause more than one mode of motion to occur. Conversely, additional bands are generated by the appearance of overtones (integral multiples of the fundamental absorption frequencies), combinations of fundamental frequencies, differences of fundamental frequencies, coupling interactions of two fundamental absorption frequencies, and coupling interactions between fundamental vibrations and overtones or combination bands (Fermi resonance). The intensities of overtone, combination, and difference bands are less than those of the fundamental bands. The combination and blending of all the factors thus create a unique IR spectrum for each compound. The major types of molecular vibrations are stretching and bending, the absorption involves discrete, quantized energy levels. However, the individual vibrational motion is usually accompanied by other rotational motions. These combinations lead to the absorption bands, not the discrete lines, commonly observed in the mid IR region.

The transmittance spectra provide better contrast between intensities of strong and weak bands because transmittance ranges from zero to hundred percent, whereas absorbance ranges from infinity to zero.

A typical IR spectrophotometer consists of components like radiation source, optical path, monochromator, radiation detector and the sample holder.

Fourier Transform Infrared spectrophotometer (FTIR) is superior to the IR spectrophotometer. The FTIR instrument is based upon Michelson interferometer. The absorbing material is placed in one of the beams and the resulting interferogram carries the spectrum characteristics of the sample in the beam. The information from the interferogram is converted into infrared spectrum through computer processing. It is easier to study small samples with weak absorption, which is an added advantage in FTIR.

IR spectra of Mn-Zn ferrite samples obtained by both the methods of preparation, were recorded in the range $4000-400\text{ cm}^{-1}$ by using FTIR Shimadzu Model IR prestige 21 series spectrophotometer.

2.3.3. SIMULTANEOUS THERMAL ANALYSER (TGA-DTA):

When a substance is heated, it undergoes certain physical and/or chemical change. This change is characteristic of the given sample. By

knowing the temperature at which such reaction occurs, the heat involved in the reaction and the loss in weight, if any, during the change, it is possible to characterize the given material.

Over the last few decades, the methods in thermal analysis have been widely used in characterization of materials as one of the most important analytical techniques. The thermal analysis is a group of technique in which physical and/or chemical changes occurring in a substance is measured as a function of temperature (heating or cooling). The different techniques commonly used include Thermogravimetry (TGA), Derivative Thermo Gravimetry (DTG), Differential Thermal Analysis (DTA), Differential Scanning Calorimetry (DSC), Thermometric Titrimetry, Dynamic Reflectance Spectroscopy (DRS), Evolved Gas Analysis (EGA), Thermo Mechanical analysis (TMA) etc. In many cases the use of a single thermal analysis technique may not provide complete information, hence the use of additional thermal technique independent or simultaneous, becomes necessary.

In the present study, simultaneous TGA and DTA is used as an analytical tool for the study of the precursor. TGA is a technique in which the weight of a substance, during heating or cooling at a controlled rate, is recorded as a function of time or temperature. In this technique, the sample is heated in an environment of which temperature is changing in a predetermined manner at a linear rate. A sensitive thermobalance records the weight during the linear increase or decrease of temperature. Results

from the programmed operation of the thermobalance are represented by a graph of weight change versus temperature. This graph is referred to as the thermogram or TG curve. From the TG curve one can draw useful information regarding the thermal stability, weight loss, composition and decomposition reaction at temperature indicated therein. This tool can also be used to confirm the composition assigned to a compound.

Differential thermal analysis (DTA) often used along with TGA, is considered to be an adjunct to TGA. Together they constitute the method that yields a data of fundamental nature. The DTA technique is simple as it records the difference in temperature between the sample and the reference material against time or temperature, as the two substances are subjected to an identical temperature regime, in an environment, while heating or cooling at a controlled rate. Thus differential temperature detector records a differential thermogram, which consists of difference in temperature of the sample and the reference (differential temperature ΔT), plotted as a function of time or reference temperature or furnace temperature. The origin of difference in temperature (ΔT) in the sample lies in the energy difference between reactant and product or between two phases of a substance, which is manifested as enthalpic changes- either endothermic or exothermic. DTA allows detection of each and every physical or chemical change whether or not accompanied by a change in weight [2-4].

TGA-DTA analysis of a few representative samples of precursors, obtained by both the methods of preparation, was carried out to ascertain

the decomposition temperature on TGA-DTA instrument Model Netzsch DSC-TG STA 409PC.

2.3.4. X-RAY DIFFRACTION SPECTROSCOPY (XRD):

A crystal lattice is considered to be made up of regular layers or planes of atoms equal distance apart. Since the wavelength of X-rays is comparable to the interatomic distances of 10^{-8} cm, Laue (1912) suggested that crystal can act as grating to X-rays. Thus when a beam of X-rays is allowed to fall on a crystal, a large number of images of different intensities is formed. If the diffracted waves are in the same phase, they reinforce each other and a series of bright spots is produced on a photographic plate placed in their path. On the other hand, if the diffracted waves are out of phase, dark spots are caused on the photographic plate. From the overall diffraction patterns produced by a crystal, we can arrive at the detailed information regarding the position of particles in the crystal [8].

X-ray powder diffraction (XRD), is an instrumental technique that is used to identify materials. XRD provides the researcher with a fast and reliable tool for routine material identification. XRD in particular can be used for identifying fine-grained minerals and mixtures or intergrowths of minerals that may not lend themselves to analysis by other techniques. Crystal structure cannot be visualized by visible light of wavelength approximately 5000\AA as arrangement of atoms or placement of atoms in

the material is too close for resolution. The interatomic spacing in crystal is of the order of 10^{-8} cm. Therefore, a wave with wavelength of similar order will give rise to diffraction phenomena. Diffraction provides information about arrangement of atoms in the crystals [9].

For crystal diffraction, X-rays are more suitable as the energy of X-ray quanta is

$$E = hc/\lambda \quad \text{-----} \quad 2.3.$$

where λ is of order 10^{-8} cm.

When X-ray radiation passes through matter, the radiation interacts with the electrons in the atoms, resulting in scattering of the radiation. If the atoms are organized in planes (i.e. the matter is crystalline) and the distances between the atoms are of the same magnitude as the wavelength of the X-rays, constructive and destructive interferences occur. These diffracted X-rays are emitted at characteristic angles based on the spacings between the atoms organized in crystal planes. Each atom can belong to many sets of crystal planes. Each set of planes has a specific interplanar distance and will give rise to a characteristic angle of diffracted X-rays. In 1913, W. L. Bragg and W. H. Bragg worked out a mathematical relation to determine interatomic distances from X-ray diffraction patterns. This relation is called the Bragg equation. They showed that: (1) The X-ray diffracted from atoms in crystal planes obey the laws of reflection. (2) The two rays reflected by successive planes will be in phase if the extra distance travelled by the second ray is an integral number of wavelengths.

If the illuminating wavelength is known and the angle can be measured then the interplanar distance can be calculated.

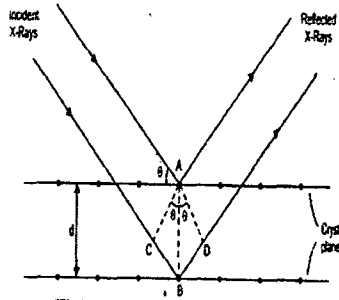


Fig.2.1. Reflection of X-rays from two different crystal planes.

From the Bragg equation, a set of d-spaces obtained from a single compound will represent the set of planes that can be passed through the atoms and can be used for comparison with sets of d-spaces obtained from standard compounds. Diffraction of monochromatic X-rays by crystal takes place according to Bragg's law

$$n\lambda = 2d\sin\theta \quad \text{-----} \quad 2.4.$$

λ = wavelength of X-rays, n = order of diffraction, d = interplanar separations, θ = Bragg angle.

This condition helps in finding the size, shape and orientation of crystallite unit cell. From Bragg's law, it is seen that intensities are stronger only at certain values of θ for specific λ and d . This intensity depends on the atomic scattering factor of each atom and position of each atom in the unit cell. The most widespread use of X-ray powder diffraction is for the identification of crystalline compounds by their diffraction pattern. One can also determine crystallite size from analysis of peak broadening.

The primary components of a powder diffractometer are the sources of X-ray, usually called X-ray tube, the sample chamber, a goniometer- for measuring angles, and a X-ray detector for measuring the intensity of diffracted X-ray beam. Apart from these there are several slits to reduce the divergence of the incident and diffracted beam and monochromator are also used.

X-ray powder diffraction pattern of Mn Zn ferrite samples obtained by both the methods of preparation, was recorded on a Rigaku, X-ray advance Power diffractometer using Cu K α radiation ($\lambda = 1.54183 \text{ \AA}$).

The step size employed was 0.02° , in the range of 20° – 80° .

2.3.4.1. LINE BROADENING ANALYSIS FOR CRYSTALLITE DIMENSION:

As the particle size decreases the peaks get broadened due to incomplete destructive interference. The broadening caused by fine crystallites relates to the size of the grains by Scherer formula [8].

$$T = 0.9 \lambda / D_p \cos \theta \quad \text{-----} \quad 2.5.$$

where 'T' = crystallite size, ' λ ' = wavelength, ' D_p ' = FWHM (full width half measure), ' θ ' = Bragg angle

The X-Ray data was used to calculate XRD density of the solid samples by method reported elsewhere (3.5.10) The XRD density values and the experimentally determined mass density values were subsequently

employed to calculate the porosity of the ferrite samples as described in Chapter Three.

2.3.5. SCANNING ELECTRON MICROSCOPY (SEM):

Scanning Electron Microscopy (SEM) technique is a widely used form of electron microscopy in the field of materials science. SEM is an instrument, which is used to observe the morphology of a sample at higher magnification, higher resolution and depth of focus compared to an optical microscope. In SEM an accelerated beam of mono-energetic electrons is focused on to the surface of the sample and a small area is scanned by it. Several signals are generated and appropriate ones are collected depending on the mode of its operation. The signal is amplified and made to form a synchronous image on the cathode ray tube, the contrast resulting from the morphological changes and the variation of atomic number over the area probed [10-12].

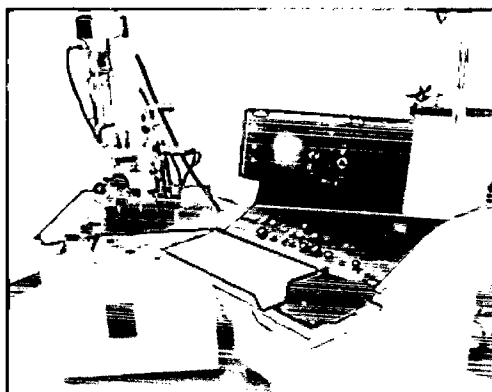


Fig.2.2.(a). Scanning Electron Microscope JEOL Model 840(SEM).

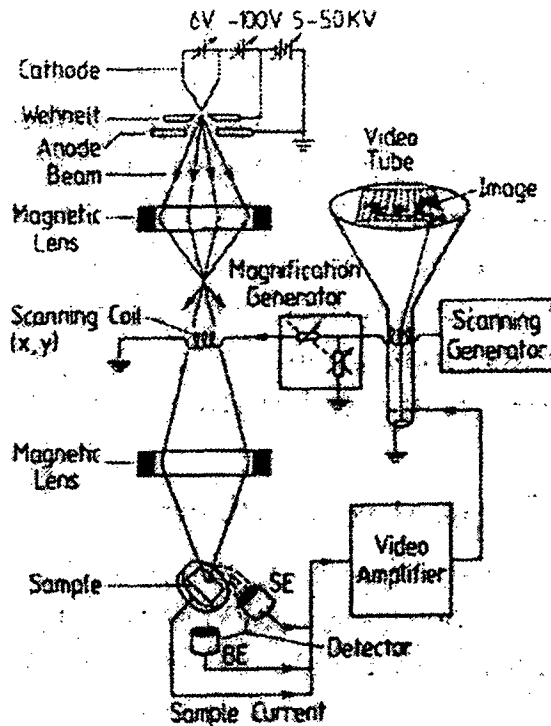


Fig.2.2.(b). Line diagram of typical Scanning Electron Microscope.

A camera is used to photograph the image which may be digitized and processed on a computer. The characteristic X-rays emitted may be analyzed for their energy and intensity energy absorption X-rays (EAX), the energy being the signature of the element emitting them and the intensity as to how much of it is present.

A well-focused mono-energetic ($\sim 25\text{KeV}$) beam is incident on a solid surface giving various signals such as scattering electrons, secondary electrons, Auger electrons and X-rays. Therefore the SEM renders imaging with radiations, which can be focused by lenses, and in addition, it can give many different views of the same specimen. Back-scattered electrons and secondary electrons are particularly pertinent for SEM applications, their intensity being dependent on the atomic number of the host atoms.

Each may be collected, amplified and utilized to control the brightness of the spot on a cathode ray tube (CRT). To obtain signals from an area, the electron beam is scanned over the specimen surface by two pairs of electro-magnetic deflection coils and so is the CRT beam in synchronization with this. The signals are transferred from point to point and the signal map of the scanned area is displayed on a long persistent phosphor CRT screen.

Changes in brightness represent changes of a particular property within the scanned area of the specimen. Some of these signals carry information about the sample which provides clues to its compositions. The performance of the SEM depends on a number of related factors; perhaps the most important is the output of the electron source.

SEM micrographs were obtained for a few samples to evaluate change in morphology of the samples after sintering them at various temperatures as well as for determining the particle size of ferrite samples prepared in the present study using Scanning Electron Microscope Model JEOL 5800LV.

2.3.6. ENERGY DISPERSIVE X-RAY ANALYSIS (EDS):

Scanning electron microscope (SEM) uses a focused beam of high-energy electrons to generate a variety of signals at the surface of solid substances. The signals that derive from electron sample interaction reveal

information about the sample including external morphology (texture), chemical composition, EDS identifies the elemental composition of materials imaged in a SEM for all elements with an atomic number greater than boron. Most elements are detected at concentrations on the order of 0.1%. crystalline structure and orientation of materials. Thus, it provides elemental analysis data of the sample.

The fundamental principle of Scanning Electron Microscopy (SEM) is that the accelerated electrons in an SEM carry significant amounts of kinetic energy, and this energy is dissipated as a variety of signals produced by electron sample interaction, when the incident electrons are decelerated in the solid sample. These signals include secondary electrons (that produce SEM images), backscattered electrons, diffracted backscattered electrons (that are used to determine crystal structures and orientations of materials), photons (characteristic X-rays that are used for elemental analysis and continuum X-rays), visible light (cathode-luminescence), and heat. Secondary electrons and backscattered electrons are commonly used for imaging samples: of these, the secondary electrons are most valuable for showing morphology and topography on samples and the backscattered electrons are most valuable for illustrating contrasts in composition in multiphase samples (i.e. for rapid phase discrimination).

Two of the most commonly used signals for investigating the composition of samples are X-rays and backscattered electrons. X-ray

signals are commonly used to provide elemental analysis by the attachment of an Energy Dispersive Spectrometer to the SEM system. X-ray emission results from inelastic scattering between the beam of incident electrons and the electrons in discrete orbitals (shells) of the atoms in the sample. As the excited electrons return to lower energy states, they yield X-rays that are of a fixed wavelength (that is related to the difference in energy levels of electrons in different shells for a given element). Thus, characteristic X-rays are produced for each element in a sample that is excited by the electron beam. As the electron beam of the SEM is scanned across the sample surface, it generates X-ray fluorescence from the atoms in its path. The energy of each X-ray photon is characteristic of the element, which produces it. The EDS microanalysis system collects the X-rays, and analyses, sorts and plots them by their energy. Thereby, it automatically identifies and labels the elements responsible for the peaks in this energy distribution.

The EDS data obtained is compared with either known or computer-generated standards to produce a full quantitative analysis showing the sample composition. The data output is either this element analysis, the original spectrum showing the number of X-rays collected at each energy, or maps of distributions of elements over areas of interest. SEM analysis is considered to be non-destructive; that is, X-rays generated by electron interactions do not lead to volume loss of the sample, so it is possible to analyze the same materials repeatedly.

EDS spectra giving percentage compositions of Mn, Zn, Fe and O are obtained and reported for the few samples using Scanning Electron Microscope JEOL Model 840 (SEM).

2.3.7. TRANSMISSION ELECTRON MICROSCOPY (TEM):

The Transmission Electron Microscope (TEM) has been used in all areas of biological and biomedical investigations because of its ability to view the finest cell structures. It is also used as a diagnostic tool in hospital pathology labs. The transmission electron microscope uses a high energy electron beam. For a crystallographer or a metallurgist or a semiconductor research scientist, current high voltage/high resolution TEMs, utilizing 200 keV to 1 MeV, have permitted the routine imaging of atoms, allowing materials researchers to monitor and design materials with custom-tailored properties. With the addition of energy dispersive X-ray analysis (EDAX) or energy loss spectrometry (EELS), the TEM can also be used as an elemental analysis tool, capable of identifying the elements in areas less than 0.5 μ m in diameter. Transmitted through a very thin sample to image and analyze the microstructure of materials with atomic scale resolution. The electrons are focused with electromagnetic lenses and the image is observed on a fluorescent screen, or recorded on film or digital camera. The electrons are accelerated at several hundred kV, giving wavelengths much smaller than that of light (with 200kV, the electrons have a wavelength of 0.025 \AA).

However, the resolution of the optical microscope is limited by the wavelength of light, while that of the electron microscope is limited by aberrations inherent in electromagnetic lenses, to about 1-2 Å. Because even for very thin samples one is looking through many atoms, one does not usually see individual atoms. Rather, the high resolution imaging mode of the microscope images the crystal lattice of a material as an interference pattern between the transmitted and diffracted beams. This allows one to observe planar and line defects, grain boundaries, interfaces, etc. with atomic scale resolution. The brightfield/darkfield imaging modes of the microscope, which operate at intermediate magnification, combined with electron diffraction, are also invaluable in giving information about the morphology, crystal phases, and defects in a material. Finally, the microscope is equipped with a special imaging lens allowing for the observation of micromagnetic domain structures in a field-free environment [12].

With its multifaceted capabilities such as nano-beam diffraction and composition analysis, and imaging abilities at angstrom level, TEM has emerged as an instrument for complete characterization of microstructure of the materials. The TEMs are available in several forms, which are referred to by different acronyms such as HRTEM (High resolution TEM), STEM (Scanning TEM) and AEM (Analytical TEM).

TEMs basically comprise of an electron gun, a vacuum system, electromagnetic lenses, a high voltage generator, recording devices and the

associated electronics. TEM also needs a source of electrons to illuminate the specimen. In order to get the best images, the best diffraction effects and the appropriately optimum suitable chemical analysis capabilities, the best available electron source needs to be used. The resolution of the modern TEM is under 0.2 nm (point to point) even with a fair amount of specimen tilt. These microscopes are therefore capable of satisfactorily resolving the structure of different phases in most metals and alloys.

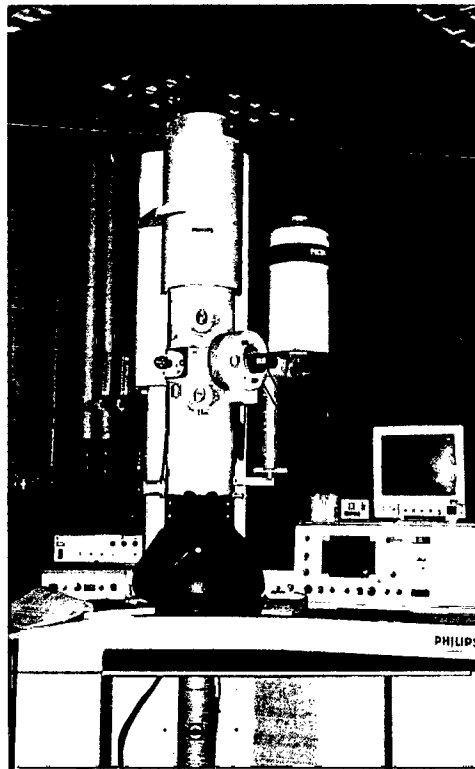


Fig.2.3(a). Transmission Electron Microscope- Philips model CM200.

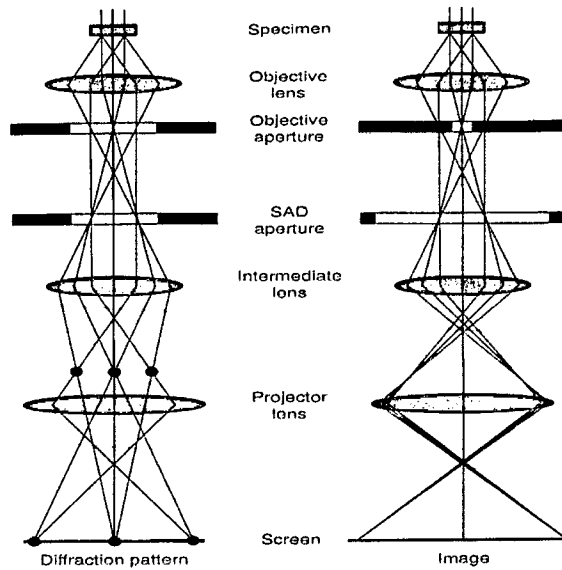


Fig.2.3(b). Sketch of radiation path in TEM.

A modern day TEM has about five to six image forming lenses. The final image is projected on the screen. The diffraction pattern is formed on the back focal plane of the objective lens and the first image is formed on the back plane of the objective lens. If the image forming lenses following the objective lens are excited in such a way that these see the back focal plane of the objective lens as the object then what one sees on the screen is the diffraction pattern. However, if the lenses are excited in such a way that these see the back image plane of the objective lens as an object then what we see on the screen is the image of sample. Therefore, in a modern TEM it is possible to switch from diffraction to imaging and vice-versa by changing the excitation of the lenses following the objective lens. TEM can be used to image the specimen by focusing the final image in the plane of the fluorescent screen or it can be used to image the diffraction pattern from the sample.

Electron diffraction can be explained on the basis of concepts of Reciprocal lattice and Ewald sphere. When combined with the reciprocal lattice concept, the Ewald sphere construction provides a very simple way of visualizing electron diffraction. Since the reciprocal of electron wavelength is much larger than the interplanar spacings in the reciprocal space, many reciprocal lattice points are simultaneously intersected by the Ewald sphere giving rise to many diffracted rays, even from a single crystal, in case of electron diffraction. The diffraction patterns can be of various types i.e. Selected Area Electron Diffraction (SAED), Convergent Beam Electron Diffraction (CBED), Reflective High-Energy Electron Diffraction (RHEED) and Low Energy Electron Diffraction (LEED). Diffraction patterns form the basis of all image formation in the TEM.

TEM micrographs were obtained for a few samples to evaluate the particle size of ultrafine ferrite samples prepared in the present study using Transmission Electron Microscope of Philips Model CM200.

2.4. MAGNETIC AND ELECTRICAL PROPERTIES:

Mn-Zn ferrites exhibit magnetic and electrical behaviour. These compounds are of technological importance because of these properties. Many techniques are available to study the magnetic properties such as saturation magnetization, permeability, susceptibility etc. as also electrical properties such as resistivity, thermo-electric power and dielectric

behaviour. A brief description of the instrumental techniques employed in the study of these properties is given below.

2.4.1. MAGNETIC PROPERTIES:

Magnetization is one of the fundamental properties of ferrites. The magnetization is the magnetic moment per unit volume of material which is induced in it when it is placed in external magnetic field. The saturation magnetization, coercivity and remanance are studied with the help of hysteresis. In ferrites, there exist the domains, which possess the magnetic moments or spins of atoms in parallel with each other. This ordering is due to the presence of internal molecular field which is found to be, maximum at 0K. Therefore, the magnetization is found to be maximum at absolute zero. An increase in the temperature of ferromagnetic substances is found to oppose this alignment because with the increase in temperature, magnetization is found to decrease.

The critical temperature at which the ferromagnet behaves as paramagnet is called the Curie temperature. It is an important intrinsic property of the ferrites. A. C. susceptibility helps in determining the existence of multidomain (MD), single domain (SD) and super paramagnetic (SP) particles in the material. From the susceptibility curves, the Curie temperature and domain structure can be studied. The origin of magnetic permeability in ferrites has been a subject of research for the last

several years. Basically two processes are responsible for permeability viz.

(i) rotations of domains and (ii) domain wall displacement.

It is generally assumed that the initial permeability is caused by the reversible displacement of the domain walls, the contribution of rotation of spin inside each domain being negligibly small on account of relatively high crystal anisotropy.

2.4.1.1 SATURATION MAGNETIZATION:

The saturation magnetization measurements of all the samples were carried out at room temperature using Pulse Field Magnetic Hysteresis Loop Tracer, supplied by Magneta India Model PFMHT-1.

In this instrument a high magnetic field is generated in a solenoid by passing a pulse current of Sinusoidal shape. A sample is placed in the pickup coil which, in turn, is kept in solenoid to detect field and magnetization signal. The signals produced are then processed by an electronic system. These transitory signals are digitized by a micro-controller and then sent to a computer for plotting a hysteresis loop observed on the monitor with calculated values of hysteresis parameters. These can be printed or stored as files. The system is useful for samples in powder or pellet form [13].

The system consists of pulsed power supply with input of 230 volts AC, generating magnetic field of 5,000 Oersteds. The output gives a pulse current in Sinusoidal Wave form in 20 ms period. Solenoid and pick-up coil assembly detect the field and magnetization signal. Signal processor is used to process signals produced in the pickup coil by integrating, amplifying and phase correcting circuits to produce signals representing magnetization of the sample and the applied magnetic field. The data acquisition system (DAQ) consists of a micro-controller with a fast digitizing and high resolution circuit. The digitized data is sent to the PC through a RS-232 port. The special software is designed to plot the hysteresis loop and display the hysteresis parameters.

2.4.1.2. A. C. SUSCEPTIBILITY:

The Curie temperature of all the Mn-Zn ferrite samples was determined. These samples were subsequently sintered at different predetermined higher temperatures and experiment was repeated for each of these temperatures. The measurements were done by using Dual Channel Data Acquisition System supplied by the Magneta India Model pfm-2.

This system consists of a power supply to run the furnace. It is a regulated digital power supply whose voltage and current are varied automatically by the PID temperature controller output which can be programmed for a set temperature and predetermined heating rate. The

instrument also has Helmholtz coil, two pick-up coils, furnace, sample holder, temperature measuring device, control unit, data acquisition system, and a PC with related software in the instrument to execute the run cycle. The information from two channels (X-T) is automatically acquired at periodic intervals and the data is sent to the PC through a RS – 232 link and thus magnetization (M_s) versus temperature (T) graph can be obtained [14].

2.4.1.3. MAGNETIC PERMEABILITY:

Magnetic permeability measurements were carried out on the torroids which had a winding of 100 turns of super enameled doubly insulated copper wire of 33 gauge. For this purpose, each powdered sample synthesized by mechano-chemical method was pressed into torroids with inner and outer diameter of 1 cm and 2 cm respectively with a thickness ranging between 3mm – 4 mm. The torroids were sintered at 1000 °C / 1100 °C / 1200 °C /1300 °C in nitrogen atmosphere for 4 hours with a heating and cooling rate of 5°C min⁻¹. The initial permeability and loss factor as a function of frequency and temperature were measured by recording the inductance values and dissipation factor starting from room temperature to 500°C and with frequency variation from 20 Hz to 1 MHz using LCRQ meter of Wayne Kerr Model 6400.

The LCRQ meter is a micro processor based instrument with a suitable software designed to plot the graph of various functions under

study for a given frequencies and temperatures. It is connected to a furnace, which can measure the different functions at various frequencies for a temperature upto 500⁰C. It can measure major functions [15], such as Impedance Z, Capacitance C, Inductance L, AC Resistance R, Susceptance B, Admittance Y, and minor functions such as Phase Angle A, Dissipation Factor D, Quality Factor Q, Conductance G, Reactance X. Any two functions, one major and one minor, (C, D, L, Q, R, G, B, and X) in combination- both as series or both as parallel- can be measured at a given time for various frequencies from 20 Hz to 10 MHz. at room temperature and for various frequencies at varied temperatures, upto 500⁰C.

2.4.2. ELECTRICAL PROPERTIES:

Ferrites are semiconductors in nature with resistivity ranging from 10⁻³ to 10¹¹ ohm cm. at room temperature. The resistivity depends on the preparative conditions, especially the temperature at which a desired ferrite is obtained, the atmosphere in which it is prepared and the presence of impurity. The conduction mechanism in ferrites has been attributed to exchange of electrons between Fe²⁺ and Me³⁺ ions. The presence of Fe²⁺ results in n-type behavior and of Me³⁺ in p-type behavior. The conductivity arises due to the mobility of the extra electron (from Fe²⁺) or the positive hole (Me³⁺) through the crystal lattice. The conductivity also depends on (a) the porosity, (b) the grain size, and (c) the chemical inhomogeneity caused during the preparation.

Thermo electric power measurement also helps in understanding the mechanism of transport of charges in the ferrite and to determine whether it shows n-type or p-type semiconductor behaviour.

Ferrites have high dielectric constants at low frequencies which decrease to low values at high frequencies. They are sensitive and depend on the method of preparation, sintering temperature as well as sintering atmosphere.

2.4.2.1. RESISTIVITY:

The resistivity of all the Mn-Zn ferrite samples was determined. These samples were subsequently sintered at different predetermined higher temperatures and experiment was repeated for each of these temperatures. Two probe method was used to measure the resistivity using this instrument supplied by Pushpa Scientific Hyderabad.

The instrument consists of a muffle type furnace, which can give temperature upto 800⁰C. It has a stable D. C. source of 10 volts (D. C. voltmeter 0 to 10 volts range), a D. C. microammeter (0 to 500 μ A ranges) and ionic conductivity cell with two brass electrodes. In a typical experiment, the Mn-Zn ferrite powder sample was pressed under 75 KN pressure applied for about 5 minutes to make pellets of 1.0 cm diameter and 2-3 mm thickness. The pellet was silver pasted on either side for establishing good ohmic contacts with the electrodes. It was then placed

between the two brass electrodes of the conductivity cell. At constant voltage, the current at various temperatures was recorded while cooling from 500⁰C to room temperature. The experiment was repeated for other samples [16].

2.4.2.2. THERMO ELECTRIC POWER (TEP):

The thermo electric power of the Mn-Zn ferrite samples was measured by using differential method. The thermo emf measurements of these samples were carried out from room temperature to 500⁰C by maintaining a temperature difference between the two ends, hot and cold junctions of electrodes, by 10⁰C.

The instrument supplied by Pushpa Scientific Hyderabad, consists of muffle type furnace, which can give temperature upto 800⁰C. D. C. Voltmeter, (0 to 500 mV range) and a TEP cell with two brass electrodes. Each electrode is connected to a temperature controller and a terminal of D.C. voltmeter. The upper electrode acts as a hot junction while lower electrode acts as a cold junction. A difference of 10⁰C is maintained between the two junctions [16].

The Mn-Zn ferrite powder sample was pressed to make pellet of the size as mentioned in the preceding section. The pellet was silver pasted on either side for establishing good ohmic contacts with the electrodes and placed between the two brass electrodes of the TEP cell. The pellet was

heated from room temperature to 500°C and simultaneously voltage at different temperatures was recorded. The experiment was repeated for other samples.

2.4.2.3. DIELECTRIC CONSTANT:

With rapid developments in solid-state electronics, the study of the A. C. electrical properties of ferrites has acquired great importance. Ferrites show high dielectric constant and also dispersion of dielectric constant in the frequency range from 20Hz to 1GHz. When a dielectric material is subjected to an alternating electric field, the positive and negative charges within the material get displaced with respect to one another and the system acquires an electric dipole moment. The dipole moment per unit volume is called polarization. The dielectric property of ferrites depends on the method of preparation, sintering temperature, chemical composition and grain size. LCRQ meter of Wayne Kerr model 6400 was used to measure the dielectric properties of ferrite in the pellet form. The capacitance and dissipation factor at various frequencies as well as variation of capacitance and dissipation factor with frequencies and at different temperature was also measured [15].

The LCRQ meter is a micro processor based instrument with a suitable software designed to plot the graph of various functions under study for a given frequencies and temperatures. It is connected to a furnace, which can measure the different functions at various frequencies

for a temperature upto 550⁰C. It can measure major functions such as Impedance Z, Capacitance C, Inductance L, AC Resistance R, Susceptance B, Admittance Y, and minor functions such as Phase Angle A, Dissipation Factor D, Quality Factor Q, Conductance G, and Reactance X. Any two functions, one major and one minor, (C, D, L, Q, R, G, B, and X) in combination- both as series or both as parallel- can be measured at a given time for various frequencies from 20 Hz to 10 MHz. at room temperature and for various frequencies at varied temperatures, upto 550⁰C.

REFERENCES:

- [1] J. W. Robinson, E. M. S. Frame, G. M. Frame II, 'Undergraduate Instrumental Analysis', 6th Ed. Marcel Dekker Publication, New York, (2005).
- [2] H. H. Willard, L. L. Merritt, J. A. Dean, F. A. Settle, 'Instrumental Methods of Analysis', 7th Ed. Wadsworth Pub. Co., California, (1988).
- [3] D. A. Skoog, F J. Holler, S. R. Crouch, 'Principles of Instrumental Analysis' 6th Ed. Thomson Brooks/Cole Pub., (2007).
- [4] G. R. Chatwal, S. K. Anand, 'Instrumental Methods of Analysis', 5th Ed. Himalaya Pub., (2005).
- [5] G. H. Jefferey, J. Bassett, J. Mendhum, R. C .Denney, 'Vogel's Text Book of Chemical Analysis', 5th Ed. (1989).
- [6] K. Nakamoto, 'Infrared and Raman Spectra of Inorganic and Coordination Compounds', 6th Ed. John Wiley and Sons Inc., Publication, (2009).
- [7] R. C. Denney, 'A Dictionary of Spectroscopy', 2nd Ed. Macmillan London, (1982) p 89.
- [8] B. D. Cullity, 'Elements of X-ray Diffraction', 2nd Ed. Addison Wesley, (1978).
- [9] M. M. Woolfson, 'An introduction to X-ray crystallography', 2nd Ed. Cambridge University Press, (2003).
- [10] L. Reimer, 'Scanning Electron Microscopy: Physics of image formation and Microanalysis', Springer Publication, (1998).
- [11] J. Goldstein, 'Scanning Electron Microscopy and X-ray Microanalysis', Kluwer Academic Plenum Publishers, (2003).

- [12] R. F. Egerton, 'Physical Principles of Electron Microscopy: an introduction to TEM, SEM, and AEM.', Springer Publication, (2005).
- [13] S. D. Likhite, C. Radhakrishnamurthy, P. W. Sahastrabudhe, Rev. Sci. Instr., 25 (1965) 302.
- [14] S. D. Likhite, C. Radhakrishnamurthy, Curr. Sci., 35 (1966) 534.
- [15] LCR meter Manual Product specification Issue B, Wayne Kerr Electronics, (2008).
- [16] Resistivity Measurement (two probe method) Product manual, Pushpa Scientific, Hyderabad, (2008).

CHAPTER THREE

SYNTHESIS, CHARACTERIZATION AND PHYSICAL PROPERTIES OF Mn-Zn FERRITES

3.1. INTRODUCTION:

Ferrites in general and Mn-Zn ferrites in particular are technologically important compounds. Performance of these materials depends on many factors. Important among them is the method of preparation. In the present study, a new method of synthesis is tried, details of which are given below. For comparison, synthesis is also carried out by a wet chemical method.

$Mn_{(x)}Zn_{(1-x)}Fe_2O_4$ mixed metal ferrites have been prepared by a novel mechano-chemical method and a wet chemical method. The final ferrite product has been characterized by known analytical and instrumental methods and the physical properties of these samples have been studied.

3.2. SYNTHESIS OF $Mn_{(x)}Zn_{(1-x)}Fe_2O_4$ MIXED METAL FERRITE:

A modified ceramic procedure coupled with a chemical method has been used for the first time to obtain ferrite material. This Mechano-Chemical method makes use of ball-mill for mixing of oxides and treating with acetate ligand for obtaining initial compound, before decomposition.

In wet chemical method, a precursor is first prepared in aqueous solution from which it is isolated in solid form and then decomposed.

3.2.1. MECHANO-CHEMICAL METHOD:

Calculated stoichiometric amounts of pure 99.9% manganese dioxide (Sigma-Aldrich make), zinc oxide (Thomas Baker make) and ferric oxide (Thomas Baker make) was taken as starting materials (Table 3.1). The mixture was then ball-milled with ball to material ratio of 10 at 80 rpm speed for 10 hrs in Acmas Technocracy Ball Mill (model Acme - 8203) to obtain a powdered mixture. This mixture was then treated with calculated amount of aqueous hydrazinium acetate and homogenized to a thick paste. The resulting paste containing mixed metal oxides and hydrazinium acetate was slowly dried on sand bath using conventional method of heating. It was observed that, on drying the paste swells and undergoes auto combustion- self decomposition- to finely divided solid powder which was found to be magnetic in nature. The procedure was repeated for various proportions of manganese and zinc as indicated in Table 3.1. As such, the final product, in each case, was used for characterization as well as to study the physical, magnetic and electrical properties.

Table 3.1. Amount of oxides taken for the mechano-chemical synthesis of Mn-Zn ferrites.

Sr. No.	Composition	Amount of MnO ₂ (M. W. = 86.94) g.	Amount of ZnO (M.W.=81.38) g.	Amount of Fe ₂ O ₃ M.W.=159.69) g.
1	Mn _{0.4} Zn _{0.6} Fe ₂ O ₄	1.7388	2.4414	7.9845
2	Mn _{0.5} Zn _{0.5} Fe ₂ O ₄	2.1735	2.0345	7.9845
3	Mn _{0.6} Zn _{0.4} Fe ₂ O ₄	2.6082	1.6276	7.9845
4	Mn _{0.625} Zn _{0.375} Fe ₂ O ₄	2.7169	1.5259	7.9845
5	Mn _{0.65} Zn _{0.35} Fe ₂ O ₄	2.8256	1.4242	7.9845
6	Mn _{0.675} Zn _{0.325} Fe ₂ O ₄	2.9342	1.3224	7.9845
7	Mn _{0.7} Zn _{0.3} Fe ₂ O ₄	3.0429	1.2207	7.9845
8	Mn _{0.8} Zn _{0.2} Fe ₂ O ₄	3.4776	0.8138	7.9845

3.2.2. WET CHEMICAL METHOD:

In the wet chemical method, aqueous solution containing hydrated salts namely manganese acetate (Merck India make), zinc nitrate (Hi Media make) and ferric nitrate (Hi Media make); having metal ions in stoichiometric proportion as given in Table 3.2, were treated with hydrazinium acetate to obtain aqueous mixture. The mixture was then slowly dried on a hot plate to give a solid acetate hydrazinate precursor. The acetate hydrazinate precursor ignites on drying, thus, undergoing auto combustion resulting in formation of fine particle product.

Apparently, nucleation of the Mn-Zn ferrite occurs as a result of the heat generated due to high exothermicity of the decomposition of hydrazinium acetate in the precursor. Further decomposition of the

precursor is self-sustained resulting in complete decomposition giving mixed metals ferrites product.

The product so obtained for each composition was characterized and further used for studying physical, magnetic and electrical properties as in the case of other method.

Table 3.2. Amount of metal salts taken for the wet chemical synthesis of Mn-Zn ferrite.

Sr. No	Composition	Amount of $\text{Mn}(\text{CH}_3\text{COO})_2 \cdot 4\text{H}_2\text{O}$ (M.W. = 245.09) g.	Amount of $\text{Zn}(\text{NO}_3)_2 \cdot 6\text{H}_2\text{O}$ (M. W. = 297.47) g.	Amount of $(\text{Fe NO}_3)_3 \cdot 9\text{H}_2\text{O}$ (M. W. = 404.00) g.
1	$\text{Mn}_{0.4}\text{Zn}_{0.6}\text{Fe}_2\text{O}_4$	49018	89241	404000
2	$\text{Mn}_{0.5}\text{Zn}_{0.5}\text{Fe}_2\text{O}_4$	61273	74368	404000
3	$\text{Mn}_{0.6}\text{Zn}_{0.4}\text{Fe}_2\text{O}_4$	73527	59494	404000
4	$\text{Mn}_{0.625}\text{Zn}_{0.375}\text{Fe}_2\text{O}_4$	76591	55776	404000
5	$\text{Mn}_{0.65}\text{Zn}_{0.35}\text{Fe}_2\text{O}_4$	79654	52057	404000
6	$\text{Mn}_{0.675}\text{Zn}_{0.325}\text{Fe}_2\text{O}_4$	82718	48339	404000
7	$\text{Mn}_{0.7}\text{Zn}_{0.3}\text{Fe}_2\text{O}_4$	85781	44620	404000
8	$\text{Mn}_{0.8}\text{Zn}_{0.2}\text{Fe}_2\text{O}_4$	98036	29747	404000

3.3. CHARACTERIZATION:

After synthesis, it is necessary to characterize the products, to ensure that the desired compounds are produced from the method employed for preparation. Various reliable analytical methods and instrumental techniques are available for characterization. The data obtained from such analysis is not only useful in fixing the composition of

the product, but it also pin points the presence and the extent of impurities in the sample under analysis.

In the present studies, different methods/techniques were used, which are listed below. This was done to confirm the composition and understand the structure of the ferrite samples.

The analytical method and instrumental techniques used for the characterization of the ferrites are:

- (i) Percentage yield in synthesis.
- (ii) Atomic Absorption Spectroscopy (AAS).
- (iii) Infrared Spectroscopy (IR).
- (iv) Simultaneous Thermal Analyzer (TGA-DTA)
- (v) X-ray Diffraction Spectroscopy (XRD).
- (v) Energy Dispersive X-ray Analysis (EDS).
- (vi) Transmission Electron Microscopy (TEM).

3.3.1. CHARACTERIZATION USING PERCENTAGE YIELD METHOD:

One of the primary methods of determining the formation of the desired product is by comparing the theoretical and experimental percentage yield. Known amounts of starting materials are taken for synthesis at the end of which theoretical percentage yield and experimental percentage yield, for the fixed composition of desired product, are calculated and compared to ascertain, the formation of the product as a

primary consideration. Percentage yield for all the samples were calculated in the present study for both methods of preparations.

3.3.2. ATOMIC ABSORPTION SPECTROSCOPY (AAS):

Atomic absorption spectroscopy is a method for elemental analysis. It is also useful in detecting, both qualitatively and quantitatively, the trace metals and it is independent of the molecular form of the metal in the sample. The method is highly sensitive and can detect different metals in concentration of less than one ppm. Experimentally when a solution containing metallic species is introduced into a flame, the vapors of the metal will be produced. When a light of the required wavelength is allowed to pass through a flame having atoms of the metal, part of that light will be absorbed and the absorption will be proportional to the density of the atoms in the flame. Thus, using atomic absorption spectroscopy, one determines the amount of light absorbed. Once this value of absorption is known the concentration of the metal is known, since absorption is directly proportional to the density of the atoms in the flame.

In the present study, this method was used to determine the amount of Mn, Zn and Fe from the ferrite samples. Analyses of most of the samples were carried out for both methods of preparations.

3.3.3. INFRARED SPECTROSCOPY (IR):

Infrared Spectroscopy (IR) is one of the versatile tools for both qualitative and quantitative analysis of molecular species. It is employed with the intensity measurements for chemical and structural identification, and for the quantitative measurements. A chemical substance shows a marked selective absorption in the infrared region. After absorption of IR radiations, the (bonds) molecules of chemical compounds vibrate with different rates of vibration producing a close packed absorption bands called IR absorption spectrum, which may extend over a wide wavelength range. Various bands corresponding to the characteristic functional groups and bonds present in the chemical substance are present in the IR spectrum which helps in identifying the compound.

Thus, it quickly provides useful information, about the structure of the molecule without any evaluation process. The instruments are simple, relatively inexpensive and easy to operate.

In a typical experiment, the solid ferrite sample was finely ground along with the pure and dry KBr, in the ratio 1:10. Fine grinding is required for the sample to be uniformly mixed with KBr. The mixture was then put in a sample holder and placed in the sample chamber of the IR spectrophotometer. The absorption spectrum for the sample was recorded in the wavelength range 4000cm^{-1} to 400cm^{-1} . The experiment was repeated for all the samples.

3.3.4. SIMULTANEOUS THERMAL ANALYSER (TGA-DTA):

In thermoanalytical method, when a substance is subjected to heating or cooling, it undergoes certain physical and/or chemical change, which is monitored commonly in the form of thermogram or differential thermal curve. This change is characteristic of the given sample and used by the thermal studies for its characterization. In present study simultaneous TGA-DTA technique was used for the study of the precursor. TGA was used for determining the change in weight of the precursor by using heating rate of $10^{\circ}\text{C min}^{-1}$ in air. The weight change was recorded as a function of temperature. DTA was employed to record the difference in temperature between the sample and the reference material against temperature, while heating at the same rate. Difference in temperature of the sample and the reference (differential temperature ΔT) was plotted as a function of furnace temperature. It represented enthalpic changes- endothermic or exothermic- occurring during the heating process.

In a typical experiment 5-10 mg of accurately weighed precursor, accurately weighed, was taken in a silica crucible for each DTA-TGA run. Heating rate of $10^{\circ}\text{C min}^{-1}$, in air, was employed. Difference in temperature between the reference material and the sample was recorded as a function of temperature. Simultaneously the change in the weight of the sample was recorded. The sample was heated up to 900°C . The thermogram of the sample was obtained on an automatic recorder connected to the instrument. This procedure was repeated for a few samples of the precursors obtained by both methods of preparation.

3.3.5. X-RAY DIFFRACTION SPECTROSCOPY:

X-ray powder diffraction (XRD) method is generally used for investigating the internal structures, and hence, for the identification of the material. This is possible because the interatomic spacing in the crystal is of the order of 10^{-8} cm, therefore, X-ray wave with wavelength of similar order will give rise to diffraction phenomena. The diffraction pattern so obtained provides information about the internal arrangement of atoms in the crystals. The XRD patterns of all the samples, obtained by both the methods of preparation, were recorded. For mechano-chemical method, the XRD patterns of the mixture of starting oxide materials Fe_2O_3 , MnO_2 and ZnO after ball-milling was also obtained.

3.3.6. ENERGY DISPERSIVE X-RAY ANALYSIS (EDS):

Scanning electron microscope (SEM) uses a focused beam of high-energy electrons to generate a variety of signals at the surface of solid substances. The signals that derive from electron - sample interaction reveal the information about the sample including external morphology (texture), chemical composition, crystalline structure and orientation of materials. It provides information about elemental analysis of the sample.

EDS spectra for a few samples of the final Mn-Zn ferrite products were recorded. The percentage composition of Mn, Zn, Fe and O, are reported in this chapter.

3.3.7. TRANSMISSION ELECTRON MICROSCOPY (TEM):

The transmission electron microscope uses a high energy electron beam with high voltage of 200 keV to 1 MeV having high resolution, which permits the routine imaging of atoms. With the addition of energy dispersive X-ray analysis (EDAX) or energy loss spectrometry (EELS), the TEM can also be used as an elemental analysis tool capable of identifying the elements in the areas less than 0.5 μ m in diameter, transmitted through a very thin sample to image and analyze the microstructure of materials with atomic scale resolution. The electrons are focused with electromagnetic lenses and the image is observed on a fluorescent screen or recorded on a film or a digital camera. The electrons are accelerated at several hundred kV, with a wavelength much lower than that of the light.

For a few samples, TEM micrographs were obtained to evaluate the particle size of Mn-Zn ferrite samples prepared in the present study.

3.4. PHYSICAL PROPERTIES:

It is always better to have the knowledge of the physical properties of any solid substance, before it is used for any specific and characteristic applications. The properties associated with solid are density, average particle size, average surface area per unit weight, porosity, etc.

In the present study on Mn-Zn ferrites, the investigations were restricted to few of these properties such as density (bulk and X-ray density), lattice constant, average particle size and porosity. These properties were determined by using methods described in Chapter Two.

3.4.1. LATTICE CONSTANT FROM X-RAY DIFFRACTION DATA:

The X-ray data is used to determine interplanar distances and the lattice constants. Due to the random orientation of the crystallites in the sample, a reflection at the particular position is due to a set of atomic planes which are satisfying Bragg's condition.

Bragg's equation is given by

$$n\lambda = 2d_{hkl} \sin\theta \quad \text{-----} \quad 3.1.$$

where 'd'_{hkl} is the interplanar spacing or distance of crystal planes of miller indices (hkl), 'θ' is the reflection angle, 'λ' is the wavelength of the X-ray radiation and 'n' is the order of reflection.

For a cubic lattice, the interplanar distance d_{hkl}, lattice parameter 'a' and the miller indices (hkl) are related by relation,

$$d_{hkl} = \frac{a}{\sqrt{h^2 + k^2 + l^2}} \quad \text{-----} \quad 3.2.$$

thus, by using the above relation (3.2), the values of lattice constants 'a' were calculated.

3.4.2. X-RAY DENSITY:

X-ray density of the Mn-Zn ferrite samples were calculated [1] by using the relation,

$$\rho_x = 8M/Na^3 \quad \text{-----} \quad 3.3.$$

where ' ρ_x ' is the X-Ray density, '8' represents the number of atoms in a unit cell of spinel lattice, 'M' is the molecular weight of the ferrite, 'a' is the lattice constant and 'N' is the Avogadro's number.

3.4.3. MASS OR BULK DENSITY:

The mass or bulk densities of the samples were determined by using pycnometric method. Carbon tetrachloride at a room temperature was used as the liquid for displacement. The bulk density ' ρ ' was calculated using the expression;

$$\rho = \text{Weight of the sample} / (\text{Weight of the liquid displaced} / \text{Density of the liquid}) \quad \text{-----} \quad 3.4.$$

3.4.4. POROSITY MEASUREMENT:

Insight into the porosity of ferrite materials is very important, especially when these substances are to be used as catalysts or sensors. Oxide materials having high porosity exhibit better catalytic property [2, 3] and are good sensors [4, 5]. Simple and reliable method [6, 7] of determining the porosity of a solid sample, adopted in the present study, involves use of its lattice constant value, X-ray density and mass density of each ferrite sample.

The percentage porosity (P) was calculated using the formula:

$$P = [1 - (\rho/\rho_x)] \quad \text{-----} \quad 3.5.$$

where 'ρ' is bulk density and 'ρ_x' is X-ray density This method was used to calculate percentage porosity of samples.

3.5. RESULTS AND DISCUSSION:

Data obtained from various analytical methods and the instrumental techniques used in the present investigations are presented below. Interpretations from these results are also discussed.

3.5.1. PERCENTAGE YIELD METHOD:

Percentage yield method is an initial procedure followed to ascertain the possibility of obtaining the desired products. Although the method is not very accurate, nonetheless, it helps in planning of the experimental procedures to achieve the desired result. Percentage yield was calculated for both the methods of preparation.

3.5.1.1. MECHANO-CHEMICAL METHOD:

This method of preparation is explained in Section 3.2.1 above. In a typical experiment, for the preparation, of $Mn_{0.4}Zn_{0.6}Fe_2O_4$, a mixture of 1.7388g, MnO_2 (0.4x0.05m), 2.4414g, ZnO (0.6x0.05m), and 7.9845g, Fe_2O_3 (0.05m) was ball milled for 10 hours. It was then treated with

aqueous hydrazinium acetate to a thick paste. Further, the mixture was dried and ignited in a previously weighed crucible to find the weight of the product. Theoretical or expected yield was calculated from the amount of the starting materials taken for the expected product. The percentage yield was then calculated from the ratio of experimentally obtained yield (weight) and the theoretical yield (calculated).

Table 3.3. Percentage yield for various compositions of $Mn_xZn_{(1-x)}Fe_2O_4$ ferrites obtained by the mechano-chemical method.

Composition	Experimental Yield g.	Theoretical Yield g.	% Yield
$Mn_{0.4}Zn_{0.6}Fe_2O_4$	11.7061	11.8447	98.83
$Mn_{0.5}Zn_{0.5}Fe_2O_4$	11.6049	11.7925	98.41
$Mn_{0.6}Zn_{0.4}Fe_2O_4$	11.6346	11.7403	99.10
$Mn_{0.625}Zn_{0.375}Fe_2O_4$	11.4739	11.7273	97.84
$Mn_{0.65}Zn_{0.35}Fe_2O_4$	11.4706	11.7143	97.92
$Mn_{0.675}Zn_{0.325}Fe_2O_4$	11.4214	11.7011	97.61
$Mn_{0.7}Zn_{0.3}Fe_2O_4$	11.4636	11.6881	98.08
$Mn_{0.8}Zn_{0.2}Fe_2O_4$	11.3019	11.6359	97.13

3.5.1.2. WET-CHEMICAL METHOD:

Preparation by this method is given in Section 3.2.2 in details. In a typical experiment, for the preparation of $Mn_{0.4}Zn_{0.6}Fe_2O_4$, 4.9018g of $Mn(CH_3COO)_2 \cdot 4H_2O$ (0.4x0.05m), 8.9241g of $Zn(NO_3)_2 \cdot 6H_2O$ (0.6x0.05m) and 40.4000g of $Fe(NO_3)_3 \cdot 9H_2O$ (0.1m), each dissolved in minimum quantity of distilled water, were mixed and then aqueous hydrazinium acetate was added to it. The resultant solution was evaporated using a hot plate to dryness. The dried powder was decomposed in a previously

weighed crucible by reheating on the hot plate in order to find the weight of the product formed.

The theoretical yield and the experimental yield were calculated for each sample as explained in the previous section.

As seen from the Table 3.3, for Mn-Zn ferrite samples prepared by the mechano-chemical method, the percentage yield is in the range 96-99%. Similarly, from the Table 3.4, it can be observed that Mn-Zn ferrite samples synthesized by the wet chemical method, the percentage yield for different compositions is in the range 77-89%

Table 3.4. Percentage yield for various compositions of $Mn_xZn_{(1-x)}Fe_2O_4$ ferrites obtained by the wet chemical method.

Composition	Experimental Yield g.	Theoretical Yield g.	% Yield
$Mn_{0.4}Zn_{0.6}Fe_2O_4$	10.3475	11.8447	87.36
$Mn_{0.5}Zn_{0.5}Fe_2O_4$	9.7453	11.7925	82.64
$Mn_{0.6}Zn_{0.4}Fe_2O_4$	10.0174	11.7403	85.32
$Mn_{0.625}Zn_{0.375}Fe_2O_4$	9.3172	11.7272	79.45
$Mn_{0.65}Zn_{0.35}Fe_2O_4$	10.1253	11.7143	86.43
$Mn_{0.675}Zn_{0.325}Fe_2O_4$	9.8839	11.7011	84.47
$Mn_{0.7}Zn_{0.3}Fe_2O_4$	10.1429	11.6881	86.78
$Mn_{0.8}Zn_{0.2}Fe_2O_4$	10.3617	11.6359	89.05

3.5.2. ATOMIC ABSORPTION SPECTROSCOPY:

Mn-Zn ferrite powder samples of different compositions of Mn and Zn were accurately weighed and dissolved in minimum quantity of AR grade concentrated hydrochloric acid and the solution was diluted to ppm level by taking care that each powder sample has concentration of Fe ions in the range of 2 to 9 ppm, Mn ions in the range of 1 to 3.6 ppm and Zn ions in the range of 0.4 to 1.5 ppm, as per the requirement of the AAS spectrophotometer of GBC Model 932AA.

The results obtained for Fe, Mn and Zn ions in each sample are given in the Table 3.5 and 3.6 and the same are in agreement with the assigned stoichiometric compositions for the ferrite samples, within the permissible experimental error, in the mechano-chemical and the wet chemical methods.

Table 3.5. AAS analysis data for ferrite samples obtained by the mechano-chemical method.

Composition	Mn content		Zn content		Fe content	
	Theor. %	Exptl. %	Theor. %	Exptl. %	Theor. %	Exptl. %
$\text{Mn}_{0.5}\text{Zn}_{0.5}\text{Fe}_2\text{O}_4$	11.65	11.78	13.86	12.98	47.36	47.80
$\text{Mn}_{0.6}\text{Zn}_{0.4}\text{Fe}_2\text{O}_4$	14.04	14.32	11.14	11.36	47.57	46.39
$\text{Mn}_{0.625}\text{Zn}_{0.375}\text{Fe}_2\text{O}_4$	14.64	15.04	10.45	11.05	47.62	48.47
$\text{Mn}_{0.65}\text{Zn}_{0.35}\text{Fe}_2\text{O}_4$	15.24	15.40	9.76	9.95	47.67	47.92
$\text{Mn}_{0.675}\text{Zn}_{0.325}\text{Fe}_2\text{O}_4$	15.84	15.84	9.08	8.72	47.73	47.45
$\text{Mn}_{0.8}\text{Zn}_{0.2}\text{Fe}_2\text{O}_4$	18.89	19.01	5.62	5.61	47.99	50.16

Table 3.6. AAS analysis data for ferrite samples obtained by the wet chemical method.

Composition	Mn content		Zn content		Fe content	
	Theor. %	Exptl. %	Theor. %	Exptl. %	Theor. %	Exptl. %
$Mn_{0.4}Zn_{0.6}Fe_2O_4$	9.27	9.81	16.56	15.92	47.15	48.82
$Mn_{0.5}Zn_{0.5}Fe_2O_4$	11.65	11.20	13.86	14.11	47.36	47.03
$Mn_{0.6}Zn_{0.4}Fe_2O_4$	14.04	13.63	11.14	11.08	47.57	50.39
$Mn_{0.7}Zn_{0.3}Fe_2O_4$	16.45	17.07	8.39	8.13	47.78	48.29
$Mn_{0.8}Zn_{0.2}Fe_2O_4$	18.89	18.53	5.62	5.84	47.99	49.64

3.5.3. INFRARED SPECTROSCOPY:

The infrared spectra of all the ferrite samples are shown in the Fig. 3.1 (for the mechano-chemical method) and Fig. 3.2 (for the wet chemical method) recorded in the range of 4000-400 cm^{-1} .

Infrared spectra of various ferrites have been studied by Waldron [8], reporting two bands in the region 1000 cm^{-1} to 200 cm^{-1} . He attributed the high frequency (ν_1) band to tetrahedral metal-oxygen bond and second frequency (ν_2) band to octahedral metal-oxygen bond. The IR spectra of all samples show two peaks, one in the range 600-550 cm^{-1} and the other 450-385 cm^{-1} corresponding to:

(a) $Me_T - O - Me_O$ stretching vibration 600-550 cm^{-1}

(b) $Me_O \leftrightarrow O$ stretching vibration 450-385 cm^{-1}

here O is oxygen, Me_O is metal in the octahedral site and Me_T in the tetrahedral site. The metal-oxygen absorption bands (a) and (b) are

pronounced for all spinel structures and essentially for ferrites, which are also seen in these samples.

IR spectral data of all the ferrite samples prepared by both methods are in agreement with the reported value [9, 10].

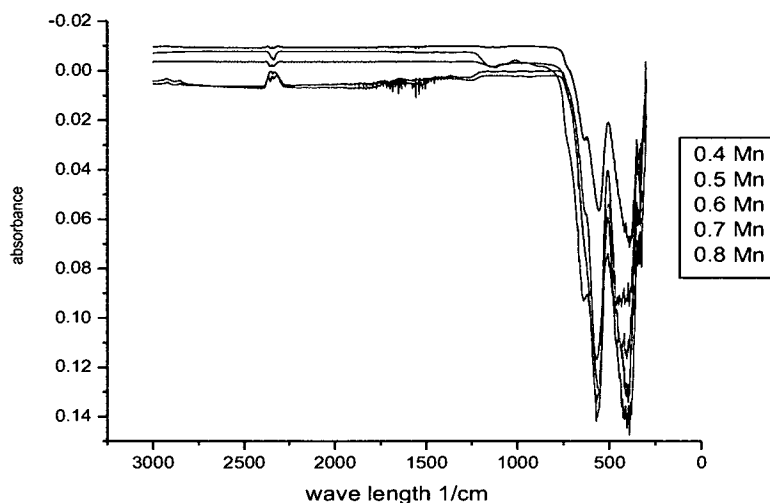


Fig.3.1. IR Spectra of various Mn-Zn ferrite samples obtained by the mechano-chemical method.

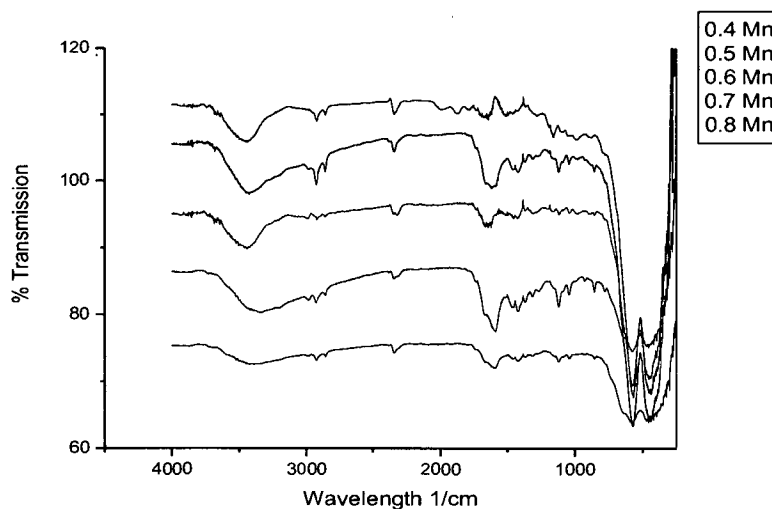
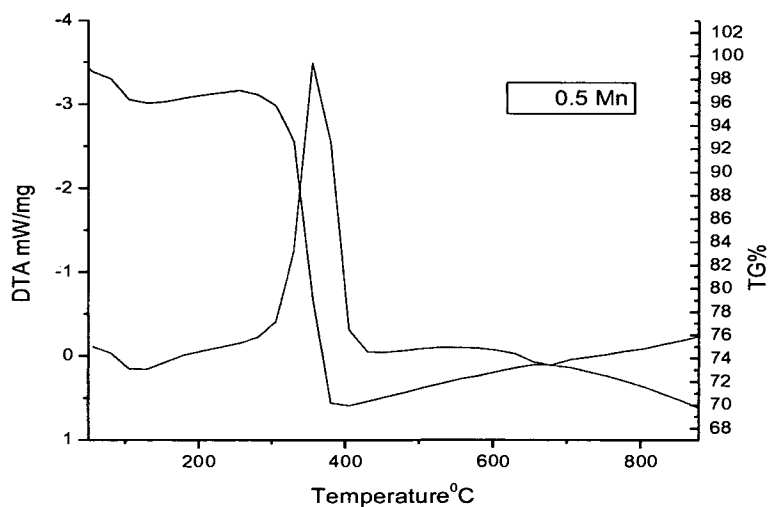


Fig.3.2. IR Spectra of various Mn-Zn ferrite samples obtained by the wet chemical method.

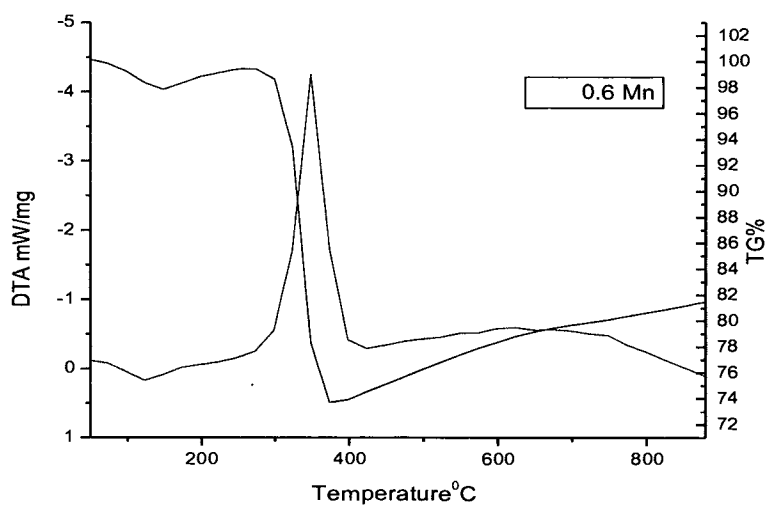
3.5.4. THERMAL ANALYSIS OF PRECURSORS:

Oxides of Mn, Zn and Fe, taken in appropriate proportion (Table 3.1), were thoroughly mixed in a ball mill. This mixture was treated with aqueous hydrazinium acetate to a thick paste. The paste was slowly heated, on a hot plate maintained at about 80-85⁰C, to dryness. Thermal analysis of the dried powder (precursor) was carried out under the conditions mentioned in Section 3.3.4 above.

In thermal analysis, it was observed that the precursor prepared by the mechano-chemical method decomposed in a single step, to yield Mn-Zn ferrite as the product. For all the compositions of the MnO₂ and ZnO in the synthesis, the weight loss was invariably in the range of 28-30% in the TGA. This loss can be attributed to the decomposition of CH₃COOH.N₂H₄ or CH₃COON₂H₅ (hydrazinium acetate), on heating. It appears that CH₃COOH.N₂H₄ is bonded to the mixture of oxides as an adduct and exothermically decomposes to the Mn-Zn ferrite as the final product. The heat released in this highly exothermic decomposition, hastens the formation of mixed metals ferrite. The gases such as N₂, NH₃, CO₂ and H₂O are released during the decomposition. Complimentary peaks were observed in the range 340-370⁰C in the DTA for precursors obtained by using various compositions of Mn and Zn oxide as seen in Fig. 3.3 (a) and (b). Thus it can be inferred that the Mn-Zn ferrite are formed at a comparatively lower temperatures in the novel method used in the present studies.



(a)



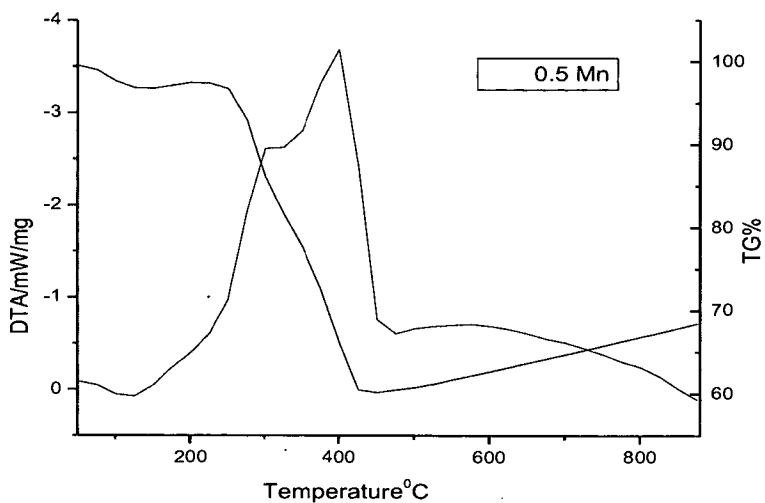
(b)

Fig.3.3. TG – DTA thermogram of precursors obtained from the mechano – chemical method for (a) $Mn_{0.5}Zn_{0.5}Fe_2O_4$ (b) $Mn_{0.6}Zn_{0.4}Fe_2O_4$.

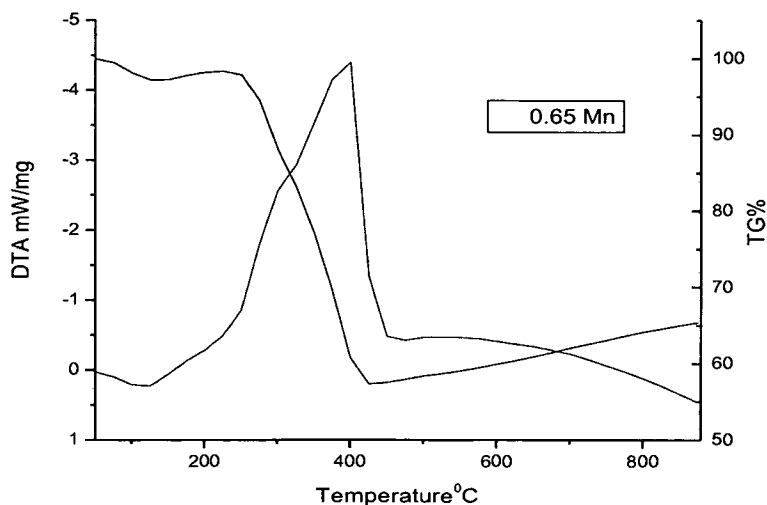
Similarly, aqueous solution of the hydrated salts: manganese acetate, zinc nitrate and ferric nitrate, having metal ions in stoichiometric proportion (Table 3.2) was treated with aqueous hydrazinium acetate. The mixture was slowly dried on a hot plate. A few mg (Section 3.3.4) of the dried powder, the precursor, was used for the thermal analysis. In the

TGA, it was observed that the precursors decomposed to Mn-Zn ferrites as the final product in a single step for all the compositions of the Mn and Zn content in the series of preparations. The weight loss was found to be between 40-42% in the temperature range of 400-425⁰C. Corresponding peaks were observed in the DTA, Fig 3.4 (a) and (b).

The wet chemical method of synthesis also gives Mn-Zn ferrite as the final product, at fairly lower temperatures, as was found in the present investigation.



(a)



(b)

Fig.3.4.TG – DTA thermogram of precursors obtained from the wet chemical method for (a) $Mn_{0.5}Zn_{0.5}Fe_2O_4$ (b) $Mn_{0.65}Zn_{0.35}Fe_2O_4$.

3.5.5. X-RAY DIFFRACTION ANALYSIS:

X-ray diffraction studies (Chapter-Two, Section 2.3.4) were carried out to examine the structure as well as to determine interplanar distances and the lattice constants. The samples of Mn-Zn ferrite prepared by the mechano-chemical and wet chemical methods were analyzed for its crystal structure by powder X-ray diffraction method using reflection angles in the range from 20° to 80° .

XRD powder patterns for all the samples, prepared by mechano-chemical method, indicate single phase cubic spinel structure formation for all the compositions of $Mn_{(x)}Zn_{(1-x)}Fe_2O_4$ (where $x = 0.40, 0.50, 0.60, 0.625, 0.65, 0.675, 0.70, 0.80$). X-ray spectra of these samples are given in Fig.3.5.(b). XRD pattern of mixture of oxides- MnO_2 , ZnO and Fe_2O_3 - prior to the synthesis is shown in Fig.3.5.(a). By comparing Fig.3.5.(a)

with Fig.3.5.(b), the formation of ferrites is confirmed. As such the mechano-chemical method is found to be useful in the synthesis of ferrites.

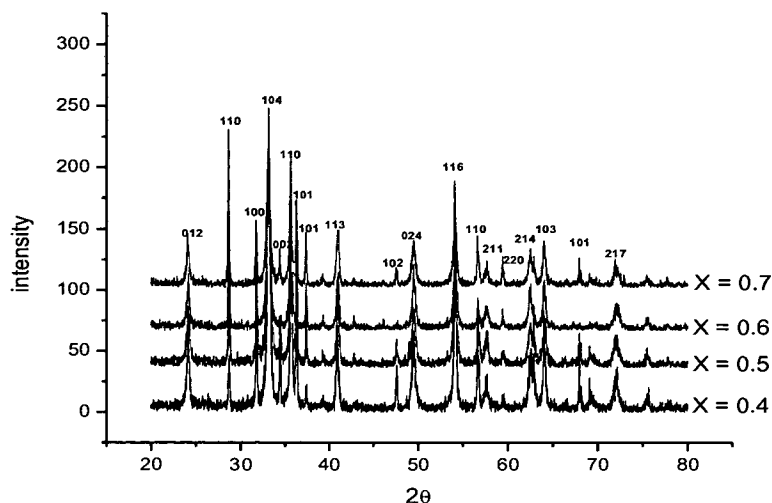


Fig.3.5.(a). X-ray diffraction patterns of mixture of oxides after ball-milling.

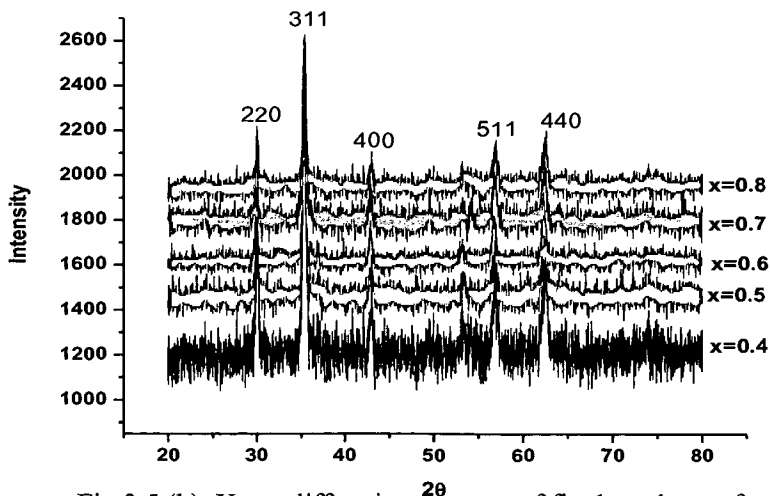


Fig.3.5.(b). X-ray diffraction patterns of final products after decomposition, obtained by the mechano-chemical method.

Similarly, the X-ray diffraction spectra for $Mn_xZn_{(1-x)}Fe_2O_4$ samples with compositions (where $x = 0.40, 0.50, 0.60, 0.625, 0.65, 0.675, 0.70, 0.80$), prepared by the wet chemical method also indicate the formation of single phase of Mn-Zn ferrite in all the cases as can be seen

in Fig.3.5.(c). The patterns obtained are similar to the XRD patterns reported in the literature for Mn-Zn ferrite [11, 12].

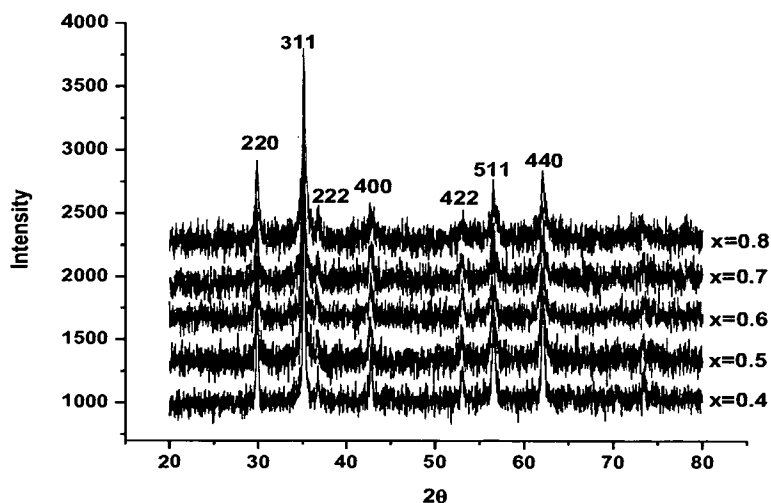


Fig.3.5.(c). X-ray diffraction patterns of Mn-Zn ferrite samples obtained by the wet chemical method.

3.5.6. EDS DATA:

Scanning electron microscope (SEM) uses a focused beam of high-energy electrons to generate a variety of signals at the surface of solid substances. The signals that derive from electron sample interaction reveal information about the sample including external morphology (texture), chemical composition, crystalline structure and orientation of materials. It also provides elemental analysis data of the sample.

The SEM spectra for two samples ($\text{Mn}_{0.5}\text{Zn}_{0.5}\text{Fe}_2\text{O}_4$ and $\text{Mn}_{0.6}\text{Zn}_{0.4}\text{Fe}_2\text{O}_4$) are illustrated in Fig.3.6. (a) and (b). Percentage compositions of elements Mn, Zn, Fe and O of these ferrite samples, determined by the EDS analysis, are given in Table 3.7. (a) and (b).

This data for the samples prepared by mechano-chemical method was fairly in good agreement with the theoretically estimated values for the compositions assigned, although oxygen deficiencies are seen in them.

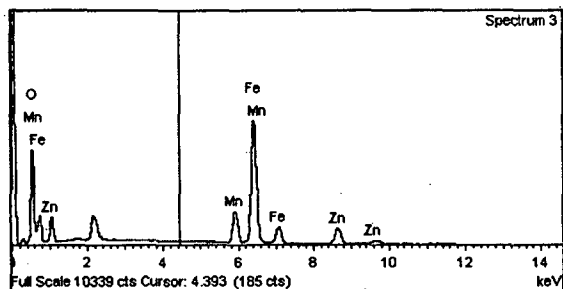


Fig.3.6.(a). EDS spectrum of $Mn_{0.5}Zn_{0.5}Fe_2O_4$.

Table 3.7.(a). EDS analysis of $Mn_{0.5}Zn_{0.5}Fe_2O_4$.

Element	Theor. %	Exptl. %
Mn	11.53	11.26
Zn	13.86	16.76
Fe	47.36	50.21
O	27.15	21.77

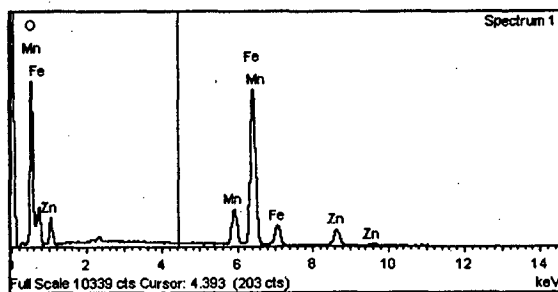


Fig. 3.6. (b). EDS spectrum of $Mn_{0.6}Zn_{0.4}Fe_2O_4$.

Table 3.7. (b). EDS analysis of $Mn_{0.6}Zn_{0.4}Fe_2O_4$.

Element	Theor. %	Exptl. %
Mn	14.04	14.58
Zn	11.13	13.84
Fe	47.57	49.71
O	27.26	21.87

3.5.7. Transmission Electron Microscopy (TEM):

TEM micrographs of the samples clearly show the formation of nano size Mn-Zn ferrite material obtained by the mechano-chemical method. The particle size is in the range of 10 to 28 nm. Two representative micrographs are shown in Fig.3.7 (a) and (b).

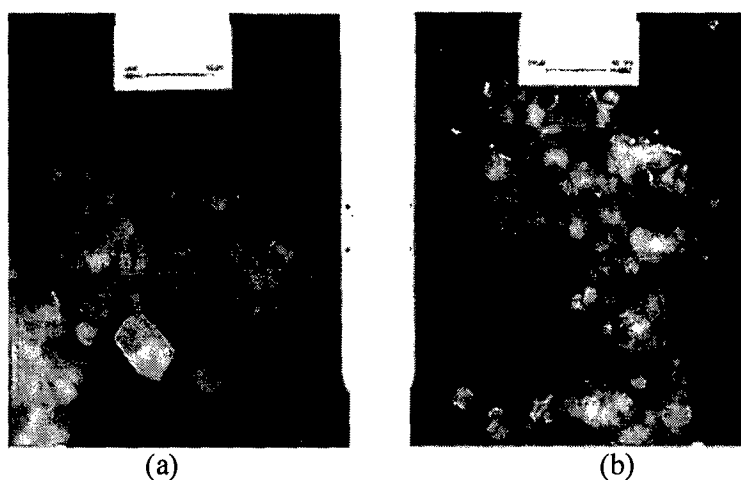


Fig.3.7. TEM micrographs of (a) $Mn_{0.5}Zn_{0.5}Fe_2O_4$ (b) $Mn_{0.6}Zn_{0.4}Fe_2O_4$.

3.5.8. LATTICE CONSTANT 'a' FROM X-RAY DIFFRACTION DATA:

The values of lattice constants 'a' calculated by using Scherer formula from the X-ray diffraction data for samples prepared by the two methods were found to be in good agreement with the reported values [13-15].

Calculated values of lattice parameters for the ferrite samples show an increase in the lattice constant value as the concentration (x) of manganese was increased (Table 3.8). In the case of mechano-chemical

method, for example, the lattice constant 8.4129Å for $\text{Mn}_{0.40}\text{Zn}_{0.60}\text{Fe}_2\text{O}_4$ increases gradually to 8.4519Å for $\text{Mn}_{0.8}\text{Zn}_{0.2}\text{Fe}_2\text{O}_4$. Similarly, in the case of the wet chemical method (Table 3.8), lattice constant 'a' for $\text{Mn}_{0.40}\text{Zn}_{0.60}\text{Fe}_2\text{O}_4$ which is 8.4529Å, increases to 8.4687Å for $\text{Mn}_{0.8}\text{Zn}_{0.2}\text{Fe}_2\text{O}_4$. This increase could be attributed to the size of the ionic radii of Mn^{2+} and Zn^{2+} cations. As the concentration of Mn^{2+} increases, bigger Mn^{2+} cations (0.91Å), replace smaller Zn^{2+} cations (0.82Å) in the samples. Similar observations have been made by some researchers [16, 17] in their study of Mn-Zn ferrites. Fig.3.8. (a) and (b) show the variation of lattice constant 'a' with concentration of Mn for both methods.

Table 3.8. Calculated lattice constant for Mn-Zn ferrites obtained by (a) the mechano-chemical method, and (b) the wet chemical method.

Composition	'a' in Å	
	(a)	(b)
$\text{Mn}_{0.4}\text{Zn}_{0.6}\text{Fe}_2\text{O}_4$	8.4198	8.4529
$\text{Mn}_{0.5}\text{Zn}_{0.5}\text{Fe}_2\text{O}_4$	8.4294	8.4587
$\text{Mn}_{0.6}\text{Zn}_{0.4}\text{Fe}_2\text{O}_4$	8.4436	8.4654
$\text{Mn}_{0.7}\text{Zn}_{0.3}\text{Fe}_2\text{O}_4$	8.4498	8.4673
$\text{Mn}_{0.8}\text{Zn}_{0.2}\text{Fe}_2\text{O}_4$	8.4519	8.4687

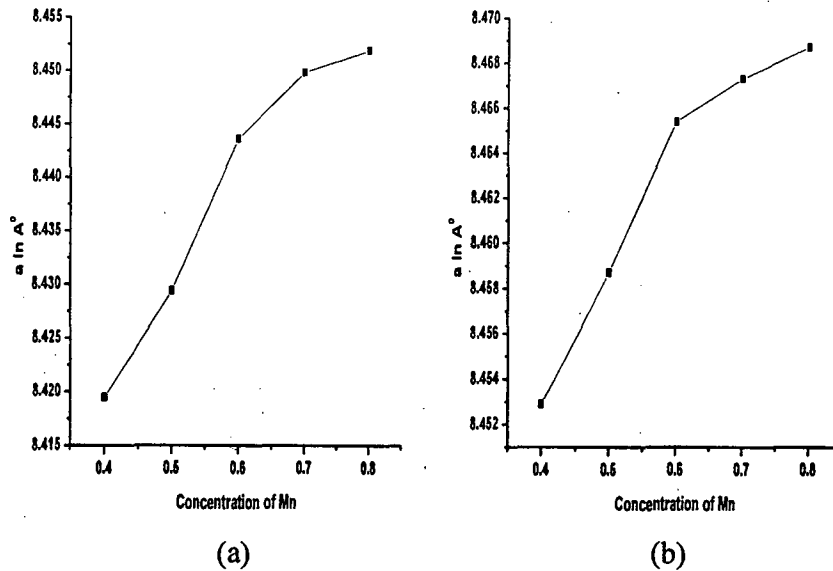


Fig.3.8. Variation of lattice value 'a' with concentration of Mn for samples prepared by (a) the mechano-chemical (b) the wet chemical method.

3.5.9. PARTICLE SIZE USING X-RAY ANALYSIS:

As the particle size decreases the peaks in the XRD patterns get broadened due to the incomplete destructive interference. This broadening caused by the fine crystallites is related to the size of the grains by the Scherer formula [18].

$$T = 0.9 \lambda / D_p \cos \theta \quad \text{-----} \quad 3.6.$$

'T' = crystallite size, ' λ ' = wavelength, ' D_p ' = FWHM (Full width half measure), ' θ ' = reflection angle.

The particle size is an important parameter in the ferrite materials with regard to their applications. Three different methods were employed to evaluate the particle size of the grains in the ferrite samples prepared by the two methods, used in the present study. One such method was by using

XRD peak broadening with the help of Scherrer formula. The particle size values calculated by this formula show that the size of Mn-Zn ferrites particles formed were in the nano-meter range for both the methods of preparations namely the mechano-chemical and wet the chemical method. The values are given in Table 3.9. (a) and 3.9.(b), respectively.

Table 3.9. Particle size of Mn- Zn ferrites obtained by (a) the mechano-chemical method, and (b) the wet chemical method.

$Mn_xZn_{1-x}Fe_2O_4$ x =	Particle size nm	
	(a)	(b)
0.40	27.40	29.76
0.50	42.20	18.14
0.60	37.16	56.80
0.625	24.00	42.47
0.65	16.12	37.88
0.675	19.70	67.29
0.70	21.36	29.64
0.80	27.32	46.23.

Interestingly, the particle size of Mn-Zn ferrite samples obtained by the mechano-chemical method was found to be smaller in comparison to the samples prepared from the wet chemical method. This could be due to breaking down of particles of individual oxide powder during ball milling.

3.5.10. X-RAY DENSITY:

X-ray densities for the samples have been calculated as explained in 3.4.2. For the mechano-chemical method (Table.3.10.(a)), for example, the X-ray density is 5.2717 g cm^{-3} for $\text{Mn}_{0.4}\text{Zn}_{0.6}\text{Fe}_2\text{O}_4$, which decreases gradually to 5.1208 g cm^{-3} for $\text{Mn}_{0.8}\text{Zn}_{0.2}\text{Fe}_2\text{O}_4$. Similarly, in the case of the wet chemical method (Table 3.10(b)), the X-ray density is 5.2097 g cm^{-3} for $\text{Mn}_{0.4}\text{Zn}_{0.6}\text{Fe}_2\text{O}_4$, which decreases to 5.0892 g cm^{-3} for $\text{Mn}_{0.8}\text{Zn}_{0.2}\text{Fe}_2\text{O}_4$. The X-ray densities of the mechano-chemical method are found to be higher than those of the samples prepared by the wet chemical method. The X-ray densities depend on molecular weight and the lattice constant of the ferrite sample. As expected, in both the cases, the X-ray densities are found to decrease with increase in the value of 'a,' since lattice constant is inversely proportional to the X-ray density. Also, the X-ray density decreases with increase in Mn content. Lattice constant 'a' for the samples is directly proportional to Mn content in the samples as reported earlier [16, 17]. Fig.3.9. (a) and (b) show the variation of X- ray densities with concentration of Mn for both methods.

Table 3.10. X-Ray Densities for ferrite samples obtained by (a) the mechano-chemical method, and (b) the wet chemical method.

Composition	X-Ray density g cm^{-3}	
	(a)	(b)
$\text{Mn}_{0.4}\text{Zn}_{0.6}\text{Fe}_2\text{O}_4$	5.2717	5.2097
$\text{Mn}_{0.5}\text{Zn}_{0.5}\text{Fe}_2\text{O}_4$	5.2303	5.1761
$\text{Mn}_{0.6}\text{Zn}_{0.4}\text{Fe}_2\text{O}_4$	5.1807	5.1407
$\text{Mn}_{0.7}\text{Zn}_{0.3}\text{Fe}_2\text{O}_4$	5.1801	5.1144
$\text{Mn}_{0.8}\text{Zn}_{0.2}\text{Fe}_2\text{O}_4$	5.1208	5.0892

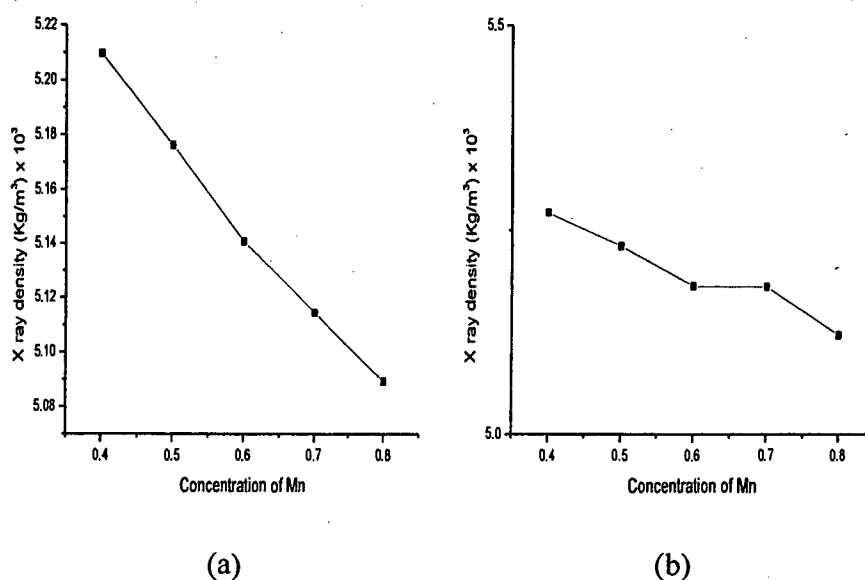


Fig. 3.9. Variation of X- ray density with concentration of Mn for samples prepared by (a) the mechano-chemical method (b) the wet chemical method.

3.5.11. MASS OR BULK DENSITY:

The mass densities of ferrites were found to be lower for the samples prepared by the mechano-chemical method as seen from Table.3.11.(a) and were in the range 2.9977 g cm^{-3} for $\text{Mn}_{0.4}\text{Zn}_{0.6}\text{Fe}_2\text{O}_4$ to

3.572 g cm⁻³ for Mn_{0.8}Zn_{0.2}Fe₂O₄. Similarly, in the case of the wet chemical method (Table 3.11 (b)), the mass densities were in the range from 3.2001 g cm⁻³ for Mn_{0.4}Zn_{0.6}Fe₂O₄ to 3.6536 g cm⁻³ for Mn_{0.8}Zn_{0.2}Fe₂O₄. This can be attributed to the fact that in the wet chemical method the formation of precursor occurs at the ionic level and hence the compactness and densification of the final ferrite material. This is not so in case of the samples obtained by the mechano-chemical method. Also, for both the methods of preparation, the mass densities of ferrite samples increase with increase in Mn content. This is due to the higher value of the specific gravity of Mn (7.21 g cm⁻³) as compared to that of Zn (7.133 g cm⁻³) [19]. Fig 3.10 (a) and (b) show the variation of mass densities with the concentration of Mn for the two methods.

Table 3.11: Mass Densities of the ferrite samples obtained by (a) the mechano-chemical method and (b) the wet chemical method.

Composition	Density g cm ⁻³	
	(a)	(b)
Mn _{0.4} Zn _{0.6} Fe ₂ O ₄	2.9977	3.2001
Mn _{0.5} Zn _{0.5} Fe ₂ O ₄	3.0919	3.2902
Mn _{0.6} Zn _{0.4} Fe ₂ O ₄	3.2396	3.313
Mn _{0.7} Zn _{0.3} Fe ₂ O ₄	3.4733	3.5474
Mn _{0.8} Zn _{0.2} Fe ₂ O ₄	3.572	3.6536

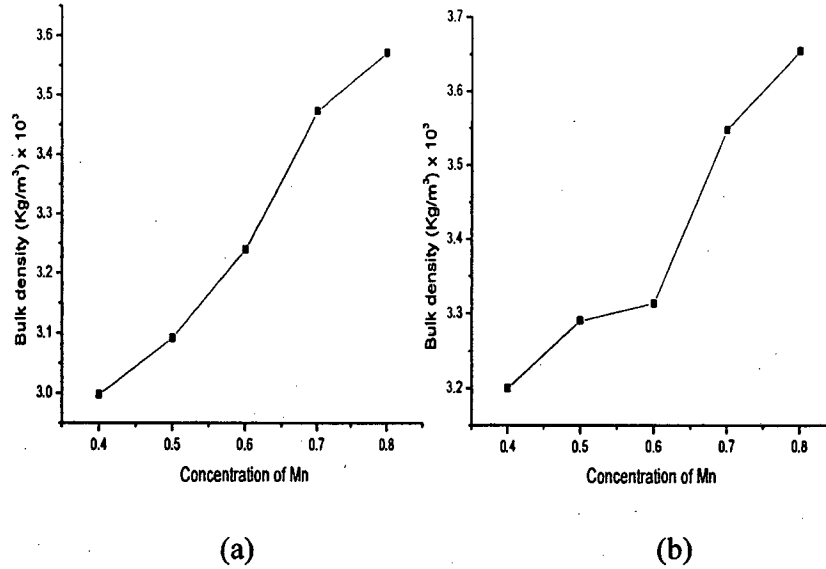


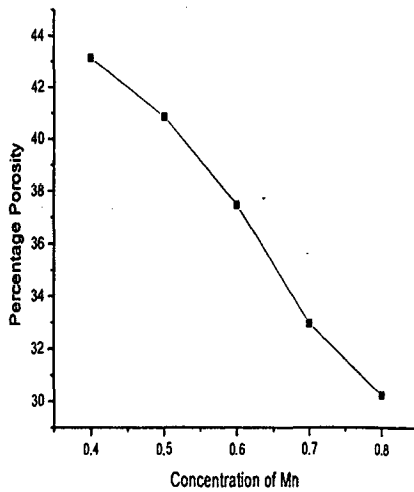
Fig. 3.10. Variation of mass density with concentration of Mn in ferrite samples obtained by (a) the mechano-chemical method and (b) the wet chemical method.

3.5.12. POROSITY MEASUREMENT:

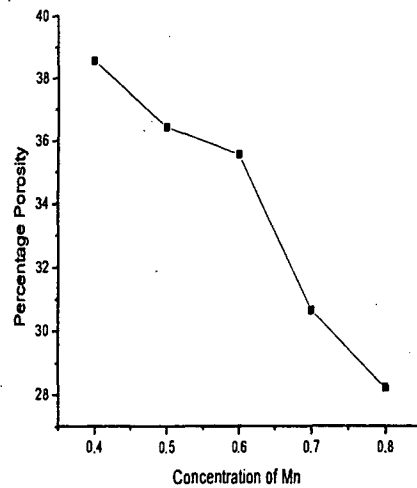
Samples obtained by both the methods have high porosity values. Among the two methods, the Mn-Zn ferrite samples obtained by the mechano-chemical method show higher porosity values ranging from 43.14 to 30.23 % as seen in Table 3. 12. (a). The values are in the range of 38.57 to 28.21 % for the samples prepared by the wet chemical method (Table.3.12.(b)). The porosity is found to decrease as the ratio (ρ/ρ_x) increases with an increasing Mn content. Fig.3.11.(a) and (b) show variation of porosity with the concentration of Mn by (a) the mechano-chemical method and (b) the wet chemical method.

Table 3.12. Porosity for Mn-Zn ferrite samples obtained by (a) the mechano-chemical method, and (b) wet chemical method.

Composition	% Porosity	
	(a)	(b)
$Mn_{0.4}Zn_{0.6}Fe_2O_4$	43.14	38.57
$Mn_{0.5}Zn_{0.5}Fe_2O_4$	40.88	36.43
$Mn_{0.6}Zn_{0.4}Fe_2O_4$	37.47	35.55
$Mn_{0.7}Zn_{0.3}Fe_2O_4$	32.95	30.64
$Mn_{0.8}Zn_{0.2}Fe_2O_4$	30.23	28.21



(a)



(b)

Fig.3.11. Variation of porosity with the concentration of Mn in samples prepared by (a) the mechano-chemical method (b) the wet chemical method.

Pannaparayil et al. [20] have calculated the porosity of Mn-Zn ferrite, prepared under mild hydrothermal conditions, to be in the range of 7–25%. The porosity values, of Mn-Zn ferrite samples prepared by both methods, namely, the mechano-chemical as well as the wet chemical method in the present study [21], were found to be higher than those reported in literature.

REFERENCES:

- [1] T.J. Shinde, A.B. Gadkari, P.N. Vasambekar, *J. Mater. Chem. Phys.*, 111 (2008), 87.
- [2] C.S. Hwang, N.C. Wang, *Mater. Chem. Phys.*, 88, (2004) 258.
- [3] L. Ma, L. Chen, S. Chen, *Mater. Chem. Phys.*, 114 (2009) 692.
- [4] N. Rezlescu, E. Rezlescu, F. Tudorache, P.D. Popa, *Roman. Rep. Phys.*, 61, (2009) 223.
- [5] N. Bagum, M.A. Gafur, A.H. Bhuiyan D.K. Saha, *Phys. Status Solidi A*, 207 (2010) 986.
- [6] R.V. Mangalaraja, S. Ananthakumar, P. Manohar, F.D. Gnanam, M. Awano, *J. Mater. Lett.*, 58, (2004) 1593.
- [7] E. C. Snelling, 'Soft Ferrites, Properties and Applications', Butter Worth and Co. (Publisher) Ltd., London, 2nd Ed. (1988).
- [8] R. A. Waldron *Phy. Rev.*, 99 (1955) 1727.
- [9] V. C. Farmer, 'The Infrared Spectra of Minerals' (ed. V. C. Farmer), Mineralogical Society, London, (1974) 18.
- [10] R. Iyer, R. Desai, R. V. Upadhyay, *Bull. Mater. Sci.*, 32, 2 (2009) 141–147.
- [11] Y. Xuan, Q. Li, G. Yang *J. Magn. Magn. Mater.*, 312 (2007) 464–469.
- [12] L. Nalbandian, A. Delimitis, V.T. Zaspalis, E.A. Deliyanni, D.N. Bakoyannakis, E. N. Peleka, *Micro. Meso. Mater.*, 114 (2008) 465– 473.
- [13] R. A. Dunlap, A. Alghamdi, J.W. O'Brien, S. J. Penney *J. Alloys Compounds*, 365 (2004) 84–88.

- [14] S. Dasgupta, K.B. Kim, J. Ellrich, J. Eckert, I. Manna, J. Alloys Compounds., 424, (2006) 13.
- [15] E.V. Gopalan, I.A. Al-Omari, K.A. Malini, P.A. Joy, D.S. Kumar, Y. Yoshida, M. R. Anantharaman, J. Magn. Magn. Mater., 321, (2009) 1092.
- [16] T. Abbas, Y. Khan, M. Ahmad, S. Anwar, Solid State Commun., 82 (1992) 701.
- [17] U. Ghazanfar, S.A. Siddiqi, G. Abbas, Mater. Sci. Eng. B, 118 (2005) 84–86.
- [18] B. D. Cullity, 'Elements of X-ray Diffraction,' 2nd Ed. Addison Wesley, (1978).
- [19] D. R. Lide, 'CRC Handbook of Chemistry and Physics', CRC Press, London, Ed. 7 (1995).
- [20] T. Pannaparayil, R. Marande, R. Komarneni, J. Appl. Phys., 69 (8), (1991) 5349- 5351.
- [21] V. J. Pissurlekar, J. S. Budkuley, A. J. Chem., 23, 4 (2011) 1677-1679.

CHAPTER FOUR

MAGNETIC PROPERTIES

4.1. INTRODUCTION:

Magnetism is a force of attraction or repulsion that acts at a distance. It occurs due to the presence of magnetic field, which is caused by moving electrically charged particles or is inherent in magnetic objects such as a magnet. Many naturally occurring compounds are magnetic in nature. The first such substance to be studied was loadstone or magnetite (Fe_3O_4), a compound of iron [1]. It was extensively studied by many researchers for its magnetic properties. P. Weiss measured its saturation magnetization and Curie temperature [2]. Subsequently, magnetism and the behaviour of magnetic materials have been well studied by several researchers [3-6]. Magnetic materials have gained wide importance due to their applications in a variety of fields. The domain structure, magnetic interaction and the basic properties of these materials are of considerable importance in modern technology. Magnetic materials are important components of electromagnetic gadgets, memory or disc storage devices, high frequency transformers, power inductors, switches, broad band pulse transformers, actuators, sensors, electromagnetic interference (EMI) suppressors, telecommunications, microwave absorbers- for special applications in defence etc.

Materials exhibit one of these magnetic behaviours viz: diamagnetism, paramagnetism, ferromagnetism, antiferromagnetism and ferrimagnetism, when placed in an external magnetic field. It also depends on the temperature. However, the ferromagnetic, antiferromagnetic and ferrimagnetic materials are classified on the basis of ordered arrangement of spins over the space lattice.

4.1.1. DIAMAGNETISM:

Diamagnetism is exhibited by all common materials. In diamagnetic materials, the orbital magnetic moment and the spin magnetic moment cancel each other. Hence there is no permanent dipole moment. In diamagnetism, weak magnetic dipole moments are produced in the atoms of the material when the material is placed in an external magnetic field. The combination of all those induced dipole moments gives the material, as a whole, only a feeble net magnetic field. The dipole moments, with them, their net field, disappear when the external field is removed. Since the magnetic moments induced by the applied magnetic field always oppose the applied field there is repulsion. The diamagnetic material has a negative susceptibility which is independent of temperature.

4.1.2. PARAMAGNETISM:

Paramagnetism is exhibited by materials containing the transition elements, the rare earth elements and the actinide elements. Each atom of

such a material has a permanent magnetic dipole moment due to incompletely filled outermost orbits, but the moments are randomly oriented in the material and the material as a whole lacks a net magnetic field. However, an external magnetic field can partially align the atomic magnetic dipole moments to give the material a net magnetic field. The alignment and thereby its field disappear when external magnetic field is removed. These materials have small positive susceptibility, which depends on temperature.

4.1.3. FERROMAGNETISM:

Ferromagnetism is a property exhibited by iron, cobalt, nickel, and certain other elements (and also by compounds and alloys of these elements). Some of the electrons in these materials have their resultant magnetic dipole moments aligned, which produces regions with strong magnetic dipole moments. An external field can then align the magnetic moments of such regions, producing a strong magnetic field for a sample of the material; the field partially persists when external magnetic field is removed. In these materials, the contribution of spin magnetic moment to the total magnetic moment is large. Neighboring atoms, having magnetic moments aligned in the same direction as illustrated in the Fig.4.1. (a), form small regions called domains. This behavior is the result of strong exchange coupling between the atoms. This interaction arises due to coupling of spins on adjacent atoms. The exchange energy between the neighboring dipoles is positive, such that the lowest energy state is the one

in which all the dipoles are aligned with their magnetic moments parallel. A ferromagnet has spontaneous magnetic moment even in zero applied field.

The electron spins and magnetic moments are arranged in a regular manner. They are supposed to occur due to a field produced within the material, which is proportional to magnetization of the sample.

4.1.4. ANTIFERROMAGNETISM:

The material in which the atomic moments from two sub lattices are such that the moment on one, equals in magnitude but is aligned antiparallel to that on the other. Thus the net magnetic moment is zero and the material is said to be antiferromagnetic (Fig.4.1. (b)). They do not produce any net magnetization at absolute zero temperature.

4.1.5. FERRIMAGNETISM:

Ferrimagnetism exists in those materials in which atomic moments are aligned antiparallel but magnetic moments are unequal as shown in Fig.4.1.(c). This is due to the fact that the opposing magnets have different moments or the number of atoms having one spin direction is different from that having opposite spin direction thus giving a magnetic moment.

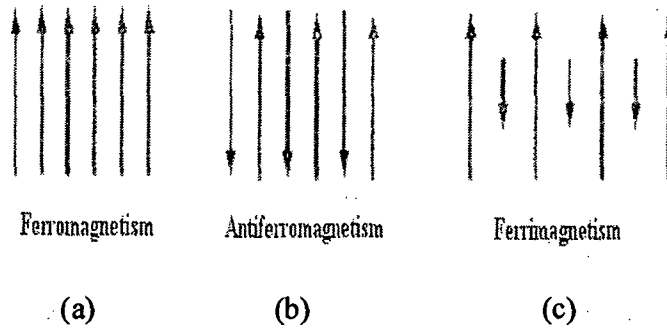


Fig.4.1. Alignment of magnetic moments.

4.1.6. SOFT AND HARD FERRITES:

Ferrites are ferrimagnetic compounds with iron oxides as the main component. They are hard and brittle like most other ceramics. In terms of their magnetic properties, the different ferrites are often classified as "soft" or "hard" ferrites, which refer to their low or high magnetic coercivity .

4.2 CHARACTERISTICS OF SOFT FERRITES:

Ferrites used in transformer or electromagnetic cores contain nickel, zinc, and/or manganese compounds. They have a low coercivity and are called soft ferrites. The low coercivity means, in such material, magnetization can easily reverse direction without dissipating much energy (hysteresis losses), while the materials' high resistivity prevents eddy currents in the core, another source of energy loss. Because of their comparatively low losses at high frequencies, they are extensively used in the cores of RF (radio frequency) transformers and inductors. Soft ferrites are also used in switched mode power supplies (SMPS). The most

common soft ferrites are manganese-zinc (with the general formula $Mn_xZn_{(1-x)}Fe_2O_4$) and nickel-zinc (with the general formula $Ni_xZn_{(1-x)}Fe_2O_4$). Ni-Zn ferrites exhibit higher resistivity than Mn-Zn ferrites, and are therefore more suitable for frequencies above 1 MHz. In comparison, the Mn-Zn ferrites have higher permeability and saturation induction.

4.2.1. MAGNETIC DOMAINS:

Weiss proposed that a magnetic material consists of physically distinct regions called domains. In a ferromagnetic domain, there is parallel alignment of the atomic moments. In a ferrite domain, the net moments of the antiferromagnetic interactions are spontaneously oriented parallel to each other (even without an applied magnetic field). The term, spontaneous magnetization or polarization is often used to describe this property. Each domain becomes a magnet composed of smaller magnets (ferromagnetic moments). Domains contain about 10^{12} to 10^{15} atoms and their dimensions are of the order of microns (10^{-4} cm.). Their size and geometry are governed by certain considerations and is dependent on the intrinsic properties of the material [7]. Domains are formed basically to reduce the magnetostatic energy which is the magnetic potential energy contained in the field lines (or flux lines as they are commonly called) connecting north and south poles outside of the material.

4.2.2. MAGNETOSTRICTION:

Ferrites change their length when they are magnetized. This small change in length is called longitudinal magnetostriction which plays an important role in domain geometry and is important in practical use of transformer materials. The incremental change may be positive or negative for different materials at saturation. Most ferrites exhibit negative incremental change except for few cases like Fe_3O_4 .

4.2.3. ANISOTROPY:

Apart from the exchange interaction between neighboring atoms, the spins have interaction with lattice atoms. The spin-lattice interaction is seen when all the spins are completely aligned and the direction of alignment is rotated relative to the crystal axis. Preferred directions of magnetic moments are then observed.

The excess work done in magnetizing a magnetic material or ferrite to saturation, in a direction which is different from the easy direction, is called crystal anisotropy and it plays an important role in determining the properties like permeability, hysteresis and magnetostriction [8].

4.2.4. HYSTERESIS:

If a demagnetized ferromagnetic or ferrimagnetic material is subjected to an external field, it gets magnetized due to the spins, as each

domain rotates parallel to the direction of the applied magnetic field until all the dipoles are aligned. And it will reach a saturation value at a certain critical field. The OABC curve is called magnetization curve as shown in Fig.4.2. The plateau region of the magnetization curve is the saturation magnetization (M_S), and it (M_S) is a measure of the magnetization (M) per gram. Its value is given by

$$M_S = M / \rho \text{ \{emu/g\}} \quad \text{----- 4.1.}$$

where, ' ρ ' is the density of the material. If the magnetizing field is reduced to zero and an increasing reverse field is applied, then, the original magnetization curve OABC is not followed but a lag (hysteresis) of the magnetization to the magnetic field occurs.

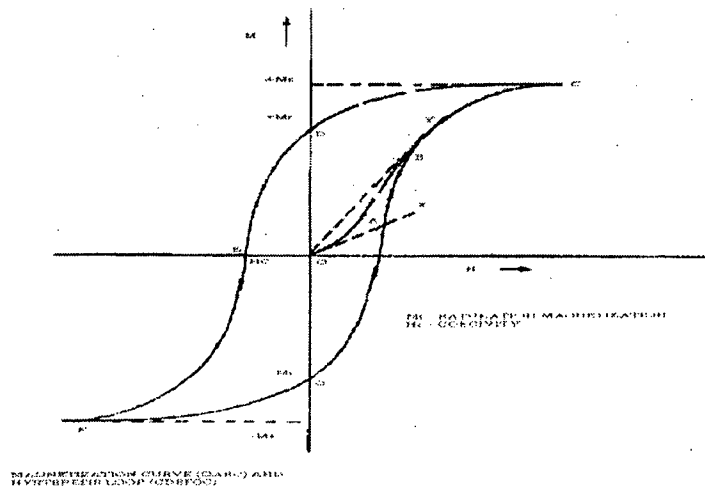


Fig.4.2. Plot of magnetization (M) versus magnetic field strength (H). ' M_S ' is the saturation magnetization, ' M_R ' is the remanance magnetization, and ' H_C ' is the coercivity in the figure.

Increasing the reverse field leads to saturation in the reverse direction, and if the field is again returned to the original direction, a complete cyclic loop CDEFGC is obtained as seen in the same Fig.4.2. The irreversibility and hysteresis in ferromagnetic material are due to the

impediments to the motion of domain walls. These impediments are the inclusions, grain boundaries, dislocations and heterogeneities which are due to other phases. The magnetization increases slowly by reversible wall motion at low fields and by irreversible wall motion above critical field and by irreversible rotation at very high field. The rotation of domains has been observed by Barkhausen [9]. The wall energy is maximum at very high field leading to irreversible increase in magneto-elastic and magneto-static energies under the action of external magnetic field. When the magnetic field is reduced to zero, the residual magnetization is retained and the opposite field is used for the reversal of domains to their original state of zero magnetization. The area inside the loop is indicative of the losses occurring due to traversal of the loop. The slope of tangent to the magnetization curve at the origin (OX) gives the magnitude of initial susceptibility χ_0 . The maximum susceptibility occurs at the knee of magnetization curve determined by the slope of OY. The smooth curve depicts the rotation of the vector moment in the domain wall as the magnetic field strength (H) is varied.

When the applied field is decreased, magnetization decreases. In multi-domain bulk materials, demagnetization occurs primarily via spin rotation through the domain walls [10, 11]. The residual magnetization (M_R) at zero applied field is remanance or retentivity. The magnetic field required to demagnetize the material completely from retentivity to zero is called [12] the coercive force (H_C). The coercive force is found to vary from 10^{-1} to 10^{+3} oersted [13].

4.2.5. A. C. SUSCEPTIBILITY:

Curie temperature is one of the most important parameters of ferrites. It is intrinsic property of the spinel ferrites, and depends on method of preparation, sintering temperature, as also on the doping by additives [14]. Rezlescu et al. [15] investigated the influence of preparation technique and cation distribution of copper manganese mixed ferrites. They observed that the migration of tetrahedral site shifts the Curie temperature to lower values. The dependence of Curie temperature on the distribution of metallic ions was suggested also by Gorter [16] and Neel [17]. Apart from the method of preparation, sintering temperature and doping by additives, the microstructure, porosity and grain size also play a dominant role in deciding the a.c. susceptibility. With respect to their magnetic properties, the ferrimagnetic materials show similarities with those of ferromagnetic. These materials show hysteresis and susceptibility below Curie temperature. A.C. susceptibility studies explore the existence of multidomain (MD), single domain (SD) and super paramagnetic (SP) particles in the material. From the susceptibility curves [18-20], the Curie temperature and the domain structure can be determined.

4.2.6. PERMEABILITY:

Permeability is one of the most important parameters used in evaluating magnetic materials. Not only is it a function of the chemical composition and crystal structure, but it is also strongly dependent on microstructure, temperature, stress, time taken for complete

demagnetization and several other factors. The permeability of the magnetic material depends on microstructural conditions and is found to be true during excitation by alternating currents and becomes extremely important at high frequencies. This is because the a. c. excitations produce rapid a movement of the magnetic domain wall and the permeability is related to the ease of movement of these walls. The presence of any imperfections in the material structure will reduce the permeability. Fewer the grain boundaries, larger will be the grains and higher the permeability, as grain boundaries act as impediments to the domain wall motion. Tebble and Craik [21] pointed out that in very high permeability metallic materials, domain walls appear to move across grain boundaries easily. In ferrites as the grain boundaries are thicker, the same kind of unhindered movement does not occur as in the case of metals. Lack of purification, presence of pores and inclusions prevent the attainment of very high permeability, which extends upto 100,000 (in the case of metals).

4.2.6.1. MODELS OF PERMEABILITY:

Different research workers have developed models of permeability to explain the behaviour of the material as regards its permeability. Some of these models are discussed in short here.

(A) TWO PINNING MODEL:

This model [22-24] is based on the assumption that a component that varies with spatial co-ordinates along the grain boundary is

responsible for permeability. The disorientation of magnetic axes of the grains gives rise to micro stress and their sources are located on the grain boundary. This results in alternation of the region with best and worst coincidence on grain boundary and the magnetostrictional deformation creates the inhomogeneous stress along grain boundary. Thus domain wall is linked near grain boundary with the regions of increased anisotropy.

$$\Delta K = (|K| - |K_i|) \quad \text{-----} \quad 4.2.$$

(B) GLOBUS MODEL:

The model developed by Globus [25, 26] is based on the reversible motion of domain walls, under a very small magnetic field, giving rise to the initial permeability in the material and it considers the contribution of the spin rotation as rather negligible. In this model the domain wall is pinned at the grain boundaries and they bulge under the application of magnetic field until the critical field is reached, when the wall gets unpinned. Such a model can be extended to the cases where the domain walls are pinned at inter- granular pores. In such a model

$$(\mu_i - 1) = 3 Ms^2 D / 16 \gamma \quad \text{-----} \quad 4.3.$$

where M_s is saturation magnetization, D is grain diameter and γ is domain wall energy per unit area as $\gamma \sim \sqrt{AK_1}$

$$\mu_i = Ms^2 D / |K_1| \quad \text{-----} \quad 4.4.$$

Such a model can be extended to the case where the domain walls are pinned at intergranular pores i.e. span of domain wall.

Further, Globus and Co-workers [25, 27] felt that, in polycrystalline ferrites the magnetization mechanism may be different due to the granular structure of ferrites. They have developed a model in which bulging of domain wall by 180° is responsible for the initial permeability rather than the domain wall displacement.

(C) NON MAGNETIC GRAIN BOUNDARY MODEL:

Johnson [28] developed the non-magnetic grain boundary model, which can explain the entire grain size dependence of μ_i (initial permeability) at low anisotropy as the Globus model cannot account for grain size dependence of permeability when inter granular domain walls are absent. This model describes the grain size dependence of rotational permeability in polycrystalline materials [29]. According to this model there is almost a linear dependence of permeability on the grain size for fine grained polycrystals, where $D \ll \mu_i \delta$.

It is given by the relation

$$\mu_e = \mu_i D / (\mu_i \delta + D) \quad \text{-----} \quad 4.5.$$

where μ_e = effective permeability, μ_i = complex (initial) permeability, D = grain size, δ = grain boundary thickness.

For larger grain size where $D \gg \mu_i \delta$, the model predicts constant rotational permeability equivalent to that in single crystal of the same material i.e. $\mu_e \approx \mu_i$.

4.2.6.2. DEPENDENCE OF INITIAL PERMEABILITY:

(A) MICROSTRUCTURE DEPENDENCE:

Microstructure plays a very important role in deciding the magnetic properties of materials because of fine grains where there is reversal of magnetization by rotation, since the domain walls are energetically favorable in fine grains. The initial permeability is dependent on grain size, density and porosity. Porosity causes hindrance to domain wall motion and it decreases initial permeability [30]. Also the coercive force increases with porosity because of internal demagnetizing field where the decrease in permeability is caused by same reason. The larger grain size causes reduction in initial permeability due to the presence of voids that induce demagnetizing field and creates impediments for domain wall motion. Therefore the grain size is a very important parameter in the permeability. A duplex structure is undesirable because it lowers the permeability. It is often due to particle impurity, which produces rapid growth locally, while other impeded areas are unaffected [31, 32].

(B) TEMPERATURE DEPENDENCE:

Temperature dependence of initial permeability is one of the important parameter in a magnetic component. From the graph of variation of initial permeability with temperature, the slope at a specific temperature can be expressed as a material parameter called the temperature factor (T.F.) which is defined as

$$\text{T.F.} = \Delta\mu/\mu^2 \Delta T \quad \text{-----} \quad 4.6.$$

where, $\Delta\mu$ is the difference in permeability ($\mu_2-\mu_1$) between the two temperatures, T_2 and T_1 respectively, while ΔT is the difference in temperature.

The temperature factor can be used to predict the variation in magnetic properties of a magnetic component. A thermal hysteresis is observed when temperature is cycled from higher temperature above T_C to lower temperature. This is explained by taking into account the domain wall pinning component between the intrinsic parameter M_S and K_1 around the transition point [33].

(C) FREQUENCY DEPENDENCE:

At low frequencies, permeability is almost independent of frequency, as the domain wall motion is dominant mechanism. Also at low frequencies, the applied field causes domain wall shift and this motion results in change in net magnetization. The domain structure is responsible for high frequency permeability. At high frequencies, the domain wall inertia precludes any appreciable wall motion but the mechanism can rotate within each domain. This mechanism is same as ferromagnetic resonance. Smit and Wijn [34] have explained the extension of the loss over a relatively broad frequency region in terms of additional effects upon the resonance condition due to demagnetizing field in the domain structure.

Various magnetic properties viz saturation magnetization, a. c. susceptibility and initial permeability of Mn-Zn ferrite samples, prepared by the mechano-chemical method and the wet chemical method, were studied.

4.3. EXPERIMENTAL MEASUREMENT:

Saturation magnetization, AC susceptibility and permeability measurements of the samples prepared by both the methods, namely, the mechano-chemical method and the wet chemical method were done by the instruments described in Chapter Two. Experimental procedures employed in the measurements are discussed below.

4.3.1. SATURATION MAGNETIZATION:

Sample preparation:

Powdered samples of $Mn_xZn_{(1-x)}Fe_2O_4$ synthesized by mechano-chemical and wet chemical methods were pressed into pellets of the size 1.0 cm in diameter and of thickness ranging between 2mm-3mm under a pressure of 75KN applied for about 5 minutes. Four sets of pellets were sintered in nitrogen atmosphere at temperatures; 1000⁰C, 1100⁰C, 1200⁰C and 1300⁰C, respectively, for 4 hours separately in a programmable Carbolite furnace model STF 15/180, with a heating and cooling rate of 5⁰C min⁻¹.

Measurement:

The saturation magnetization measurements of the samples were carried out using a high field hysteresis loop tracer supplied by Magneta India, Mumbai. This instrument works on the principle that high magnetic field is generated in a solenoid by passing a pulse current of sinusoidal shape. A pickup coil system is kept in the solenoid to detect field and the magnetization signal of a sample placed in the pickup coil. The signals produced are then processed by an electronic system. These transitory signals are digitized by a micro- controller and then sent to computer for plotting a hysteresis loop, which is observed on the monitor with calculated values of hysteresis parameters. The applied magnetic field was of 5 KOe. The magnetization sensitivity: was of 10 EMU. The accuracy of measurement was in the range of 95-100 %.

The calibration of the instrument was carried out using pure nickel as a standard having magnetization- 53.34 emu/g.

Magnetic measurements were also carried out by using vibrating sample magnetometer (VSM) OXFORD (Oxford Instruments) Mag LabVSM.

4.3.2. A. C. SUSCEPTIBILITY:

A.C. susceptibility measurements of the unsintered as well as sintered samples were made using computerized pulse field A. C. susceptibility apparatus described by Likhite et al. [35]. The apparatus consists of Helmholtz coil, two pick-up coils, furnace, sample holder, temperature measuring device, control unit, data acquisition system, power supply to run the furnace and PC with related software to execute the run cycle. The Helmholtz coil is powered to produce pulsating magnetic field. To avoid the over heating of coils, a glass jacket with water circulation was used. In a typical experiment, 0.5 g of the Mn-Zn ferrite powder was placed in the sample holder, a quartz tube fused at one end, which was then inserted in glass jacket and placed at the centre of the pick-up coil for uniform heating. The data, that is, magnetization (emu/g) as a function of temperature collected by the data acquisition system was directly saved in a file on the PC simultaneously showing the progress of the experiment by way of a graph on the PC monitor. The temperature of the furnace was maintained by a power supply and was measured by using platinum rhodium thermocouple. It is a regulated digital power supply whose voltage and current are varied automatically by the PID temperature controller output which can be programmed for a set temperature and a set heating rate. The magnetic moments were recorded at various temperatures, while the sample was heated to the preset heating rate. The heating was continued till the magnetization (emu/g) signal reduced to zero. This happens when the Curie temperature is attained.

4.3.3. INITIAL PERMEABILITY:

Sample preparation:

Magnetic permeability measurements were carried out on the torroids which had a winding of 100 turns of super enameled doubly insulated copper wire of 33 gauge. For this purpose, each powdered sample was pressed into a torroid with inner and outer diameter of 1 cm and 2 cm, respectively, with thickness ranging between 3-4 mm by applying a pressure of 75KN for about 5 minutes. The torroids were sintered at 1000⁰C, 1100⁰C, 1200⁰C and 1300⁰C in nitrogen atmosphere for 4 hours with a heating and cooling rate of 5⁰C min⁻¹.

Measurement:

The initial permeability and loss factor as a function of frequency and temperature were measured by recording the inductance and dissipation factor (tan δ) values starting from room temperature to 500⁰C and with frequency variation from 20Hz to 1MHz using LCRQ meter.

The initial permeability (μ_i) was calculated from the formula

$$L=0.0046\mu_i N^2 h \ln (OD/ID) \quad \text{-----} \quad 4.7.$$

where 'L' is inductance in Henry, 'N' is the number of turns of copper wire on torroid, 'h' is the height of the core in meters, OD and ID are the outer and the inner diameters of torroid in meters, respectively.

4.4. RESULTS AND DISCUSSION:

The results obtained in the study of the magnetic properties of the Mn-Zn ferrite samples, prepared by two different methods as stated earlier, are tabulated and discussed in the following Sections. These ferrite samples are found to be nanomaterials having the particle sizes in the range 10-67 nm.

4.4.1. SATURATION MAGNETIZATION:

Ferrite samples prepared by mechano-chemical method:

The variation of the saturation magnetization with Mn contents for the Mn-Zn ferrite samples of various compositions, prepared by the mechano-chemical method, is given in Table 4.1. It can be observed that the maximum value for saturation magnetization (M_s) was 50.91 emu/g for the unsintered $Mn_{0.625}Zn_{0.375}Fe_2O_4$ sample. The value of M_s decreases for all the samples when sintered at 1000°C. Saturation magnetization of $Mn_{0.7}Zn_{0.3}Fe_2O_4$ was found to be 22.53 emu/g, which was the highest as compared to all the samples sintered at this temperature. On further sintering of the samples, at 1100°C and beyond, the saturation magnetization values showed an increasing trend with the highest value shown by $Mn_{0.675}Zn_{0.325}Fe_2O_4$ sample being 44.57 emu/g. However, the maximum value of M_s at 1200°C was 63.39 emu/g for $Mn_{0.675}Zn_{0.325}Fe_2O_4$ whereas at 1300°C it was 68.59 emu/g for $Mn_{0.65}Zn_{0.35}Fe_2O_4$. Fig.4.3 and Fig.4.4 (a), (b) and (c) illustrate the variation of saturation magnetization

of Mn-Zn ferrite samples with the amount of Mn for different sintering temperatures.

Table 4.1. Saturation magnetization values of unsintered and sintered Mn-Zn ferrite samples, of various compositions, obtained by the mechano-chemical method.

Composition	Saturation magnetization values (emu/g)				
	Unsintered	Sintered 1000 ^o c	Sintered 1100 ^o c	Sintered 1200 ^o c	Sintered 1300 ^o c
Mn _{0.4} Zn _{0.6} Fe ₂ O ₄	16.68	12.63	18.58	22.15	28.99
Mn _{0.5} Zn _{0.5} Fe ₂ O ₄	28.20	7.92	24.15	27.62	29.96
Mn _{0.6} Zn _{0.4} Fe ₂ O ₄	39.47	11.92	35.22	55.08	52.86
Mn _{0.625} Zn _{0.375} Fe ₂ O ₄	50.91	9.50	38.30	52.70	41.13
Mn _{0.65} Zn _{0.35} Fe ₂ O ₄	45.46	11.37	40.46	58.27	68.59
Mn _{0.675} Zn _{0.325} Fe ₂ O ₄	43.90	18.75	44.57	63.39	53.60
Mn _{0.7} Zn _{0.3} Fe ₂ O ₄	32.35	22.53	29.64	28.42	38.48

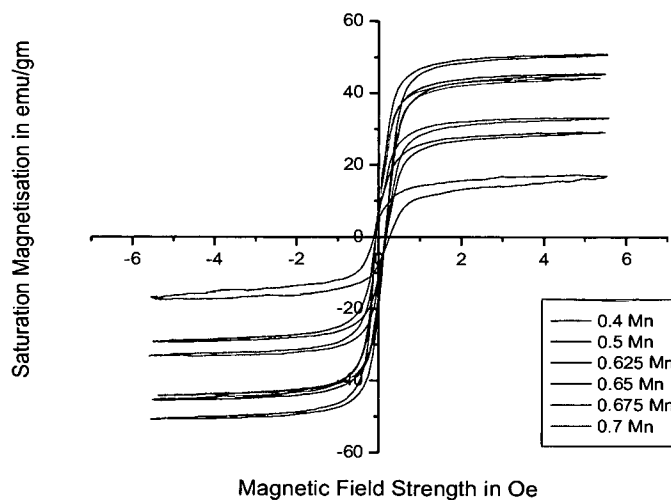


Fig.4.3. Variation of saturation magnetization value of Mn-Zn ferrite unsintered samples with Mn contents, prepared by the mechano- chemical method.

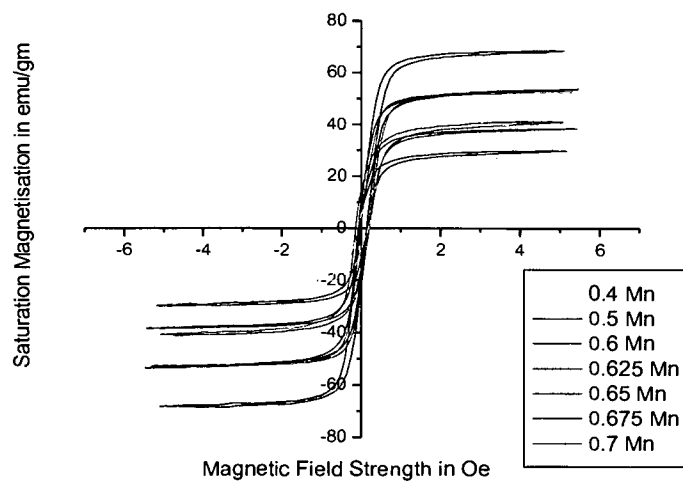
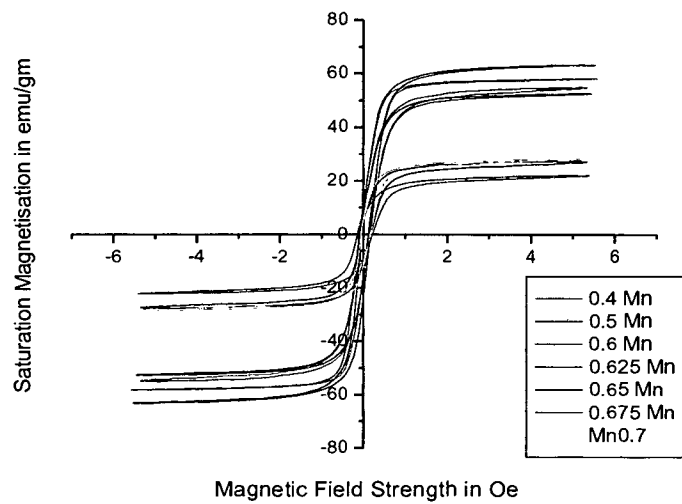
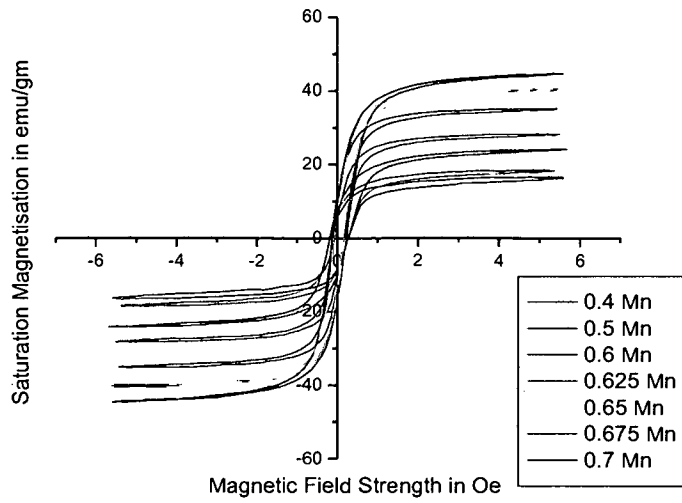


Fig.4.4. Variation of saturation magnetization of Mn-Zn ferrite samples, with Mn contents sintered at (a)1100°C (b) 1200°C and (c) 1300°C.

Ferrite samples prepared by wet chemical method:

For the samples synthesized by the wet chemical method, the variation of the saturation magnetization with Mn contents is given in Table 4.2. The saturation magnetization values for unsintered samples were found to be lower when compared with the samples prepared by the mechano-chemical method. The highest value of M_S being 43.66 emu/g, for the $Mn_{0.7}Zn_{0.3}Fe_2O_4$ sample. When sintered at $1000^{\circ}C$, the Mn-Zn ferrite samples prepared by the wet chemical method were found to show a similar trend as observed in the case of samples from the mechano-chemical method. Initially, there was a decrease in the saturation magnetization value for all the samples. The maximum M_S value of 22.37 emu/g was observed in the case of $Mn_{0.675}Zn_{0.325}Fe_2O_4$ sample. When the samples were further sintered at temperatures $1100^{\circ}C$, $1200^{\circ}C$ and $1300^{\circ}C$, increase in the saturation magnetization at each higher temperature was observed. And the maximum value of M_S was found to shift from $Mn_{0.65}Zn_{0.35}Fe_2O_4$ to $Mn_{0.625}Zn_{0.375}Fe_2O_4$ and to $Mn_{0.675}Zn_{0.325}Fe_2O_4$ with values being 42.86 emu/g, 61.63 emu/g and 68.36 emu/g, respectively, at three sintering temperatures. Fig.4.5. and Fig.4.6. (a) and (b) show variation of saturation magnetization of Mn-Zn ferrite samples with amount of Mn for different sintering temperatures.

Table 4.2. Saturation magnetization values of unsintered and sintered Mn-Zn ferrite samples, of various compositions, obtained by the wet chemical method.

Composition	Saturation Magnetization (emu/g)				
	Unsintered	Sintered 1000 ^o c	Sintered 1100 ^o c	Sintered 1200 ^o c	Sintered 1300 ^o c
Mn _{0.4} Zn _{0.6} Fe ₂ O ₄	14.93	8.25	20.73	32.53	28.36
Mn _{0.5} Zn _{0.5} Fe ₂ O ₄	17.40	6.56	19.31	38.65	39.54
Mn _{0.6} Zn _{0.4} Fe ₂ O ₄	21.06	14.95	28.66	49.23	44.21
Mn _{0.625} Zn _{0.375} Fe ₂ O ₄	34.08	20.61	37.18	61.63	54.84
Mn _{0.65} Zn _{0.35} Fe ₂ O ₄	27.41	11.40	42.86	52.17	53.09
Mn _{0.675} Zn _{0.325} Fe ₂ O ₄	39.99	22.37	39.09	42.56	68.36
Mn _{0.7} Zn _{0.3} Fe ₂ O ₄	43.66	17.94	26.41	36.67	42.27

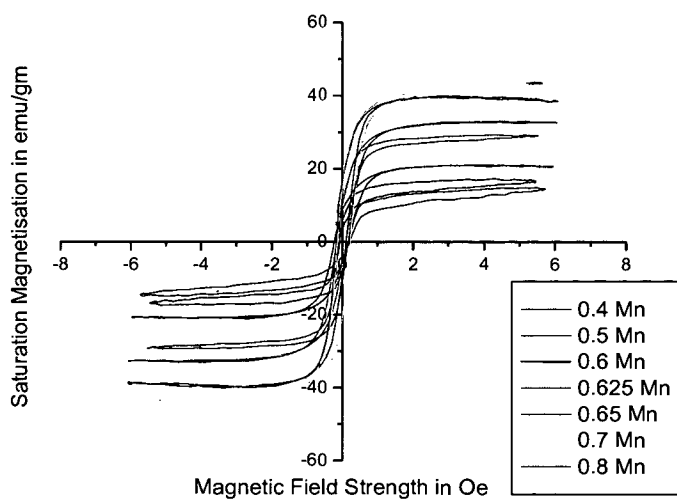
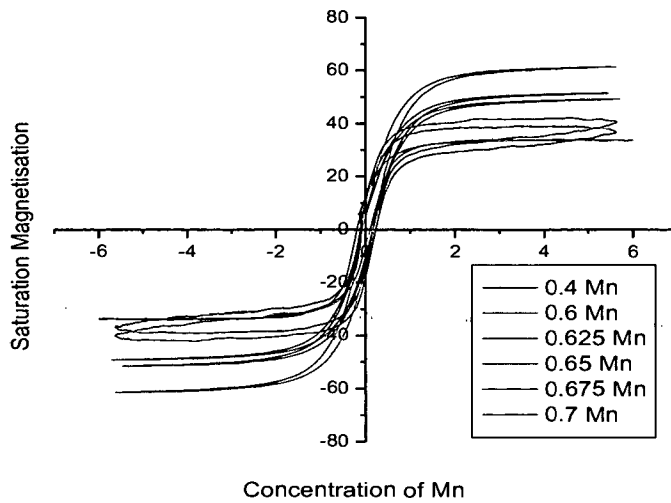
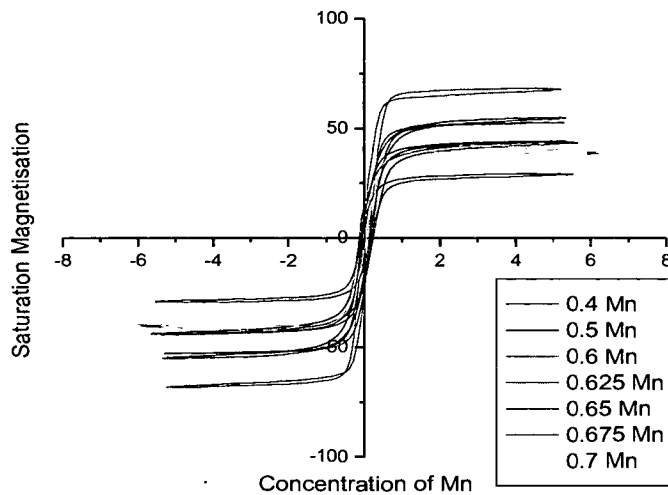


Fig.4.5. Variation of saturation magnetization of Mn-Zn ferrite unsintered samples, with Mn contents, prepared by the wet chemical method.



(a)



(b)

Fig.4.6. Variation of saturation magnetization of Mn-Zn ferrite samples, with Mn contents sintered at (a) 1200^oC and (b)1300^oC.

Zinc ferrite, $ZnFe_2O_4$, is a normal spinel, and the unit cell has no net magnetic moment ($ZnFe_2O_4/Zn^{2+} [Fe^{3+}Fe^{3+}]O_4/d^0[d^5d^5]$). In contrast, the manganese ferrite is an inverse spinel and, consequently, the two magnetic sublattices are antiferromagnetically aligned ($MnFe_2O_4/Fe^{3+}[Mn^{2+}Fe^{3+}]O_4/d^5[d^5d^5]$). When the nonmagnetic zinc

ion (d^{10}) is substituted into the manganese ferrite lattice, it has a stronger preference for the tetrahedral site than does the ferric ion and thereby reducing the amount of Fe^{3+} on the A site. Because of the antiferromagnetic coupling, the net result is an increase in magnetic moment on the B lattice and an increase in saturation magnetization. Therefore the addition of nonmagnetic zinc ferrite to the inverse spinel manganese ferrite raises the saturation magnetization in Mn–Zn ferrite. However, the change in the magnetic properties of Mn–Zn ferrites depends on the solubility of cations (Mn^{2+} or Zn^{2+}) in the ferrite lattice and the occupying positions of tetrahedral or octahedral sites.

On the other hand, magnetic properties of the ferrites depend on the microstructure [36, 37]. The microstructure of the ferrite is determined by a variety of factors such as: raw material quality, sintering temperature, sintering time and material composition. This fact is very important because the microstructures developed during sintering are determined, to a large extent, by the powder's characteristics namely crystallite size, shape, size distribution, porosity, state of agglomeration, chemical and phase composition, which are closely associated with the preparation method.

Various investigators [38, 39] have studied the saturation magnetization values for Mn–Zn ferrites and have observed that the saturation magnetization is the highest for the samples when the Mn content is around 0.8 in the Mn–Zn ferrites. The changes in the magnetic

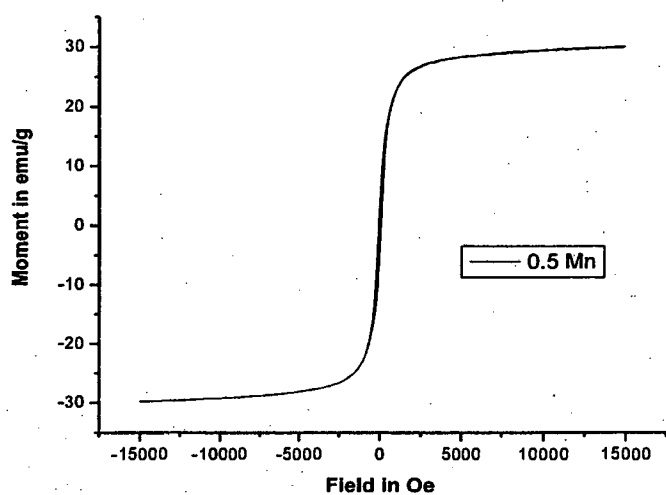
properties, due to sintering of the nano sized Mn–Zn ferrites at various temperatures, are because of the influence of cationic stoichiometry and their occupancy in the specific sites. In addition, it is also due to the formation of dead layers on the surfaces, existence of random canting of particle surface spins, non-saturation effects caused by a random distribution of particle size and deviations from the normal cation distribution [40].

A decrease in the coercivity value H_C was observed for higher sintering temperatures of the samples as well as for increased Mn value. This decrease can be attributed to an increase in grain size and the decrease in porosity of the samples.

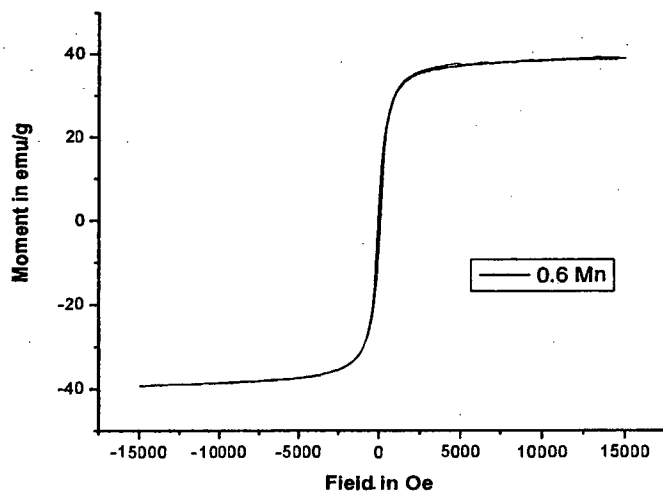
For most of the unsintered samples, the values of retentivity (M_R) and the coercivity (H_C) were found to be higher indicating single domain (SD) behavior of the samples, whereas on sintering the samples beyond 1200°C the values of retentivity M_R and the coercivity H_C were found to be lower pointing towards multi domain (MD) behavior of the samples. The hysteresis losses were found to be low for the unsintered as well as for the sintered samples and were found to depend on the amount of Mn and the sintering temperature.

In the present investigation, from among all the samples prepared by mechano-chemical method as well as wet chemical method, sintered (at higher temperature) at 1100°C , 1200°C and 1300°C , the maximum value of

M_s was found for the samples with Mn contents ('x' value) around 0.65. Saturation magnetization and hysteresis study was also carried out on VSM and the results obtained confirm of the low loss in the magnetic behaviour. The VSM results are illustrated in Fig. 4.7., and Fig.4.8.

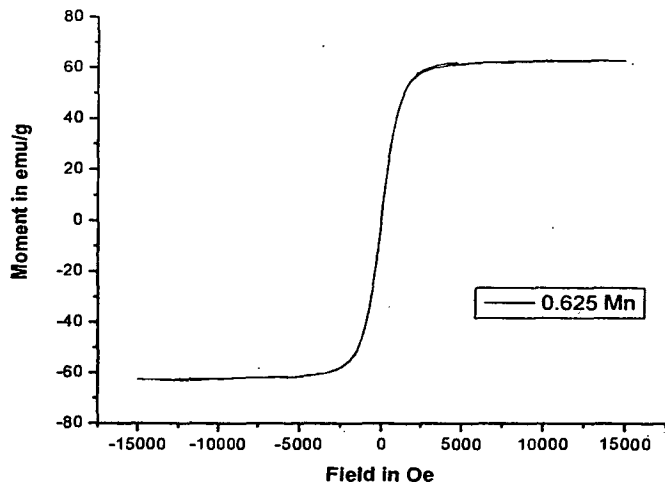


(a)

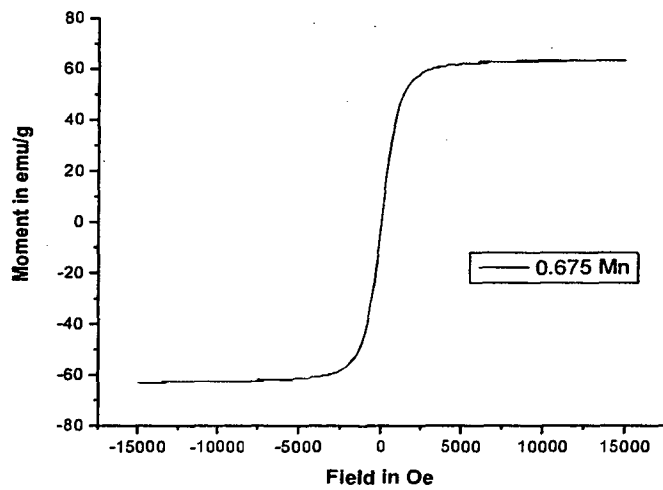


(b)

Fig. 4.7. Magnetic hysteresis curves obtained by VSM at room temperature for unsintered samples (a) $Mn_{0.5}Zn_{0.5}Fe_2O_4$ and (b) $Mn_{0.6}Zn_{0.4}Fe_2O_4$, for the mechano-chemical method.



(c)



(d)

Fig. 4.8. Magnetic hysteresis curves obtained by VSM at room temperature for (c) $\text{Mn}_{0.625}\text{Zn}_{0.375}\text{Fe}_2\text{O}_4$ sintered at 1200°C and (d) $\text{Mn}_{0.675}\text{Zn}_{0.325}\text{Fe}_2\text{O}_4$ sintered at 1300°C for the wet chemical method.

4.4.2. A.C. SUSCEPTIBILITY:

Ferrite samples prepared by mechano-chemical method:

The variation of the Curie temperature with increasing Mn content in unsintered Mn-Zn ferrite samples prepared by the mechano-chemical method is given in Table 4.3. It can be seen that, there was a systematic increase in the value of the Curie temperature (T_C) from 447K for $Mn_{0.4}Zn_{0.6}Fe_2O_4$ to 603K for $Mn_{0.8}Zn_{0.2}Fe_2O_4$ as the manganese amount increases in these ferrites [41]. This is due to the substitution of non-magnetic Zn^{2+} ions by the magnetic Mn^{2+} ions in the samples. The value of T_C was found to be higher in the case of the ultrafine powder than that in bulk ferrites. This is due to the deviation of cation distribution in a nanosized particle as in comparison with its bulk counterparts [42].

In general, magnetic properties are controlled by exchange interaction of the metallic ions on the two interactive sub-lattices A and B. The change in T_C may be positive or negative depending on the boundaries, the geometry, and the interaction. It is also possible that T_C decreases due to some unknown surface effect. For small particles a significant fraction of atoms are on the surface, and it is reasonable to expect their magnetic interactions to be different. As such, a different average Curie temperature [43] is observed. The graph of the variation of the magnetization with temperature for each sample with different Mn content is shown in Fig. 4.9 and Fig. 4.10. Chandana Rath et al. in 2002 [42] and others [44, 45] observed a cusp (i.e. the magnetization increased beyond a

point instead of approaching zero) in some specific compositions among many samples of Mn-Zn ferrite.

In our present study of variation of Curie temperature of Mn-Zn ferrite, a small cusp was observed for the samples as can be seen from Fig. 4.9. The nature of the M_S versus T plots of the samples indicates near single domain behavior.

When the samples were sintered at 1100°C and 1300°C , the Curie temperature was found to decrease for all the samples. The decrease in this value of T_C was due to the increase in the grain size from initial nano-size, on sintering, changing to the bulk, which allows redistribution of cations to occupy their preferential site. T_C values were found to be in the range 413K to 588K for the samples sintered at 1100°C . For the samples sintered at 1300°C , the T_C further decrease, and the values were in the range 354K to 549K. The samples thus show a multidomain behavior as can be seen from the Fig. 4.10.

Table 4.3. Curie temperature of unsintered and sintered Mn-Zn ferrite samples obtained by the mechano-chemical method.

Composition	Temperature (K)		
	Unsintered	Sintered 1100°C	Sintered 1300°C
$\text{Mn}_{0.4}\text{Zn}_{0.6}\text{Fe}_2\text{O}_4$	447	413	354
$\text{Mn}_{0.5}\text{Zn}_{0.5}\text{Fe}_2\text{O}_4$	520	442	366
$\text{Mn}_{0.6}\text{Zn}_{0.4}\text{Fe}_2\text{O}_4$	534	467	402
$\text{Mn}_{0.7}\text{Zn}_{0.3}\text{Fe}_2\text{O}_4$	551	513	468
$\text{Mn}_{0.8}\text{Zn}_{0.2}\text{Fe}_2\text{O}_4$	603	588	549

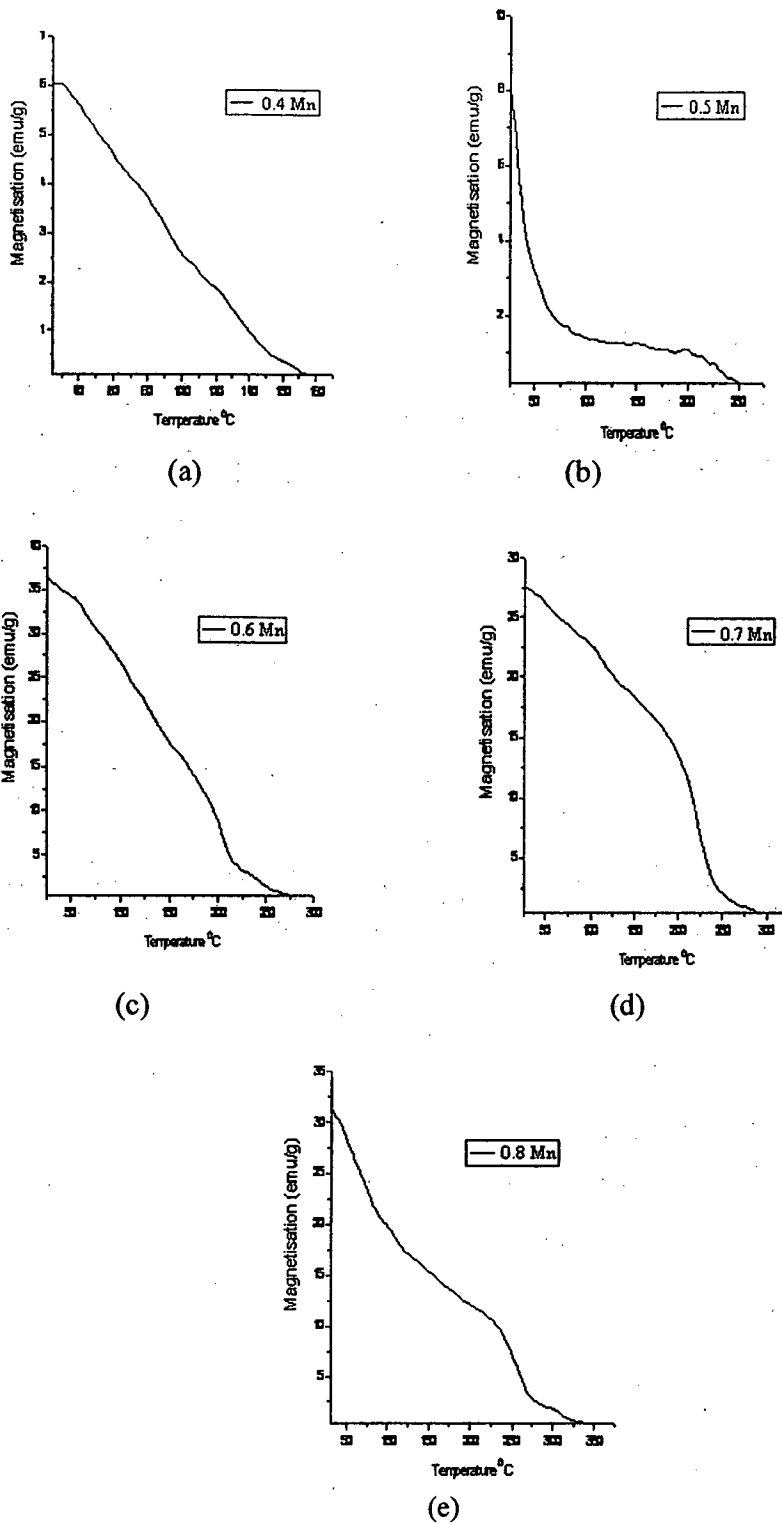
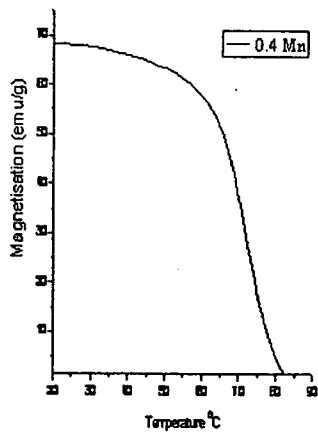
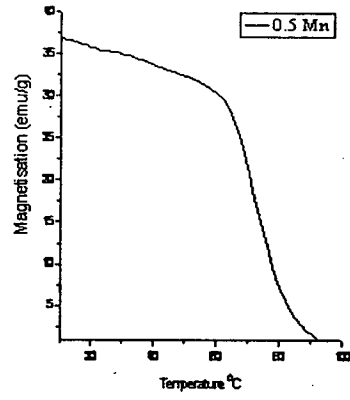


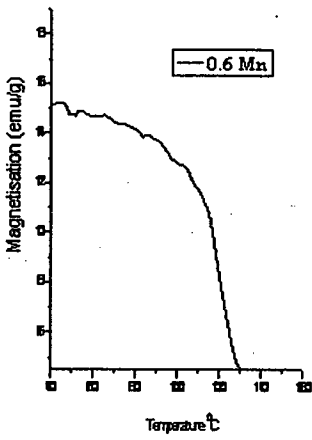
Fig.4.9. Curie temperature for various unsintered Mn-Zn ferrites samples with different Mn content, prepared by the mechano-chemical method.



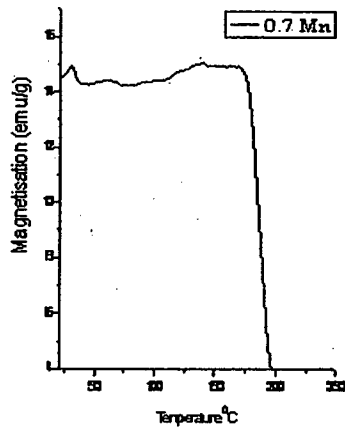
(a)



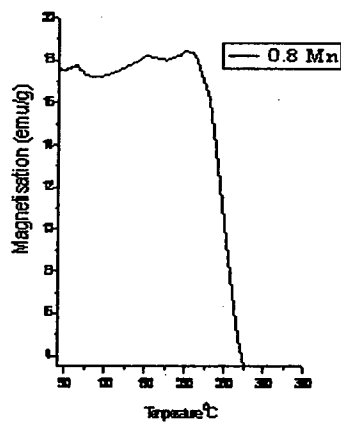
(b)



(c)



(d)



(e)

Fig.4.10. Curie temperature for various Mn-Zn ferrite samples with different Mn content sintered at 1300°C, prepared by the mechano-chemical method.

Ferrite samples prepared by wet chemical method:

Similarly, the Curie temperature for Mn-Zn ferrite samples prepared by the wet chemical method varies with increasing Mn content as can be seen in Table 4.4. For the same composition, the Curie temperature was marginally higher than that for the samples prepared by mechano-chemical method in the range from 481K for $Mn_{0.4}Zn_{0.6}Fe_2O_4$ to 628K for $Mn_{0.8}Zn_{0.2}Fe_2O_4$

The graph of variation of the magnetization with temperature for Mn-Zn ferrite samples for different compositions of Mn is shown in Fig. 4.11. Cusp for the samples with Mn proportion of 0.7 and 0.8 is pronounced in the figure. When the samples are sintered at $1100^{\circ}C$ and $1300^{\circ}C$, invariably, the Curie temperature is found to decrease for all the samples. The decrease in the T_c can again be attributed to the increase in the grain size, on sintering, to form the bulk material. This allows stable cation, redistribution of Mn^{2+} , Zn^{2+} and Fe^{3+} in their preferential site. T_c was found to be in the range of 446K to 609K for the samples sintered at $1100^{\circ}C$, whereas for the samples sintered at $1300^{\circ}C$, the T_c further decrease to the range 378K - 563K.

Table 4.4. Curie temperature of Mn-Zn ferrite sample of various composition, obtained by the wet chemical method.

Composition	Temperature (K)		
	Unsintered	Sintered 1100 ⁰ c	Sintered 1300 ⁰ c
Mn _{0.4} Zn _{0.6} Fe ₂ O ₄	481	446	378
Mn _{0.5} Zn _{0.5} Fe ₂ O ₄	509	463	390
Mn _{0.6} Zn _{0.4} Fe ₂ O ₄	578	542	459
Mn _{0.7} Zn _{0.3} Fe ₂ O ₄	613	575	513
Mn _{0.8} Zn _{0.2} Fe ₂ O ₄	628	609	563

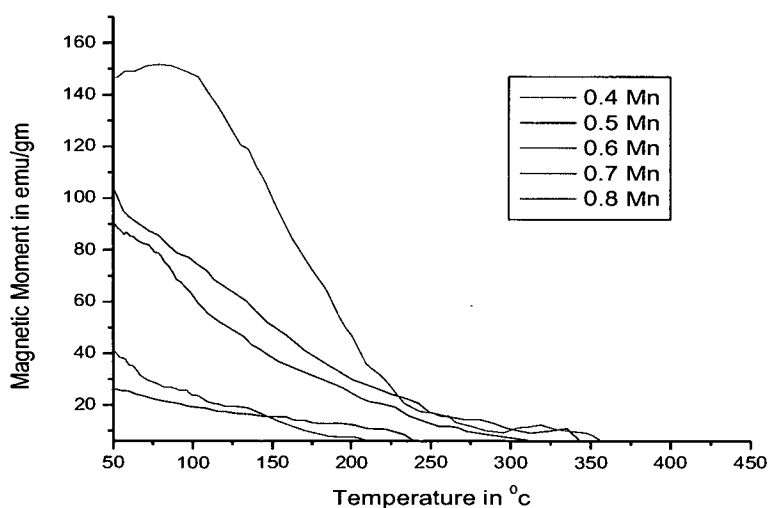


Fig.4.11. Curie temperature for various unsintered Mn-Zn ferrite samples with different Mn content, prepared by the wet chemical method.

4.4.3. PERMEABILITY:

The variation of permeability with temperature at frequency 20 Hz for the samples prepared by the mechano-chemical method sintered at 1000⁰C, 1100⁰C, 1200⁰C and 1300⁰C is shown in Fig. 4.12 (a), (b), (c) and (d). It is observed that the initial permeability slowly increases, reaches a certain peak value at a specific temperature and drops gradually to zero at

Curie temperature. The increase in permeability with temperature is due to the fact that the anisotropy decreases faster with temperature than the saturation magnetization. However, most of the samples sintered at 1000⁰C show two peaks. The peak at the far right drops to zero at the Curie point when ferrimagnetism is lost. The peak to the left is called the secondary maximum of permeability (SMP). This peak most often occurs close to the temperature at which the magnetostriction goes through zero. In 1957, Guillaud has shown [46] the existence of secondary maxima of permeability for Mn-Zn ferrite. Lescroel and Pierrot (1960) have reported that many manganese ferrites containing ferrous ions have a secondary permeability maxima [47].

For the samples sintered at this temperature (1000⁰C), the initial permeability (μ_i) of $Mn_{0.5}Zn_{0.5}Fe_2O_4$ is 1791 at 120⁰C and secondary maximum of permeability is at 60⁰C. However, the highest value of μ_i equal to 2433 at SMP of 170⁰C and curie peak of 210⁰C was observed in the case of $Mn_{0.675}Zn_{0.325}Fe_2O_4$, among all the samples sintered at this temperature. The Curie temperature values for various Mn-Zn ferrite samples were found to be in the range 240⁰C to 380⁰C.

When the samples were sintered at 1100⁰C, $Mn_{0.4}Zn_{0.6}Fe_2O_4$ was found to show permeability value of 4522 at 100⁰C, while, within the series $Mn_{0.65}Zn_{0.35}Fe_2O_4$ has the highest value of permeability i.e. 9202 at 120⁰C. A few samples show the secondary maximum of permeability at this sintering temperature.

In the case of $\text{Mn}_{0.625}\text{Zn}_{0.375}\text{Fe}_2\text{O}_4$, when sintered at 1200°C , the samples showed highest value of initial permeability equal to 15234 at 100°C . Similarly, $\text{Mn}_{0.6}\text{Zn}_{0.4}\text{Fe}_2\text{O}_4$ was found to have the value of 16183 at 90°C for the samples sintered at 1300°C . The Curie temperature was found to decrease from about 180°C to about 150°C as the sintering temperature increased from 1200°C to 1300°C .

Chikazumi (1964) co-related permeability to saturation magnetization. He suggested [48] that both the permeabilities, due to the domain rotation and that in turn, the domain wall movement, are in one manner or another related to $(M_s)^2$. It is not surprising therefore to find the higher permeabilities in ferrites in the higher saturation Mn-Zn ferrites as compared to the others. Of course, low anisotropy and magnetostriction, are also responsible for the same. Keluskar et al. [49] have found the initial permeability values for Mn-Zn ferrite samples to be more than 25000. Also manganese-zinc ferrites certainly have higher permeabilities at low or medium frequencies. When the frequencies involved are in the upper megahertz range, the permeability drops off due to the higher increase in the losses.

In 1966, Roess, Beer and Schwartz [50, 51] and later on Perduijn and Peloschek, [52] have confirmed the linear dependence of grain size to permeabilities. The relationship between grain size and permeability will generally be linear only if the grain growth is normal, that is if all the grains grow almost at the same rate and same time. This leads to a rather

narrow range of final grain sizes. If, indeed, some grains grew very rapidly, they would trap pores, which can limit the permeability by pinning domain walls. When conditions permit this type of grain growth to occur, with many intragranular pores included, it is called exaggerated or discontinuous grain growth.

Drofenik [53, 54] has reported results that indicate that the distances between the pores account for variations in permeability. Samples with giant grains and included porosity owing to exaggerated grain growth still had higher permeabilities than those with normally grown grains, provided the distances between pores were the same. Drofenik concludes that the large grained samples are less sensitive to grain boundary effects and thus the μ_i versus T curve is more peaked.

SEM micrographs of two samples prepared by mechano-chemical method are given in Fig.4.13. and Fig.4.14. The morphology of $Mn_{0.6}Zn_{0.4}Fe_2O_4$ sample (Fig. 4.13.) and that of $Mn_{0.5}Zn_{0.5}Fe_2O_4$ (Fig. 4.14.) at various temperatures is clearly visible. These ferrite powders have particle size in the range 20-90nm before sintering. However, the particle size increases gradually, as the sample is subjected to heating from 1000^oC upwards. SEM data for samples heated at 1000, 1100 °C, 1200 °C and 1300 °C show normal uniform crystalline growth for almost all the particles visible in the micrographs, with very little aberration. In the present studies, it is observed that the permeability of the samples

increases with the sintering temperature indicating that there is uniform compact growth of the particles.

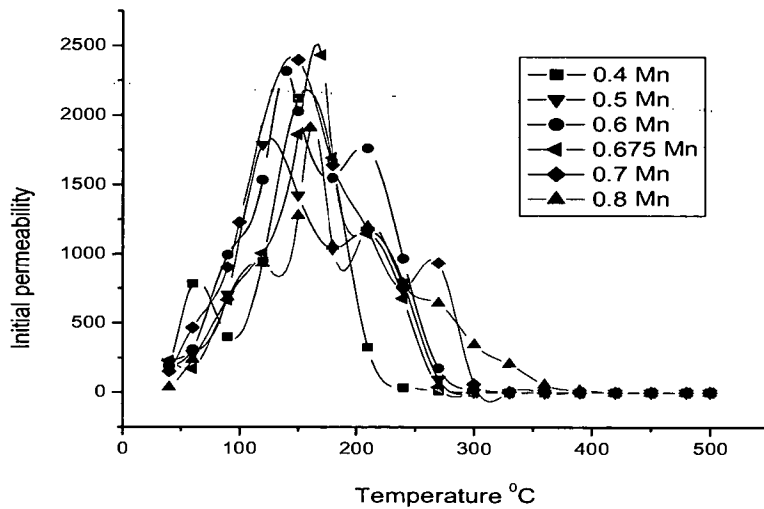


Fig. 4.12.(a). Variation of magnetic permeability of Mn-Zn ferrite with temperature for sintered (1000°C) samples obtained by mechano-chemical method.

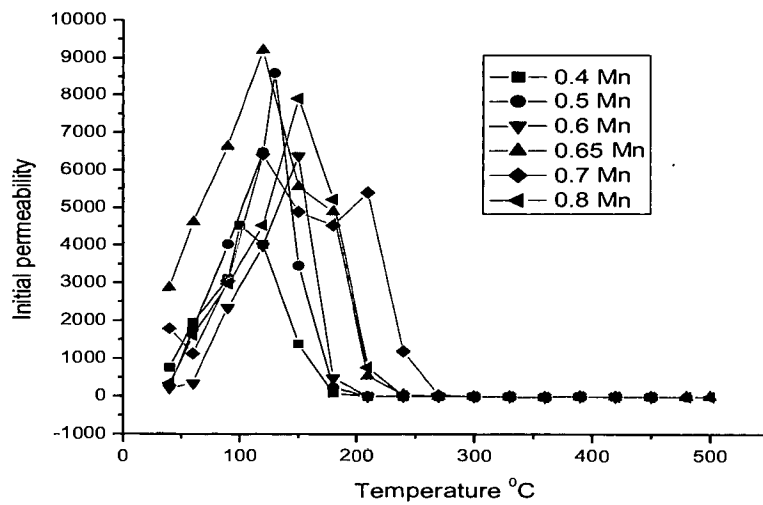


Fig. 4.12.(b). Variation of magnetic permeability of Mn-Zn ferrites with temperature for sintered (1100°C) sample obtained by mechano-chemical method.

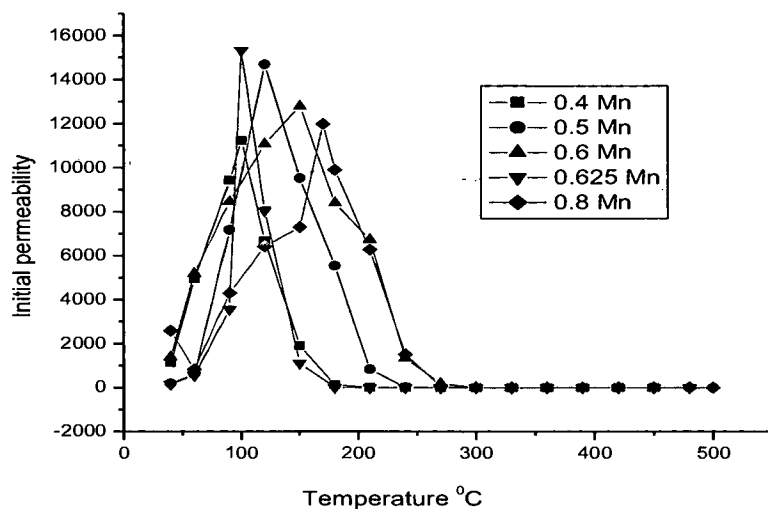


Fig.4.12.(c). Variation of magnetic permeability of Mn-Zn ferrites with temperature for sintered (1200°C) sample obtained by mechano-chemical method.

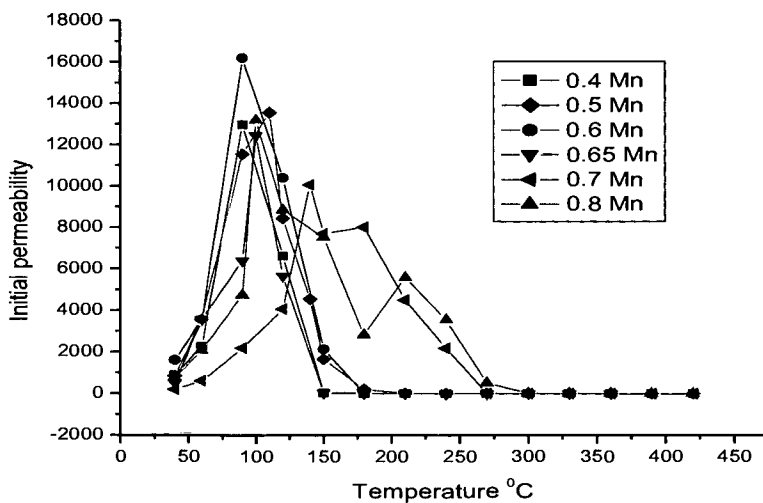


Fig .4.12.(d). Variation of magnetic permeability of Mn-Zn ferrites with temperature for sintered (1300°C) sample obtained by mechano-chemical method.

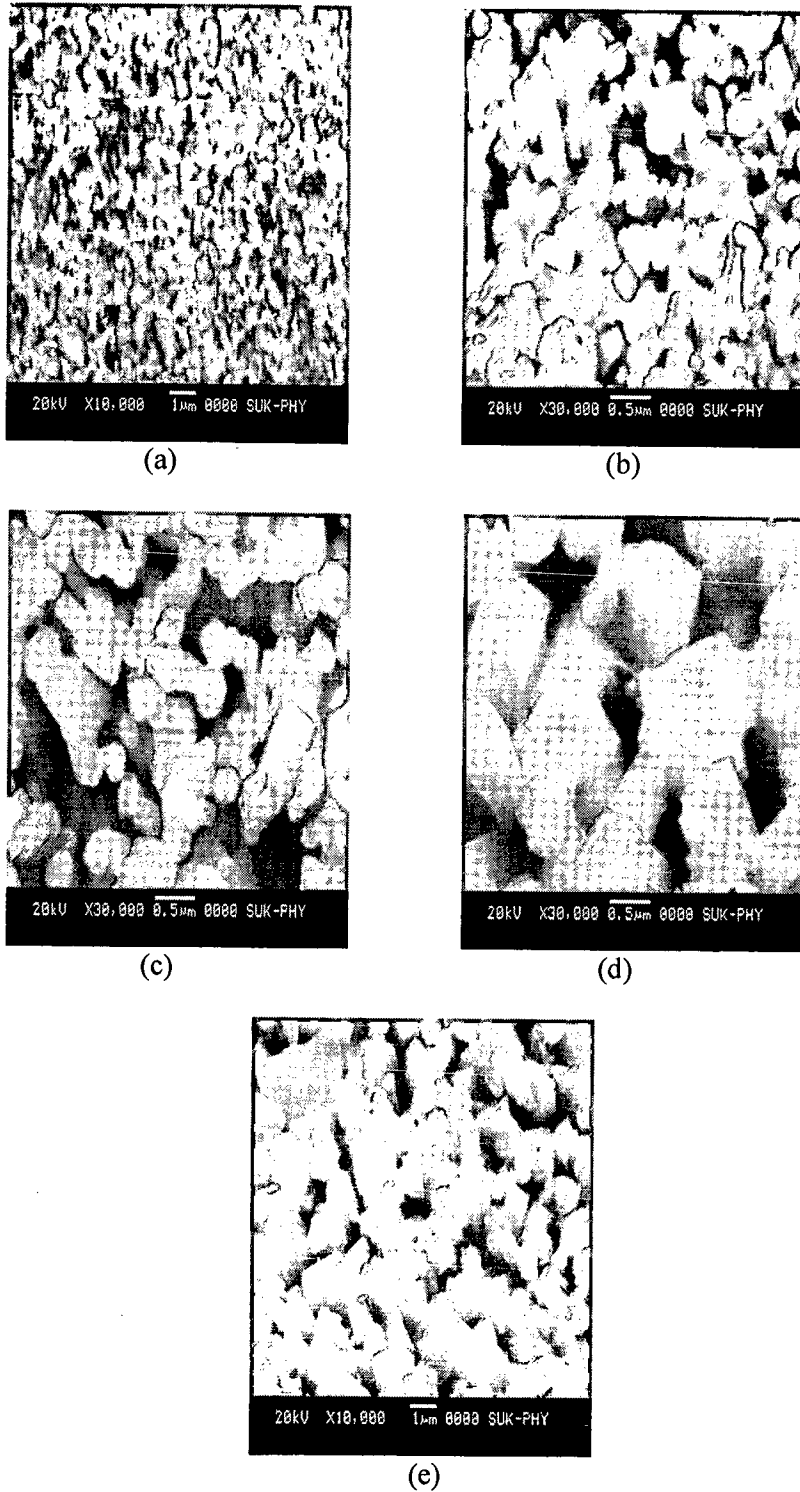


Fig. 4.13. SEM micrographs of $Mn_{0.6}Zn_{0.4}Fe_2O_4$ ferrite (a) unsintered sample, and sintered at (b) $1000^{\circ}C$, (c) $1100^{\circ}C$, (d) $1200^{\circ}C$, (e) $1300^{\circ}C$.

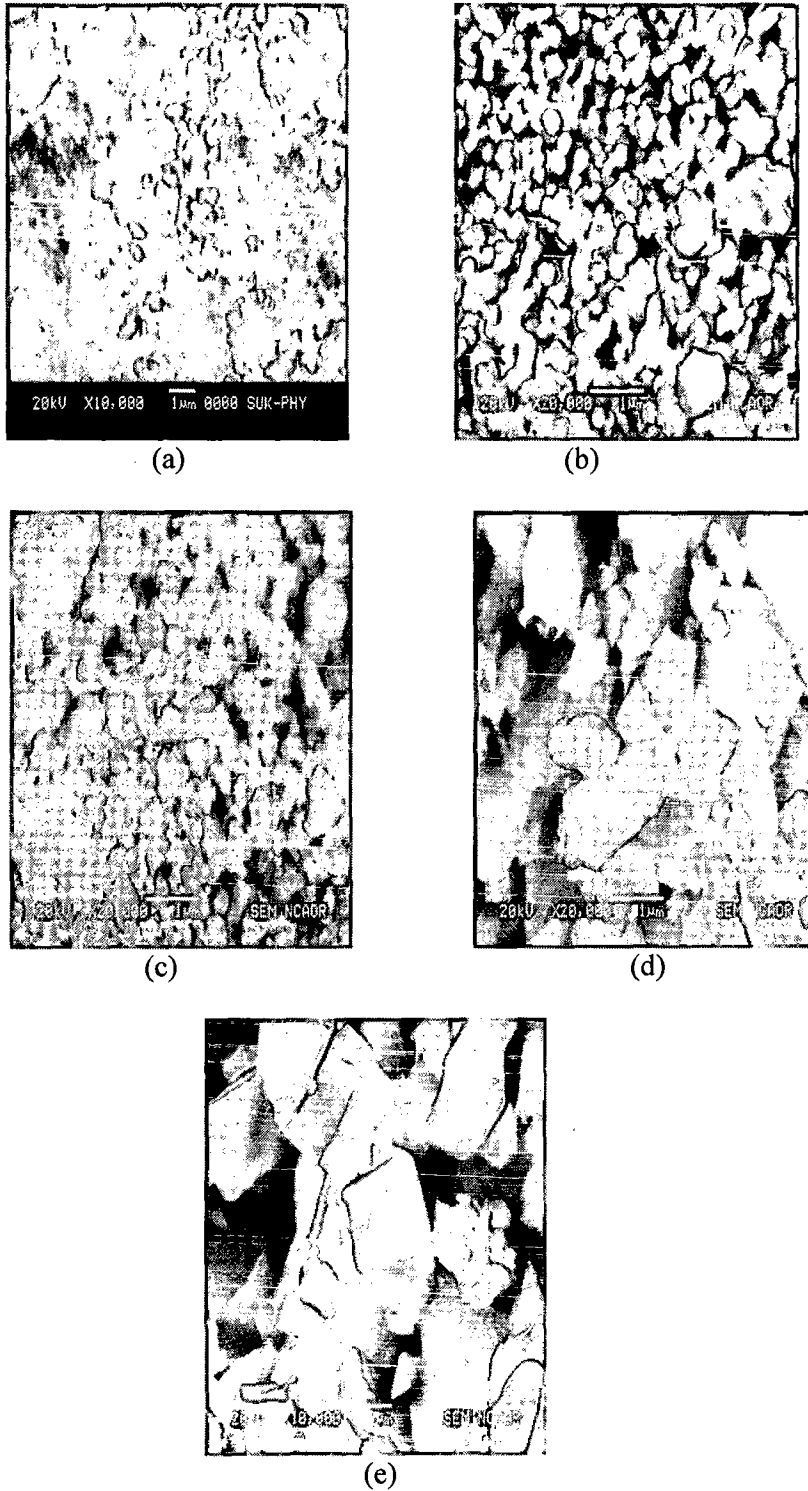
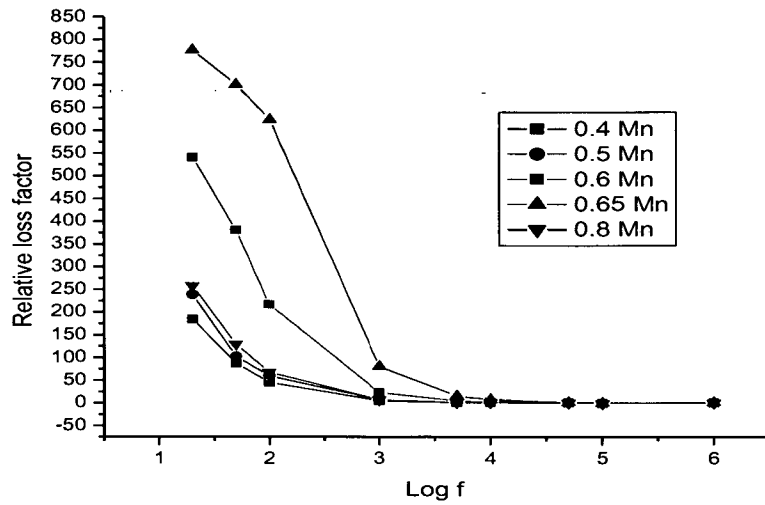


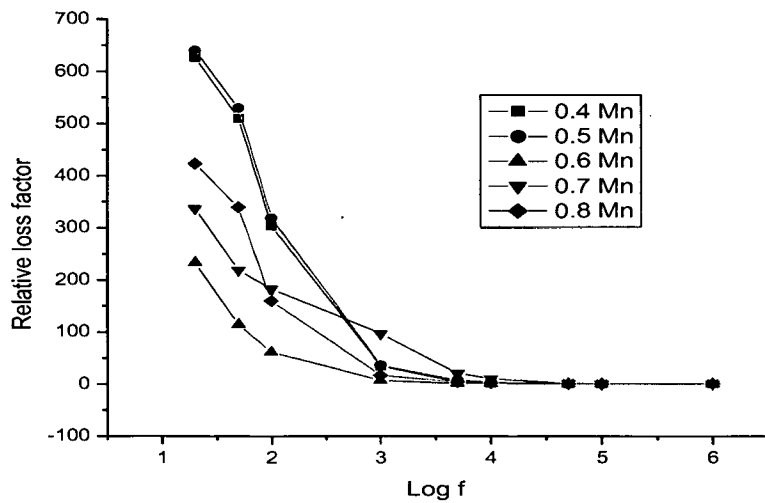
Fig.4.14. SEM micrographs of $Mn_{0.5}Zn_{0.5}Fe_2O_4$ ferrite (a) unsintered sample, and sintered at (b)1000°C, (c)1100°C, (d)1200°C, (e)1300°C.

4.4.4. RELATIVE LOSS FACTOR:

Relative loss factor (rlf) is the ratio of $\tan \delta$ (dissipation factor) to μ_i (initial permeability). The relative loss factor versus frequency is graphically represented in Fig.4.15. For most of the samples, the value of relative loss factor rapidly decreases as the frequency is increased. At higher frequencies, the 'rlf' touches very low value for samples at different sintering temperatures. For a few samples, the 'rlf' value is low at lower frequencies. The 'rlf' is found to depend on the composition and the microstructure of the Mn-Zn ferrites which is dependent on the sintering profile of the samples. The 'rlf' values obtained in the present investigation were from 8×10^2 to as low as 10^{-6} , in the frequency range of 20Hz to 1MHz



(a)



(b)

Fig.4.15. Variation of relative loss factor with log f for various Mn-Zn ferrites sintered at (a)1000°C and (b)1200°C, obtained by the mechano-chemical method.

REFERENCES:

- [1] H. E. Du Bois, *Phil Mag.*, 29 (1890) 293.
- [2] P. J. Weiss, *J. Phys.*, 6(4) (1907) 66.
- [3] B. D. Cullity, C. D. Graham, 'Introduction to Magnetic Materials', 2nd Ed. John Wiley and Sons, (2009), chapter 4.
- [4] *MRS Bulletin*, Vol. 31 (2006).
- [5] A. P. Guimaraes, 'Principles of Nanomagnetism', Springer Publication, (2009).
- [6] N. A. Spaldin, 'Magnetic Materials Fundamentals and Applications', Cambridge University Press, New York, (2010).
- [7] D. J. Dunlop, *Science*, 41 (1972) 176.
- [8] V. G. Broese, P. P. Bongers, A. L. Stuyts, *Mater. Sci. Eng.*, 391 (68/69) 317.
- [9] H. Barkhausen, *Phys. Zeits.*, 20 (1919) 401.
- [10] C. Kittel, 'Introduction to Solid State Physics', Wiley, New York, (1976).
- [11] S. R. Elliott, 'The Physics and Chemistry of Solids', John Wiley and Sons, New York, (1998).
- [12] D. L. Leslie-Pelecky, R. D. Rieke, *Chem. Mater.*, 8 (1996) 1770.
- [13] A.M. Alper 'High Temperature Oxides', Acad. Press, New York, (1971).
- [14] A. A. Sattar, K .M. El-Shokrofy, *J. Phys. IV France* 7 Colloq, (1997) C1-245.

- [15] N. Rezlescu, S. Instrate, E. Rezlescu, J. Luca. J. Phys. Chem. Solid., 35 (1974) 43.
- [16] E.W. Gorter Phil. Res. Rept., 9 (1954) 321.
- [17] L. Neel Proc. Phys. Soc. London, A-65 (1952) 869.
- [18] G. J. Baldha, R. G. Kulkarni, Solid Stat. Commun., 53 (1985)11.
- [19] C. Radhakrishnamurthi, J. Goel. Soc. India, 26(9) (1985) 640.
- [20] R. V. Uphadhay, G. J. Baldha, R. G. Kulkarni, Mater. Res. Bull., 21 (1986) 1015.
- [21] R. S. Tebble, D. J. Craik 'Magnetic Materials', John Wiley and Sons, London, (1969) p. 592.
- [22] J. Gieraltowski, Proc. I.C.F., Japan, (1980) 277
- [23] H. Piscard , A. Globus , Phys. Rev., B 24 (1981) 6610.
- [24] G. Rankis, Bull. Latv. Acad. Sci., Phys. Tech. Sci., N 2 (1984) 27.
- [25] A. Globus, J. Physique Coll., C 1 (1963) C1.1-C1.15.
- [26] A. Globus, Cardiff Conf. USA, (1975).
- [27] A. Globus, P. Duplex, Phys. Stat. Solidi, 31 (1968) 75.
- [28] M. T. Johnson, E. G. Vissar, IEEE Trans. Magn. MAG-26, (1990) 1987.
- [29] P. J. Vender Zaag, J. J. M. Ruigrok, A. Noordermeer, M. H. W. M. van Deiden, P. J. Por, Recveltk, D. M. Sonnet, J. N. Chapman, J. Appl.Phys.,74 (6) (1993) 4085.
- [30] C. Guillaud, Proc. IEEE, 704 (B) (1957) 165.
- [31] C. P. Bean, J. D. Livingston, J. Appl. Phys., 30 (1959) 120.
- [32] C. Kittel, Phys. Rev., 70 (1946) 965.
- [33] H. Rikukawa, IEEE Trans. On Magn., 18 (1982) 1535.

- [34] J. Smit, H. P. J. Wijn, 'Ferrites', John Wiley, New York, (1959).
- [35] S. D. Likhite, C. Radhakrishnamurthy, *Curr. Sci.*, 35 (1966) 534.
- [36] M. A. El Hiti, A.I. El Shora, S.M. Hammad, *Mater. Sci. Technol.*, 13 (1997).
- [37] T. Nakamura, Y. Okano, *J. Phys. IV Fr.*, 7 (C1) (1997) 101.
- [38] S. Dasgupta, J. Das, J. Eckert, I. Manna, *J. Magn. Magn. Mater.*, 306 (2006) 9.
- [39] M. M. Hessien, M. M. Rashad, K. El-Barawy, I. A. Ibrahim, *J. Magn. Magn. Mater.*, 320 (2008) 1615–1621.
- [40] P. Papazoglou, F. Eleftheriou, V.T. Zaspalis, *J. Magn. Magn. Mater.*, 296 (2006) 25.
- [41] R. Iyer, R. Desai, R. V. Upadhyay, *Bull. Mater. Sci.*, 32, 2 (2009) 141–147.
- [42] C. Rath, S. Anand, R. P. Das, *J. Appl. Phys.*, 91(2002) 2211.
- [43] J. P. Chen, C. M. Sorenson, K. J. Klabunde, G. G. Hadjipanayis, E. Delvin, A. Kostidas, *Phys. Rev.*, B 54 (1996) 9288.
- [44] W Wolski, A Wolska, J Kaczmarek, P. Piszora, *Phys. Status Solidi A*, 152 (1995) K19.
- [45] R. Arulmurugan, B. Jeyadevan, G. Vaidyanathan, S. Sendhilnathan, *J. Magn. Magn. Mater.*, 2889 (2005) 470.
- [46] C. Guillaud, *Proc. IEE. Supp.*, 5 (1957) 165.
- [47] Y. Lescroel, A. Pierrot, *Cables and Transmissions*, 14 (1960) 220.
- [48] S. Chikazumi, *Phys. Magne.* John Wiley and Sons, New York, (1964) 263.

- [49] S. H. Keluskar, R. B. Tangsali , G. K. Naik, J. S. Budkuley, J. Magn. Mater., 305 (2006) 296–303.
- [50] E. Roess, Electronic Component Bull., (1966) 1,138.
- [51] A. Beer, T. Schwartz, ibid, (1966) 2,470.
- [52] D. J Perduijn, H. P. Peloschek, Proc. Br. Cer. Soc., 10 (1968)263.
- [53] M. Drofenik, S. Besenicar, M. Lempel, Advances in Ceramics, 16 (1985) 229.
- [54] M. Drofenik, Am. Ceram Soc. Bui., 65(1986) 656.

CHAPTER FIVE

ELECTRICAL PROPERTIES

5.1. INTRODUCTION:

Mechanism of charge transport can be understood from the measurement of electrical conductivity, thermo-electric power, Hall coefficient and magneto-resistance. Density and mobility of charge carriers are the key quantities for obtaining inner details of the conductivity. The ferrites in general are semiconductors and have low conductivity as compared to the metals and thus greatly influence their various applications. The principle application of dielectric and the ac electrical properties is the capacitive element in the electronic circuits and as electrical insulators, therefore the knowledge of parameters such as dielectric constant, dielectric loss factor and dielectric strength is highly important for their use.

Most of the high frequency applications related to electric properties are concerned with dielectrics. The advantages of the ferrites, which are ceramic in nature, over the other available dielectric materials are elastic properties, and greater resistance to environmental changes, particularly at higher temperature.

Hall-effect and thermoelectric properties are widely used in interpretation of the conduction mechanism in semiconductors. The

interpretation of Hall-effect is straight forward and it gives precise results. However, in the case of low mobility materials, like the ferrites, it is sometimes difficult to measure the Hall-effect. In such cases, the thermoelectric power measurement is the only alternative. The sign of the thermoelectric emf gives vital information about the type of conduction in the semiconductors, whether it is p-type or n-type. Another important significance is that it enables one to calculate the value of carrier concentration.

The frequency dependent dielectric behaviour of ferrites created considerable interest among researchers [1-4] to understand many physical and chemical properties of ferrites. Verway [5] attributed high conductivity to the presence of Fe^{2+} and Fe^{3+} ions on equivalent sites (octahedral sites). However Koops [6] proposed that it is largely due to the preparation technique. According to Koops, iron deficiency results in high resistivity, while low resistivity is due to excess of iron.

The temperature dependence of conduction in ferrite is studied by Guillaud and Bertrand [7] and also by Bradburn and Rigby [8]. The effect of small concentrations of manganese on magnesium ferrite is investigated by Van Uitert [3]. Rosenberg et al. [9] have investigated variation of resistance and thermoelectric power with temperature for manganese ferrite and observed ferrimagnetic transition near the Curie temperature.

Maizen [10], amongst many investigators, studied the conduction mechanism on the basis of band picture and hopping model. Band picture takes into account the temperature dependence of conductivity to charge carrier concentration, whereas, hopping model considers that conductivity is because of changes in mobility of charge carriers with temperature.

The dependence of resistivity and activation energy of nickel-zinc ferrite on the sintering temperature and porosity has been studied by Naik and Powar [11]. It was found that there is more densification or less porosity at the higher sintering temperature. The electrical conductivity is also increased when the sintering temperature was high. The observed results were explained on the microstructural changes brought about by sintering conditions.

5.2. RESISTIVITY:

Ferrites are semi conductors in nature having a wide range of resistivity from 10^{-3} to 10^{11} ohm cm at room temperature [3]. These low and high resistivities of ferrites are explained on the basis of location of cations in the spinel structure and also the hopping mechanism. High conductivity in the ferrite is found to be due to the presence of ferrous and ferric ions in the crystallographically equivalent sites (octahedral sites). Both Fe^{2+} and Fe^{3+} ions are at B-site and conduction takes place when electrons move from Fe^{2+} to Fe^{3+} ions. The high resistivity in ferrites is attributed to the occupation of B-sites by other divalent metal ions and trivalent iron ions.

The resistivity of the ferrites is sensitive to temperature. The diffusion of charge carriers from one state to the other state takes place only when the charge carriers acquire the activation energy. The thermal lattice vibrations consistently give rise to phonons, and electrons hop between the pairs of states either by absorption or by emission of phonons. In this way transport of charge carriers is achieved by the hopping process through an interaction with phonons. On the basis of this, the temperature dependence of resistivity of ferrites is given by the relation.

$$\rho = \rho_0 \exp(-\Delta E/kT) \quad \text{-----} \quad 5.1.$$

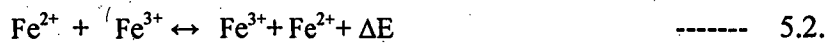
Where, ' ρ_0 ' is temperature dependent constant, ' ΔE ' is the activation energy, ' k ' is Boltzmann constant and ' T ' is absolute temperature.

Unlike in the semiconductors, wherein the charge carriers occupy states in wide energy band, the charge carriers in the ferrites, are localized at the magnetic atoms. In the ferrites, the cations are surrounded by close packed oxygen anions and can be treated as isolated from each other. There will be little direct overlap of the anion charge clouds or orbitals. Alternatively, the electrons associated with particular ion will largely remain isolated and hence a localized electron model is more appropriate in the case of ferrites rather than the collective electron (band) model.

These factors that differentiate the electrical behavior of ferrites from that of the semiconductors, lead to the hopping model of electrons [12, 13]. Conduction is due to exchange of the 3d electrons, localized at the metal ions, from Fe^{3+} to Fe^{2+} [14]. Assuming that all the Fe^{2+} in the B

sites participates in the hopping transport, the number of charge carriers works out to be of the order of 10^{22} cm^{-3} . Since the mobility is very low, the conductivity is also low, even though the charge carriers may be high. Many models have been suggested to account for the electrical properties like the hopping electron model, the small polaron model and the phonon induced tunneling.

The mechanism of transport phenomena in ferrites mainly follows the two following routes for conductivity [15].



where ' ΔE ' is the activation energy, required for transfer of electron from Fe^{2+} to Fe^{3+} or Me^{2+} to Fe^{3+} and vice versa. The valence states of two ions get interchanged. Under the influence of an electric field, these extra electrons are responsible for the generation of current by the jumping or the hopping process [16].

The free electron model cannot explain the electrical conductivity of ferrites because of the fact that the electrons in ferrites are not free and energy band model is not suitable to explain the electrical conductivity for the lack of Bloch type wave functions for electrons in ferrites. The conductivity of ferrites can be, however, explained in terms of electronic charge carriers, like electrons and holes, by the relation

$$\sigma = e [n_e \mu_e + n_h \mu_h] \quad \text{-----} \quad 5.4.$$

where, n and μ are the concentration and mobility of electrons (e) and holes (h), respectively.

In ferrite lattice, the electrostatic interaction between electron and the neighboring ions results into the polarization field called polaron. When such an association is weak, it constitutes a large polaron. Such polarons are found in ionic crystals.

When electron plus lattice deformation have a linear dimension smaller than the lattice constant, they constitute small polarons. Such polarons are found in covalent crystals.

Using mechanism of hopping of polarons, the electrical resistivity, the change in activation energy at Curie temperature and the relation of activation energies with composition have been successfully employed to explain the electrical properties of ferrites [17, 18]. These polarons have low activation energy in magnetic region, while high activation energy in non-magnetic regions.

In the electrostatic interaction between conduction electron or a hole and the nearby ions may result in a displacement of the latter and hence lead to the polarization of the surrounding region. So the carrier gets situated at the centre of the polarization potential well. If this well is deep enough, a carrier may be trapped at a lattice site and its transition to a neighboring site may be determined by thermal activation. If this

activation is sufficient, the conduction can take place by the hopping of electrons, from one lattice to another.

In ferrites, having spinel structure, the B-B distances are smaller than A-A and A-B distances. Even then, the B-B distance is much larger than the sum of the ionic radii of the cations involved, indicating a little or no overlap between d-d wave functions of the ions on adjacent octahedral sites. This gives rise to a situation in which electrons are not free to move through the crystal but remain fixed on B- sites, necessitating a hopping process. However, in the ferrite samples, conductivity is decided mainly by the availability of a pair of cations [19] that facilitate hopping.

5.2.1. MODELS FOR THE ELECTRICAL PROPERTIES:

Various models are proposed by many research workers after investigating the electrical properties of the ferrites under various conditions. Some of these models are discussed in brief in this section.

5.2.1.1. HOPPING ELECTRON MODEL:

Jonker [20] has observed that in cobalt ferrites the transport properties differ considerably from those of normal semiconductors, as the charge carriers are not free to move through the crystal lattice but jump from one ion to the other ion. It was further observed that in this type of materials the possibility of a change in the valency of a considerable fraction of metal ions and especially in that of Fe ions.

Assuming the number of electrons contributing to the conductance to be equal to the number of Fe^{2+} ions and the number of electron holes to be equal to the number of Co^{3+} ions, Jonker has calculated (from resistivity data) extremely low values of mobilities for electrons and holes, and showed a fairly strong exponential dependence of resistivity on temperature. The temperature dependence of conductivity arises only due to mobility and not due to the number of charge carriers in the sample.

5.2.1.2. SMALL POLARON MODEL:

A small polaron is a defect created when an electron carrier becomes trapped at a given site as a consequence of the displacement of adjacent atoms or ions. The entire defect (carrier as well as distortion) then migrates by an activated hopping mechanism. Small polaron formation can take place in materials whose conduction electrons belong to incomplete inner (d or f) shells, which due to small electron overlap tend to form extremely narrow bands. The possibility for the occurrence of hopping conductivity in certain low mobility semiconductors, especially oxides, has been widely recognized for some time, and extensive theoretical discussion which considers the small polaron model and its consequences has been reported [21- 26].

The migration of small polaron requires the hopping of both the electron and the polarized atomic configuration from one site to its adjacent site [27]. The small polaron model also explains the low value of

mobility, temperature independent, Seebeck coefficient and thermally activated hopping. In addition to these properties, if the hopping electron becomes localized by virtue of its interaction with phonons, then a small polaron is formed and the electrical conduction occurs due to the hopping motion of small polarons.

5.2.1.3. PHONON INDUCED TUNNELING:

Srinivasan and Srivastava [27] have explained electrical properties of ferrites on the basis of tunneling of electrons amongst Fe^{2+} and Fe^{3+} atoms on B sites. It has been assumed that the electrons, which take part in the $\text{Fe}^{2+} \leftrightarrow \text{Fe}^{3+} + e^-$ exchange process, are strongly coupled to the lattice and tunnel from one site to the other due to a phonon-induced transfer mechanism.

5.3. THERMO-ELECTRIC POWER:

In the case of low mobility semiconductor materials like ferrites, the thermo-electric power measurement is used to determine the type of conduction mechanism responsible for the conduction. It is the sign of the thermo-emf which gives the information about whether it is p-type or n-type [28].

Zinc ferrite and lithium ferrite are found to be n-type semiconductors. Murthy et al. [29] have investigated the dc conductivity

and Seebeck coefficient of some nickel-zinc ferrite as a function of temperature from room temperature to 300°C. The ferrites with excess iron show n-type semiconduction and those with iron deficiency show p-type semiconduction. Gabelle et al. [30] has measured the electrical conductivity and Seebeck effect of nickel ferrite as a function of temperature. Fayek et al. [31] have studied thermo-electric power of Zn substituted Cu-Ga ferrite and has shown that there are two types of conduction mechanism mainly due to Cu^{2+} - Cu^{2+} and Fe^{3+} - O^{2-} - Fe^{3+} interaction. At lower concentration of Zn it shows p-type behaviour as Cu^{2+} - Cu^{2+} interaction dominate, while at higher concentration of Zn it is n-type as Fe^{3+} - O^{2-} - Fe^{3+} interaction dominates. Sattar et al. [32] have shown that in Mn substituted Ni- Zn ferrite; it is n-type conductor with polaron hopping mechanism.

There are two known methods to measure the thermo-electric power [33]. They are as follows:

a) **Integral method:** In this method one end of the sample is kept at the fixed temperature ' T_1 ', while at the other end the temperature ' T_2 ' is made to vary through the desired temperature range. Thermo-electric voltage ' V ', developed across the sample is measured as a function of the temperature.

$$V(T) = \int_{T_1}^{T_2} QdT \quad \text{----- 5.5.}$$

b) **Differential method:** In this method, a small temperature difference ' ΔT ' is established across the sample to induce a small

thermoelectric voltage ' ΔV '. The Seebeck Coefficient is then determined by an equation

$$Q(T) = \lim_{\Delta T \rightarrow 0} \Delta V(T) / \Delta T \quad \text{-----} \quad 5.6.$$

The accuracy of this method depends on ' ΔT ' being sufficiently small at which ' $Q(T)$ ' changes in the temperature interval ' ΔT '. On the other hand ' ΔT ' should be large enough to generate a voltage that can be detected to the desired precision.

5.4. DIELECTRIC CONSTANT:

Ferrites have wide range of applications from microwave to radio frequencies. With rapid expansion in the field of solid-state electronics it is important to study their behaviour at different frequencies [6, 34]. Ferrites show high dielectric constant and the dispersion of dielectric constant in the frequency range from 20Hz to 1GHz. Ferrites have low conductivity, which is one of the important considerations for microwave applications. The order of the magnitude of conductivity greatly influences the dielectric and magnetic behaviour of ferrites this has aroused considerable interest in the electrical conductivity and the frequency dependent dielectric behaviour of ferrites [35, 36].

The dielectric properties of ferrites are sensitive to method of preparation [36], chemical composition and the substitution [37], porosity and grain size [38]. Krammer [39] has explained the relation between grain size and dielectric constant. The polycrystalline ferrites have very high

dielectric constants of the order of several thousands at low frequencies, falling to very low values at microwave frequencies. The very low conductivity of these materials makes them useful for microwave applications. Several research workers have studied the frequency dependence of the dielectric behaviour of ferrite [40, 41].

Koops [6] suggested a theory in which relatively good conducting grains and insulating grain boundary layers of ferrite material can be understood as given by inhomogeneous dielectric structure, as discussed by Maxwell [42] and Wagner [43]. Since an assembly of space requires finite time to line up their axes parallel to an alternating electric field, the dielectric constant naturally decreases, if the frequency of the field reversal increases. Iwachi [44, 45] studied the low frequency dielectric behaviour of Fe_3O_4 , Mn and Mn-Zn ferrites in powder form and attributed this behaviour to Maxwell Wagner polarization arising from the heterogeneity in oxidation. He pointed out that the powder samples of oxides prepared by calcination at high temperature may have conducting and non conducting layers similar to the sintered oxides, because a considerable amount of sintering takes place in these samples.

The dielectric material reacts to an electric field differently from free space because it contains charge carriers that can be displaced. For an alternating field the time required for polarization show a phase retardation of the charging current instead of 90° further.

It is advanced by some angle $90-\delta$ where δ is the loss angle, which gives,

$$\tan \delta = K'' / K = \epsilon'' / \epsilon' \quad \text{-----} \quad 5.7.$$

where K 's represent dielectric constants and ϵ 's the permittivities. The loss factor $\tan \delta$ is the primary criterion for usefulness of dielectric as an insulating material.

The frequency dependence can be explained with the help of Maxwell-Wagner two-layer Model or the heterogeneous model of the polycrystalline structure of ferrites given by Koops (1951). According to this theory, in a dielectric structure two layers are formed: the first layer consists of ferrite grains of fairly well conducting (ferrous) ions, which is separated from the second layer a thin layer of poorly conducting substances, which forms the grain boundary. These grain boundaries are more active at lower frequencies. Hence the hopping frequency of electron between Fe^{2+} and Fe^{3+} ion is less at lower frequencies. As the frequency of the applied field increases, the conductive grains become more active by promoting the hopping of electron between Fe^{2+} and Fe^{3+} ions, thereby increasing the hopping rate (frequency). Thus, a gradual increase in conductivity with applied field frequency is observed. But at higher frequencies the rate of hopping between the ions can not follow the applied field frequency and it lags behind. This causes a dip in conductivity at higher frequencies.

5.5. EXPERIMENTAL MEASUREMENT:

The samples were subjected to various tests to assess their potential applications. The tests were carried out to investigate the electrical properties such as resistivity, thermo-electric power and the dielectric constant.

5.5.1. RESISTIVITY:

Sample preparation:

Powdered samples of $Mn_xZn_{(1-x)}Fe_2O_4$, synthesized by the mechano-chemical and the wet chemical methods, were pressed into pellets of the size 1.0 cm in diameter and of thickness between 2-3 mm under 75KN pressure applied for about 5 minutes. Four sets of pellets were sintered in nitrogen atmosphere at temperatures: 1000⁰C, 1100⁰C, 1200⁰C and 1300⁰C, respectively, for 4 hours separately in a programmable Carbolite furnace with a heating and cooling rate of 5⁰C min⁻¹. The pellets were silver pasted on either side for establishing good ohmic contacts with the electrodes.

Measurement:

The dc resistivity measurements on these samples were then carried out using standard two-probe method.

5.5.2. THERMO-ELECTRIC POWER:

Sample preparation:

Powdered samples of $Mn_xZn_{(1-x)}Fe_2O_4$ prepared by mechano-chemical and wet chemical methods were pressed into pellets of the size 1.0 cm in diameter and of thickness between 2-3mm under 75KN pressure applied for about 5 minutes. The pellets were silver pasted on either side for establishing good ohmic contacts with the electrodes.

Measurement:

The thermo-emf measurements of these samples were carried out from room temperature to 500⁰C by maintaining a temperature difference between the two ends - hot and cold junction - of electrodes by 10⁰C.

5.5.3. DIELECTRIC CONSTANT:

Sample preparation:

Powdered samples of $Mn_xZn_{(1-x)}Fe_2O_4$ synthesized by mechano-chemical and wet chemical methods were pressed into pellets of the size 1.0 cm in diameter and of thickness between 2mm-3mm under a pressure of 75KN applied for about 5 minutes. Four sets of pellets were sintered in nitrogen atmosphere at temperatures: 1000⁰C, 1100⁰C, 1200⁰C and 1300⁰C, respectively, for 4 hours separately in a programmable Carbolite furnace with a heating and cooling rate of 5⁰C min⁻¹. The pellets were

silver pasted on either side for establishing good ohmic contacts with the electrodes.

Measurement:

The dielectric measurements were carried out from room temperature to 550°C, with the variation of frequencies from 20Hz to 1MHz using Wayne Kerr precision LCR meter. The capacitance C was measured and the dielectric constant was calculated using the relation

$$\epsilon' = ct / \epsilon_0 A \quad \text{-----} \quad 5.8.$$

where 't' is the thickness of pellet, 'A' is Area of cross section of the pellet, ' ϵ_0 ' is the permittivity of free space.

5.6. RESULTS AND DISCUSSION:

The results obtained in the study of the resistivity, thermo –electric power and dielectric constant of the Mn-Zn ferrite samples, are tabulated and discussed in the following Sections.

5.6.1. RESISTIVITY:

Ferrite samples prepared by mechano-chemical method:

Variation of dc resistivity ($\log\rho$) with different sintering temperatures ($1000/T$) K for $Mn_xZn_{(1-x)}Fe_2O_4$ ferrite samples (with different compositions) prepared by the mechano-chemical method, is illustrated in the Fig.5.1 (a, b, c and d). It was observed that the dc resistivity decreases with increasing temperature indicating the semiconducting nature of the samples. This was due to the increase in drift

mobility of the charge carriers. Although the resistivity depends on the concentration of the Mn in the ferrite samples, in present study it was observed that it strongly depend on the sintering temperature. Resistivity values at 310K were varying between 5.721×10^7 ohm-cm and 9.365×10^7 ohm-cm for unsintered samples. The lowest was observed for $Mn_{0.7}Zn_{0.3}Fe_2O_4$ and the highest value was obtained for $Mn_{0.4}Zn_{0.6}Fe_2O_4$. These values of resistivity were found to be higher than that for bulk material [46]. This was because, in the case of nano material, microstructure with smaller grain contains a greater number of grain boundaries. The grain boundaries are the region of mismatch between the energy states of the adjacent grains and hence act as a barrier to the flow of electrons. The higher resistivity observed in this method thus may be attributed to the smaller grain size. The smaller grain size is also advantageous from the point of view of reducing Fe^{2+} ions as oxygen advances faster in smaller grains thus keeping iron in the Fe^{3+} state [47].

For the samples sintered at $1000^{\circ}C$, the resistivity at 310K was found to vary between 3.962×10^6 ohm-cm and 3.526×10^7 ohm-cm with the value being highest for $Mn_{0.6}Zn_{0.4}Fe_2O_4$ sample. The values of resistivity for samples sintered at $1200^{\circ}C$ were found in the range between 1.194×10^6 ohm-cm and 7.850×10^6 ohm-cm. While the resistivity values obtained for samples sintered at $1300^{\circ}C$ at 310K were having the lowest value of 6.615×10^5 ohm-cm for $Mn_{0.7}Zn_{0.3}Fe_2O_4$ and the highest value being 4.481×10^6 ohm-cm. for $Mn_{0.4}Zn_{0.6}Fe_2O_4$.

Many models have been suggested to account for the electrical properties and conduction mechanism in ferrites by various investigators, which have been reviewed by Klinger et al. [48]. However, the thermally activated hopping model is found to be the one, which can qualitatively and appropriately explain the electrical properties and behavior of Mn-Zn ferrite. In the hopping process the additional electron on a Fe^{2+} ion requires lesser energy to move to an adjacent Fe^{3+} ion on the equivalent octahedral lattice sites (B sites).

When external electric field is applied, these extra electrons hopping between Fe ions are responsible for the electrical conduction. Therefore, any change in the Fe^{2+} ion content in the spinel ferrite lattice as also the distance between them is important for the intrinsic resistivity of Mn-Zn ferrite grains, including the intrinsic grain boundaries. If the introduction of another cation into the lattice causes a change in the valency distribution on the B sites, then the number of electrons potentially available for the transfer will be altered. On the other hand, the addition of foreign ions (impurity) can also change the distance between the B lattice sites; this is crucial for the conduction mechanism.

Thus, the formation of an intrinsic grain boundary in doped samples by the segregation of aliovalent ions must increase the resistivity. This gives rise to polycrystalline Mn-Zn ferrite with non ferrimagnetic grain boundary, ferrimagnetic outer grain region and ferrimagnetic conductive core. Thus the contribution to the bulk resistivity may be

considered as resistivity contribution coming from three different regions [49]. In order to establish a relation between the power loss due to eddy currents and the average grain diameter, a hypothetical brick wall model is applied. As per this model each layer can be represented by a resistance – capacitance (R-C) lumped circuit of high ohmic layers. When the resistivity of the bulk is much lower than the grain boundary layers, the equivalent circuit of the ferrite can be represented by a series of lumped R-C circuits of the grain boundary layers.

As the samples in the present study were sintered from nanosized Mn-Zn ferrite particles in nitrogen atmosphere (reducing) without any additives, there was no possibility of formation of high resistivity ferrimagnetic outer grain boundary. Thus the resistivity will exclusively depend on the contribution from the non-ferrimagnetic grain boundaries and ferrimagnetic conductive core. It can be seen from SEM micrographs in Fig.5.2 (a, b, c and d) and 5.3 (a, b, c and d) that the samples sintered at 1000⁰C show small grain sizes with large non ferrimagnetic grain boundaries. Higher total surface area of the sample, which further increases due to the formation of fine (small) crystals, results in the high resistivity for the samples. With the increase in the sintering temperature for the samples, viz. 1100⁰C, 1200⁰C and 1300⁰C, the grain size increases without forming perfect crystals. This leads to low surface area and lower resistivity non-ferrimagnetic grain boundaries which accounts for the low value of resistivity at 310K for the samples sintered at these increasing temperatures.

Many researchers [50, 51] have observed that the increase in electrical conductivity as a function of sintering temperature and time results in higher density and grain growth. As a result, porosity correspondingly decreases and so does the number of grain boundaries. This is due to an increase in grain size. Therefore, it is concluded that sintering temperature and time play dominant role in deciding the electrical conductivity and microstructure of the particular ferrite.

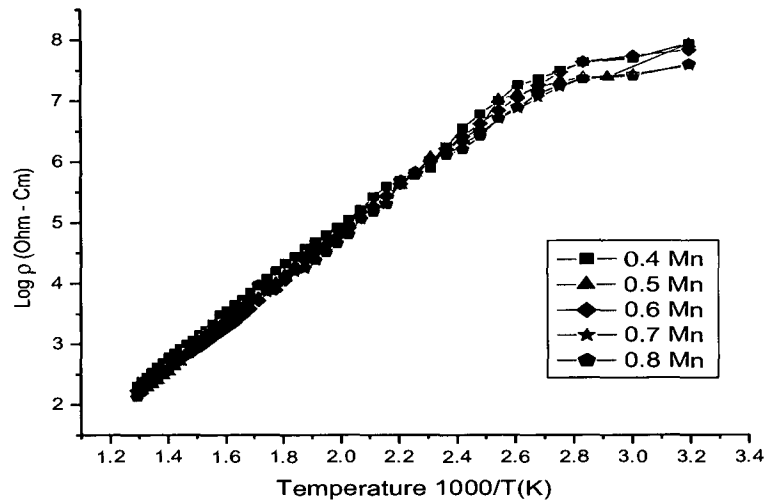


Fig. 5.1.(a). Variation of resistivity ($\log \rho$) with $1000/T$ (K) for different unsintered Mn-Zn ferrite samples obtained by the mechano-chemical method.

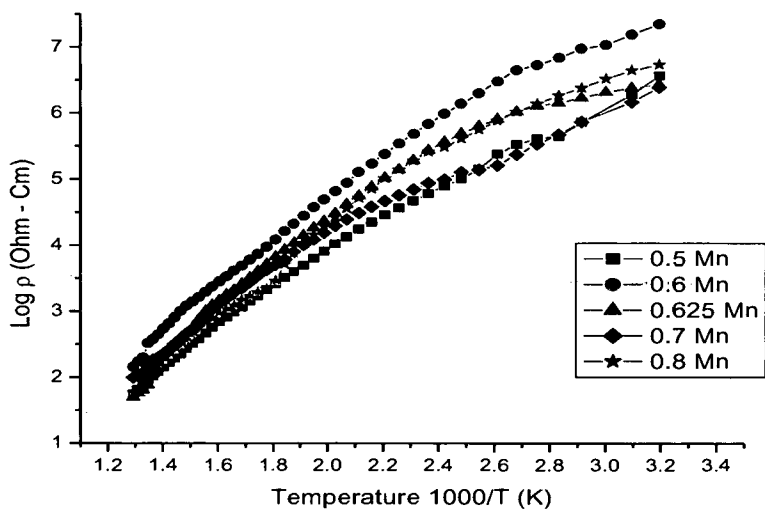


Fig. 5.1.(b). Variation of resistivity ($\log \rho$) with $1000/T$ (K) for different sintered Mn-Zn ferrite (1000°C) samples obtained by the mechano - chemical method.

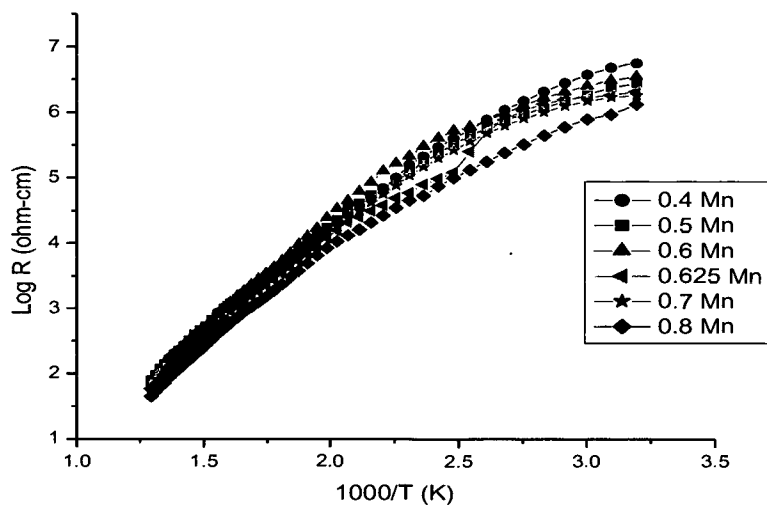


Fig.5.1.(c). Variation of resistivity ($\log \rho$) with $1000/T$ (K) for different sintered Mn - Zn ferrite (1200°C) samples obtained by the mechano - chemical method.

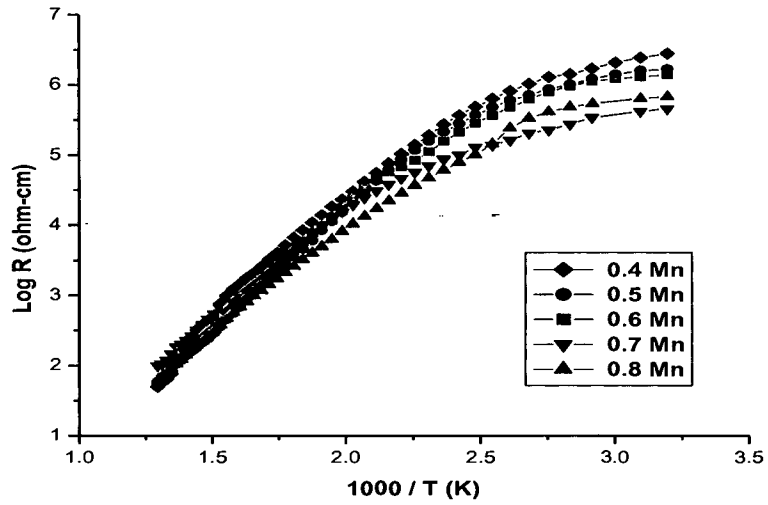


Fig.5.1.(d). Variation of resistivity ($\log\rho$) with $1000/T$ (K) for different sintered Mn-Zn ferrite (1300°C) samples, obtained by the mechano - chemical method.

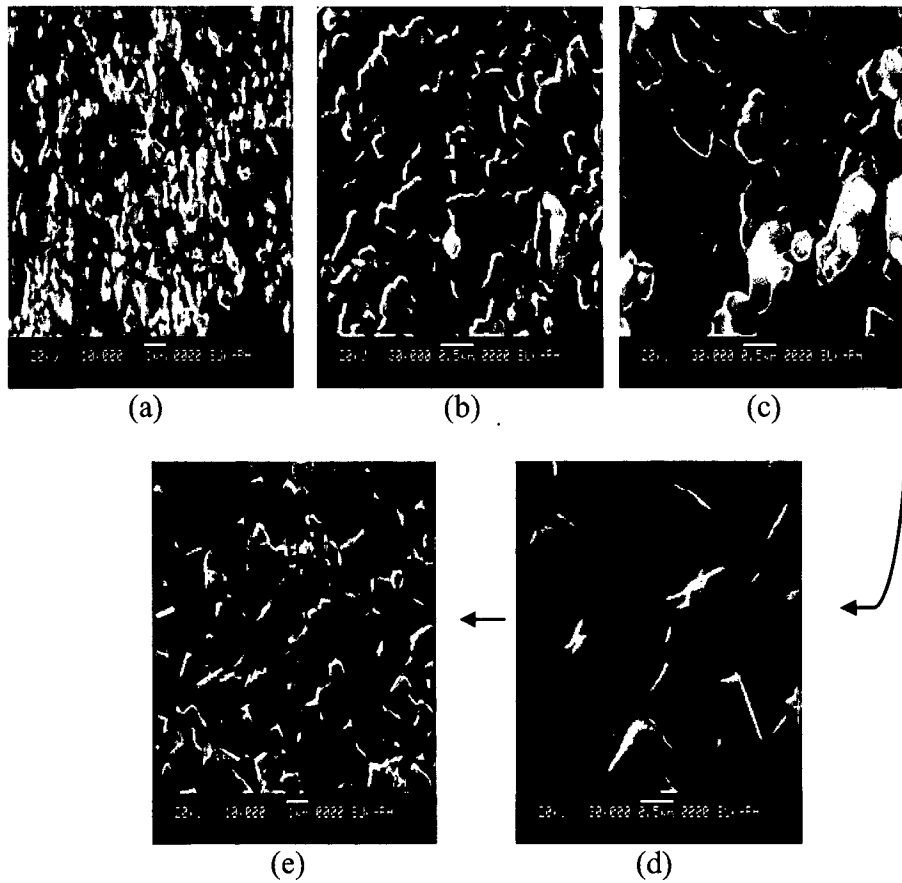
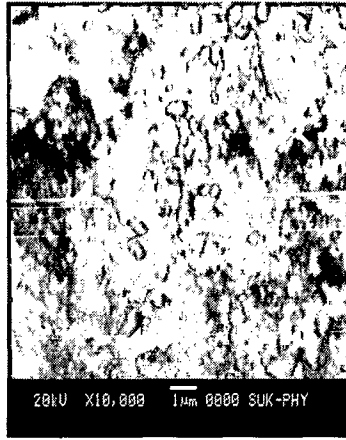


Fig.5.2. SEM micrographs of $\text{Mn}_{0.6}\text{Zn}_{0.4}\text{Fe}_2\text{O}_4$ ferrite (a) unsintered sample, and sintered, at (b) 1000°C , (c) 1100°C , (d) 1200°C , (e) 1300°C by the mechano-chemical method.



(a)



(b)



(c)



(d)



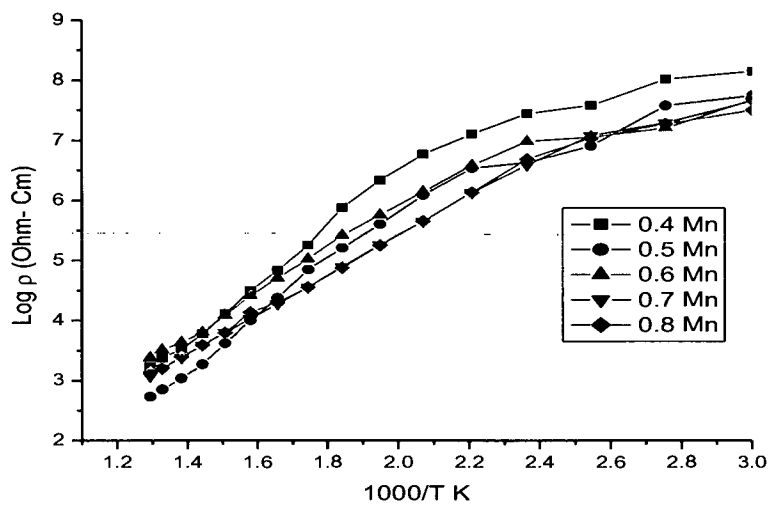
(e)

Fig.5.3. SEM micrographs of $Mn_{0.5}Zn_{0.5}Fe_2O_4$ ferrite (a) unsintered sample, and sintered, at (b) $1000^{\circ}C$, (c) $1100^{\circ}C$, (d) $1200^{\circ}C$, (e) $1300^{\circ}C$ by the mechano-chemical method.

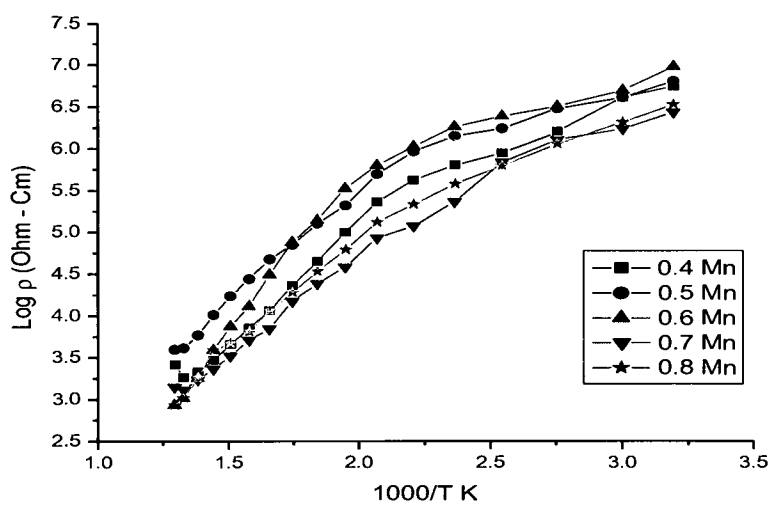
Ferrite samples prepared by wet chemical method:

Similar variation of dc resistivity ($\log\rho$) with sintering temperatures ($1000/T$ K) was noticed in the case of samples prepared by the wet chemical method. Fig.5.4 (a, b and c) illustrate these changes for samples with different Mn content. These samples also exhibit semiconducting nature as their dc resistivity decreases with increasing temperature. This phenomenon occurs due to an increase in the drift mobility of the charge carriers. In these samples the resistivity also is found to be strongly dependent on the sintering temperatures. Resistivity values at 310K are seen to vary between 7.281×10^7 ohm-cm and 2.176×10^8 ohm-cm for unsintered samples. The lowest for $\text{Mn}_{0.8}\text{Zn}_{0.2}\text{Fe}_2\text{O}_4$ and the highest value is seen for $\text{Mn}_{0.4}\text{Zn}_{0.6}\text{Fe}_2\text{O}_4$. These values of resistivity were found to be marginally higher than those samples obtained from the mechano-chemical method. The higher values of dc resistivity may be attributed to the stoichiometric compositions, better crystal structure and the improved nanostructure due to atomic level mixing in the aqueous medium in this wet chemical method.

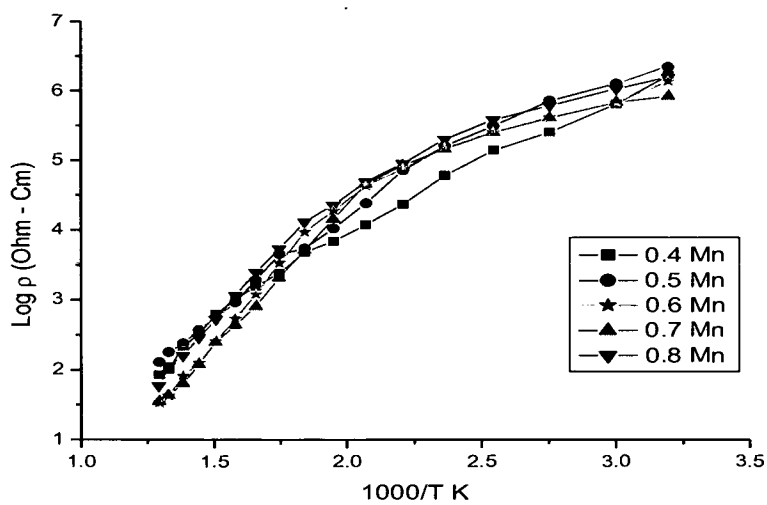
For the samples sintered at 1200°C the resistivity at 310K was found to vary between $4,380\times 10^6$ ohm-cm and 9.841×10^6 ohm-cm with the highest being for the $\text{Mn}_{0.6}\text{Zn}_{0.4}\text{Fe}_2\text{O}_4$ sample. The values of resistivity for samples sintered at 1300°C at 310K were found in the range- 9.179×10^5 ohm-cm. as the lowest for $\text{Mn}_{0.7}\text{Zn}_{0.3}\text{Fe}_2\text{O}_4$ and 3.418×10^6 ohm-cm as the highest value, for $\text{Mn}_{0.5}\text{Zn}_{0.5}\text{Fe}_2\text{O}_4$.



(a)



(b)



(c)

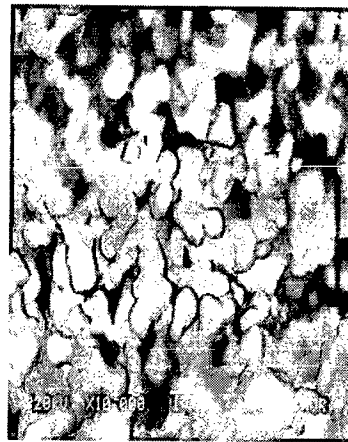
Fig. 5.4. Variation of resistivity ($\log \rho$) with $1000/T$ (K) for various Mn-Zn ferrite (a) unsintered samples, and sintered, at (b) 1200°C and (c) 1300°C samples obtained by the wet chemical method.



(a)



(b)



(c)



(d)



(e)

Fig. 5.5. SEM micrographs of $Mn_{0.6}Zn_{0.4}Fe_2O_4$ ferrite (a) unsintered sample, and sintered, at (b) $1000^{\circ}C$, (c) $1100^{\circ}C$, (d) $1200^{\circ}C$, (e) $1300^{\circ}C$ obtain by the wet chemical method.

The resistivity values obtained in the present studies for both the methods of preparation, namely mechano-chemical and wet chemical method, were higher compared to the resistivity values of 10^5 ohm-cm reported [52, 53] in the surveyed literature.

The higher resistivity values seen for the samples obtained by the mechano-chemical method as well as those prepared by the wet chemical method amply confirm that both these methods yield Mn-Zn ferrite having grain size in the nanometer range. This observation is in conformity with the particle size calculated from the XRD data (3.5.9, Table 3.9) and with the conclusion drawn from the other experimental results (3.5.7, Fig.3.7).

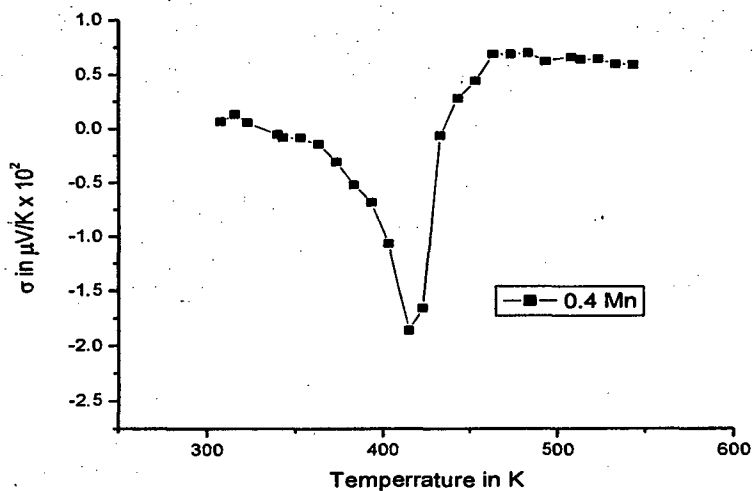
5.6.2. THERMO-ELECTRIC POWER:

Ferrite samples prepared by mechano-chemical method:

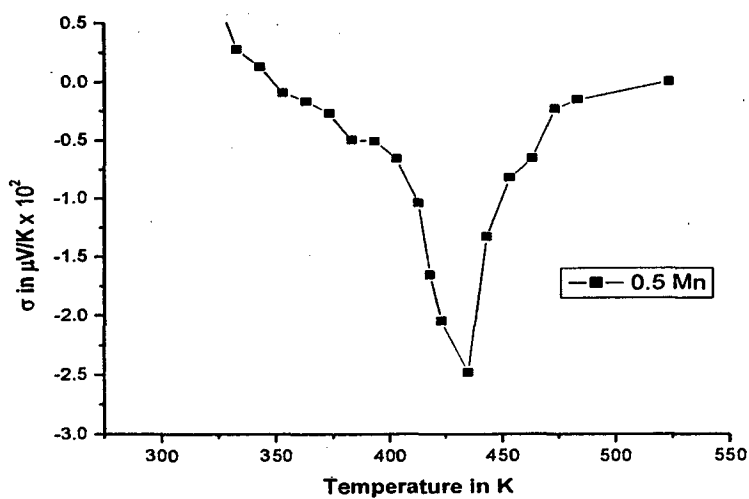
The variation of Seebeck coefficient (Q) with temperature (K) for the $Mn_{(x)}Zn_{(1-x)}Fe_2O_4$ (where $x = 0.40, 0.50, 0.60, 0.80$) unsintered samples prepared by the mechano-chemical method is shown in Fig.5.6. (a, b, c and d).

It can be seen from the figures that all the samples prepared by this method show a negative value of Seebeck coefficient (Q), indicating that the electrons were the majority charge carriers. Thus all the samples show n-type semiconductor behaviour. The mechanism of conduction in all these samples is predominantly due to the hopping of electrons from

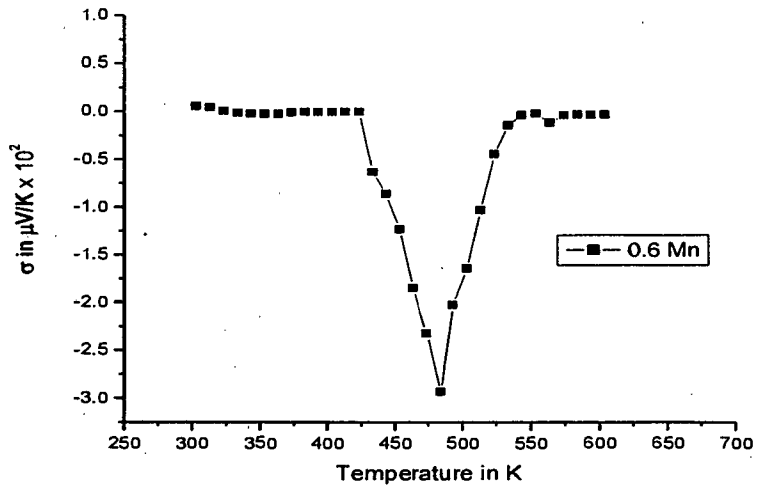
Fe^{2+} to Fe^{3+} ions. It is also evident from the figures that the value of Seebeck coefficient increases with increasing Mn content in the samples. Among all the samples prepared by the mechano-chemical method, $\text{Mn}_{0.4}\text{Zn}_{0.6}\text{Fe}_2\text{O}_4$ sample show lower (numerical) Q value of -186 $\mu\text{V}/\text{K}$ while $\text{Mn}_{0.8}\text{Zn}_{0.2}\text{Fe}_2\text{O}_4$ has the highest (numerical) Q value of -452 $\mu\text{V}/\text{K}$.



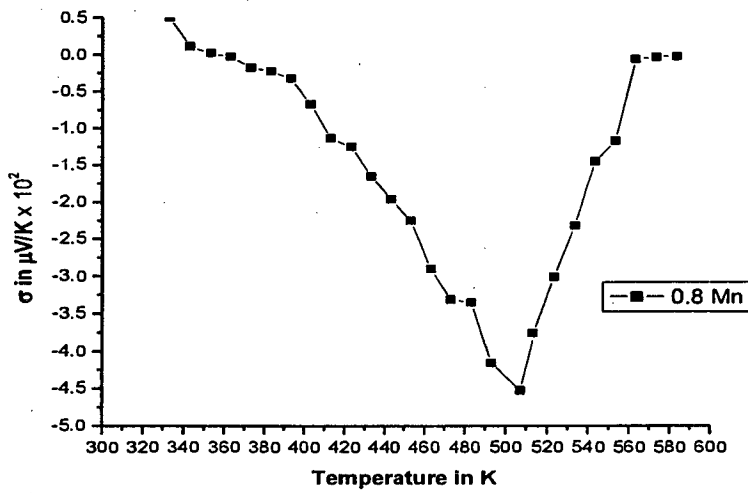
(a)



(b)



(c)



(d)

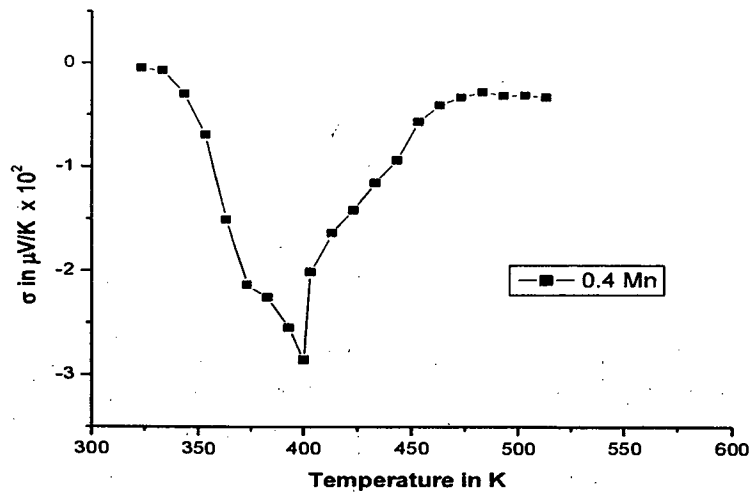
Fig.5.6. Variation of Seebeck coefficient with Temperature (K) for various Mn-Zn ferrite unsintered samples obtained by the mechano-chemical method.

Ferrite samples prepared by wet chemical method:

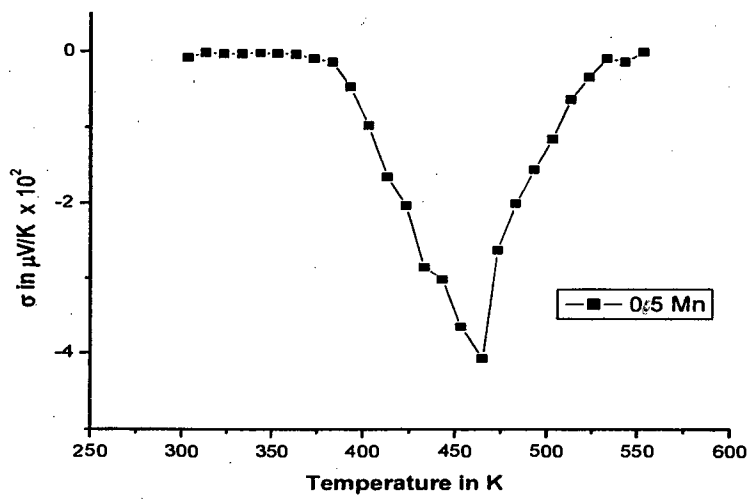
Similarly, the variation of Seebeck coefficient (Q) with temperature (K) for $Mn_{(x)}Zn_{(1-x)}Fe_2O_4$ unsintered samples, with various compositions, prepared by wet chemical method is shown in Fig.5.7. (a, b, c, d).

It can be seen from the figures that, like the samples prepared by the mechano-chemical method, all the samples prepared by the wet chemical method also show an identical trend of a negative value of Seebeck coefficient (Q), indicating that the electrons are the majority charge carriers. In other words, all the samples show n-type semiconductor behaviour. The mechanism of conduction in all these samples is also predominantly due to the hopping of electrons from Fe^{2+} to Fe^{3+} ions. It is also evident from the graphs that the values of Seebeck coefficient increases with decreasing zinc concentration.

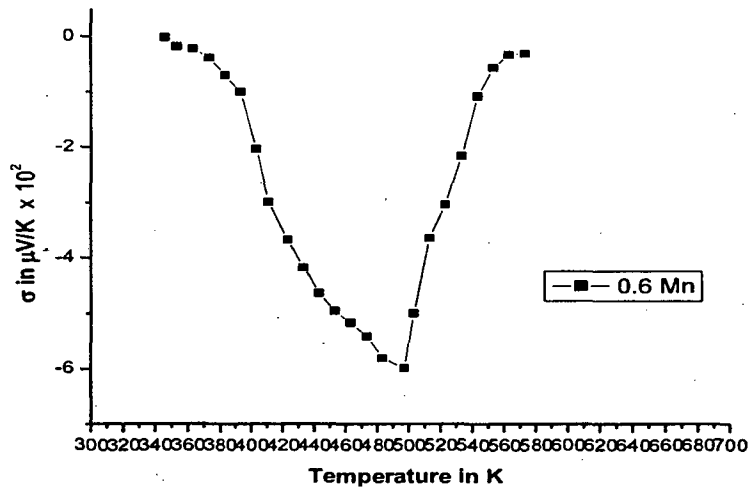
However, the samples prepared by the wet chemical method were found to show overall higher values of Seebeck coefficient as compared to the mechano-chemical method. The lowest (numerical) value was seen in case of $Mn_{0.4}Zn_{0.6}Fe_2O_4$ which is -285 $\mu V/k$ and the highest (numerical) was for $Mn_{0.8}Zn_{0.2}Fe_2O_4$ equal to -782 $\mu V/K$.



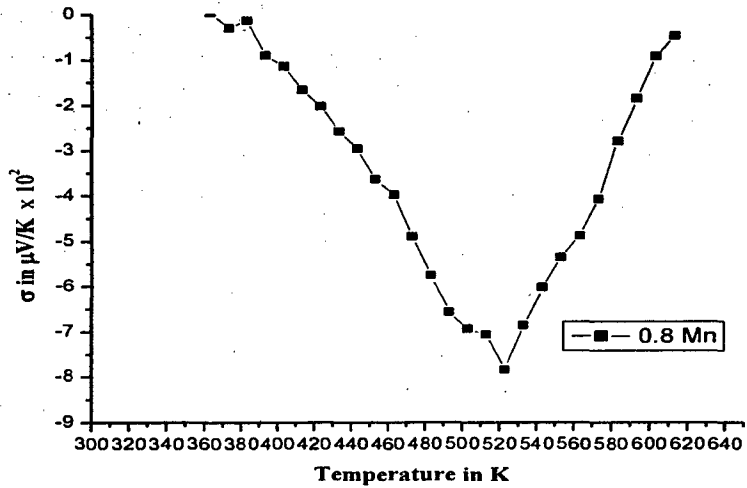
(a)



(b)



(c)



(d)

Fig.5.7. Variation of Seebeck coefficient with Temperature (K) for various Mn-Zn ferrite unsintered samples obtained by the wet chemical method.

While investigating the thermo-electric power of Mn-Zn ferrite with various compositions of Mn (0.2, 0.4, 0.6, 0.8 and 1.0), Ravinder and Latha [54] observed that except for the composition of 0.8 in Mn-Zn ferrite, all other compositions showed n-type of behaviour, where as,

sample with Mn composition of 0.8, indicated p-type behaviour. However all the Mn-Zn ferrite samples prepared by both the methods discussed in the present study showed n-type behaviour for all the compositions of Mn (0.4, 0.6, 0.7 and 0.8).

Ravinder et al. [55-57], further in their studies on substituted Mn-Zn ferrite with cerium, erbium and gadolinium also observed that in all these substituted Mn-Zn ferrites the conduction is due to the electrons. These substituted ferrites show n- type of semiconductor behaviour.

5.6.3 DIELECTRIC CONSTANT:

Results of variation of dielectric constant, with the frequency and the temperature, are given in this section.

5.6.3.1 FREQUENCY DEPENDENCE OF DIELECTRIC CONSTANT:

Ferrite samples prepared by mechano-chemical method:

The capacitance values were recorded at various frequencies for the ferrite samples prepared by the mechano-chemical method. The variation of dielectric constant with the frequency for $Mn_{(x)}Zn_{(1-x)}Fe_2O_4$ samples is shown in Fig.5.8. (a), (b) and (c).

It can be seen from the figures that the value of the dielectric constant decreases with increasing frequencies and that a very low value is shown at higher frequencies for all the unsintered as well as sintered samples at different sintering temperatures. This can be explained on the basis of space charge polarization model of Maxwell [42] Wagner [43], and the Koop's phenomenological theory [6]. The decrease of dielectric constant at higher frequency can be explained on this basis, by assuming that the solid is composed of well conducting grains separated by poorly conducting grain boundaries. The electrons reach the grain boundary by hopping and if the resistance of the grain boundary is high enough, electrons pile up at the grain boundaries and produce polarization. However, as the frequency of the applied field is increased beyond a certain value, the electrons cannot follow the alternating field. This decreases the possibility of further electrons reaching the grain boundary and as a result the polarization decrease [6, 42].

The decrease of dielectric constant with increase in frequency as observed in the case of mixed ferrites is a normal dielectric behavior. This normal dielectric behavior was also observed by several other investigators [58, 59]. Reddy et al. have studied the variation of dielectric constant with frequency for ferrites [60]. They have explained the behavior qualitatively as due to the fact that the electron exchange between Fe^{3+} and Fe^{2+} ions cannot follow the frequency of the externally applied alternating field beyond a certain limit. The large decrease in dielectric constant validates the two-layer model assumption [61]. The large values of dielectric

constant at lower frequencies have been attributed to the predominance of the species like Fe^{2+} ions, interfacial dislocation pile ups, oxygen vacancies, grain boundary defects etc.

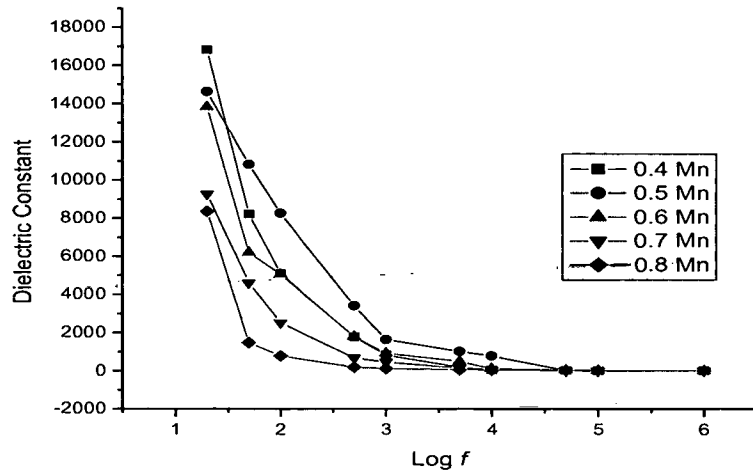
The values of dielectric constant at 310K and 20Hz frequency were seen to vary between 8.3587×10^3 and 1.6803×10^4 for unsintered samples. The lowest was observed for $\text{Mn}_{0.8}\text{Zn}_{0.2}\text{Fe}_2\text{O}_4$ and the highest value for $\text{Mn}_{0.4}\text{Zn}_{0.6}\text{Fe}_2\text{O}_4$ respectively.

The dielectric constant for all the unsintered samples is lower than the corresponding bulk value at room temperature. Latha et al. [62] have reported a dielectric constant of $(17-32) \times 10^5$ at 308K measured at a frequency of 5 kHz for Mn-Zn ferrite in bulk form synthesized by ceramic method. This low value of dielectric constant may be attributed to homogeneity, better symmetry, uniform smaller grains. Smaller grains contain large surface boundaries and are the regions of high resistance. This reduces the interfacial polarization and hence the dielectric constant was found to be lesser than that reported for the bulk materials.

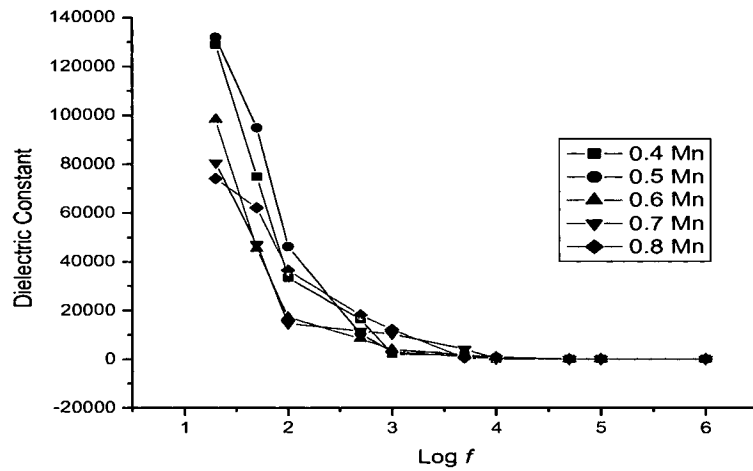
For the samples sintered at 1100°C , the values vary between 7.4730×10^4 and 1.3472×10^6 , the lowest and the highest were for $\text{Mn}_{0.8}\text{Zn}_{0.2}\text{Fe}_2\text{O}_4$ and $\text{Mn}_{0.5}\text{Zn}_{0.5}\text{Fe}_2\text{O}_4$ respectively. It can be seen that samples sintered at 1300°C have higher values of dielectric constant. The highest value 1.9268×10^7 was obtained for $\text{Mn}_{0.4}\text{Zn}_{0.6}\text{Fe}_2\text{O}_4$ sample (at ambient temperature) for 20Hz frequency which is comparable to the

reported values. In the case of samples sintered at 1300⁰C, the lowest value of dielectric constant was 6.8240×10^5 for Mn_{0.8}Zn_{0.2}Fe₂O₄ sample.

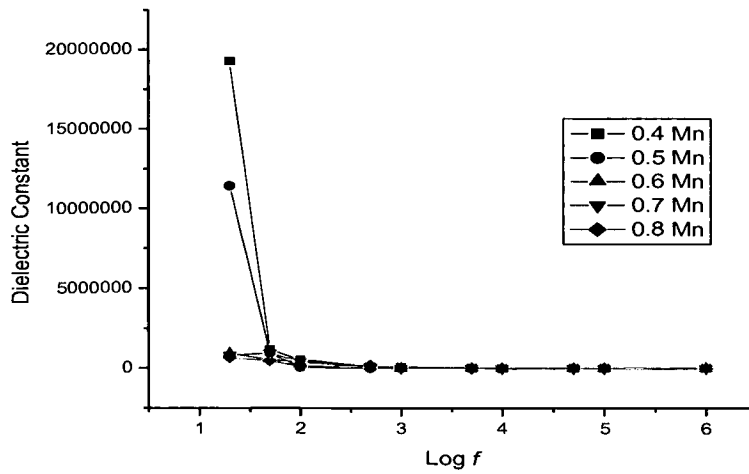
Some investigators [47, 63] have reported that there is a strong correlation between the conduction mechanism and the dielectric behavior of the ferrites, with the conjecture that the mechanism of the polarization process in ferrites is similar to that of the conduction process. They observed that the electronic exchange between $Fe^{2+} \leftrightarrow Fe^{3+}$ results in local displacement that determine the polarization behavior of the ferrites. The dependence of the dispersion of dielectric constant on composition can be explained on the basis of the available ferrous ions on octahedral sites [64]. As the frequency of the externally applied electric field increases gradually, and though the same number of ferrous ions are present in the ferrite material, the dielectric constant decreases. This reduction occurs because, beyond a certain value of frequency of the externally applied field, the electronic exchange between ferrous and ferric ions cannot follow the alternating field, since the field changes are too fast. The variation of dispersion with composition can also be explained on the same basis.



(a)



(b)



(c)

Fig.5.8. Variation of dielectric constant with Log f for various Mn-Zn ferrites (a) unsintered samples, and sintered, at (b) 1100°C and, (c) 1300°C samples prepared by the mechano-chemical method.

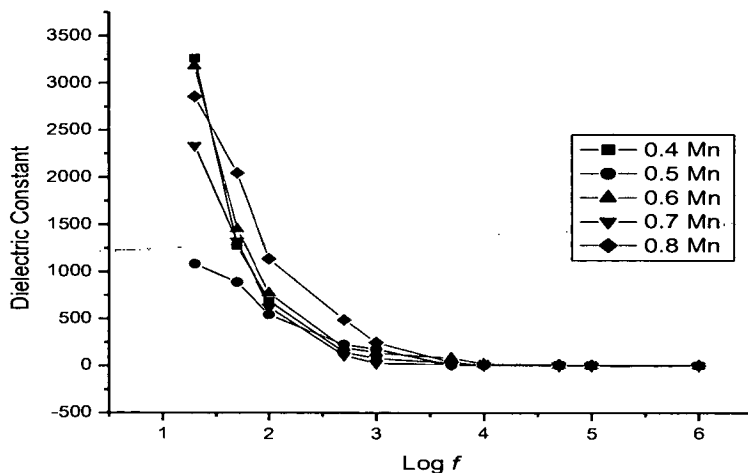
Ferrite samples prepared by wet chemical method:

As in the case of the samples prepared by the mechano-chemical method, the variation of dielectric constant with frequency for $Mn_{(x)}Zn_{(1-x)}Fe_2O_4$ samples prepared by the wet chemical method can be seen in Fig.5.9.(a), (b) and (c).

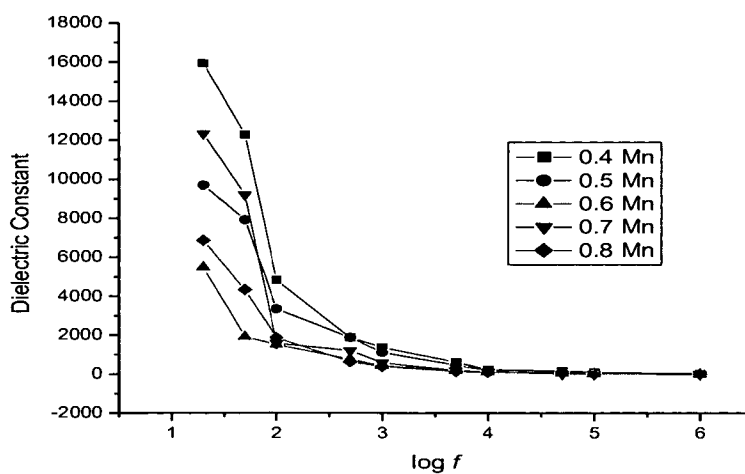
The value of the dielectric constant decreases with increase in frequency as in the case of samples prepared by mechano-chemical method. These samples were also found to have very low values at higher frequencies for all the unsintered as well as sintered samples.

The dielectric constant values at 310K and 20Hz frequency were in the range of 1.0811×10^3 and 3.2613×10^3 for unsintered samples. The observed lowest was for $Mn_{0.5}Zn_{0.5}Fe_2O_4$ and the highest for $Mn_{0.4}Zn_{0.6}Fe_2O_4$ samples. For the samples sintered at $1100^\circ C$ the values vary between 5.4980×10^3 and 1.5942×10^4 for $Mn_{0.6}Zn_{0.4}Fe_2O_4$ and $Mn_{0.4}Zn_{0.6}Fe_2O_4$, respectively. Samples sintered at $1300^\circ C$, have the dielectric constant value in the range 7.5735×10^5 and 1.8704×10^6 measured at room temperature at 20Hz frequency. The highest was for the $Mn_{0.4}Zn_{0.6}Fe_2O_4$ sample.

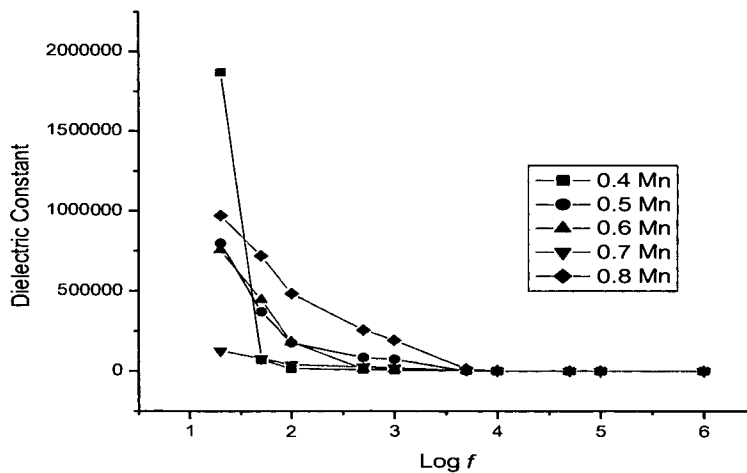
The dielectric constant values for wet chemical method were found to be on the lower side in comparison with the samples prepared by the mechano-chemical method. These low values of dielectric constant may be attributed to the homogeneity, better symmetry and the uniform smaller grains in the case of samples prepared by wet chemical method.



(a)



(b)



(c)

Fig.5.9. Variation of dielectric constant with Log f for various Mn-Zn ferrites (a) unsintered samples, and sintered, at (b) 1100°C and, (c) 1300°C samples prepared by the wet chemical method.

5.6.3.2 TEMPERATURE DEPENDENCE OF DIELECTRIC CONSTANT:

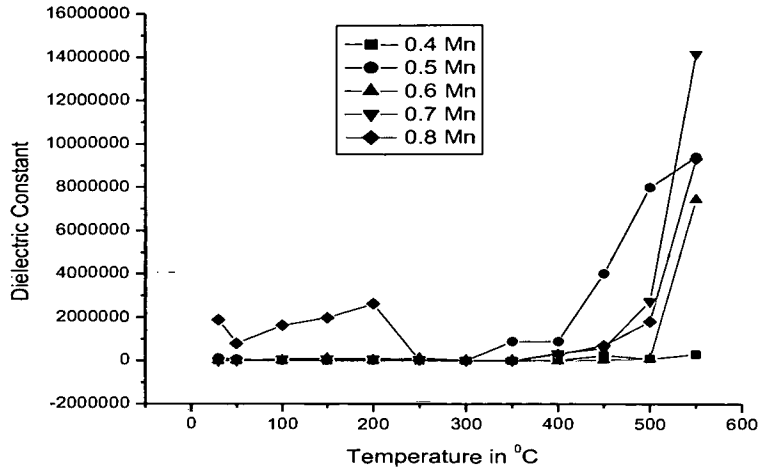
Ferrite samples prepared by mechano-chemical method:

In the case of ferrites, the dielectric constant is found to be directly proportional to the temperature up to a certain value. There are several reports [65-67] wherein the variation of dielectric constant of ferrites with temperature has been studied. In the present study, the dielectric constant values were recorded as a function of temperature at a fixed frequency of 20Hz. The results obtained for the $Mn_xZn_{(1-x)}Fe_2O_4$ samples prepared by the mechano-chemical method are illustrated in Fig.5.10 (a), (b) and (c).

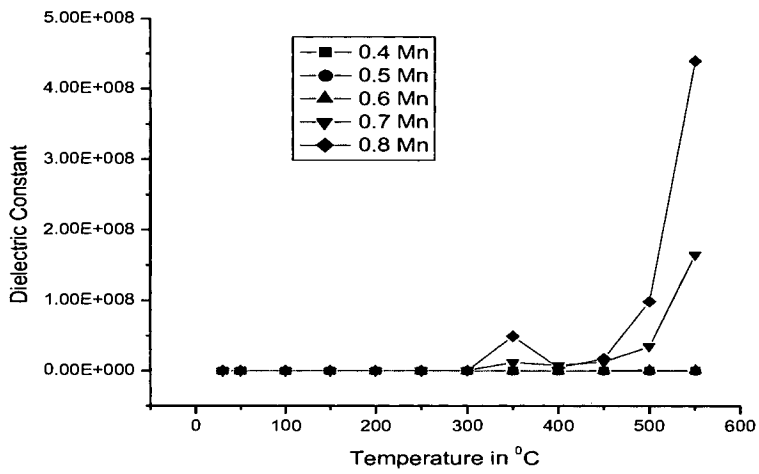
It can be seen from these figures that for all the samples dielectric constant (ϵ') increase with increasing temperature. Initially at lower temperature, the (ϵ') increases gradually as the thermal energy supplied to the samples is not sufficient to free the localized dipoles. When a certain temperature is reached, the thermal energy liberates more localized dipoles, and the field accompanying the applied frequency tries to align them in its direction. Thus, there is a sharp increase in the dielectric constant, reaching a peak. The temperature at which the dielectric constant is maximum (peak) is called the transition temperature. Beyond the transition temperature, the thermal energy added to the system overcomes the field effect and decreases the internal viscosity of the system giving rise to more degrees of freedom to the dipoles, and increasing the entropy (degree of randomness) of the system, thus resulting in the decrease in the

dielectric constant (ϵ'). This peak is also attributed to the presence of two types of charge carriers as reported by Rezlescu [63].

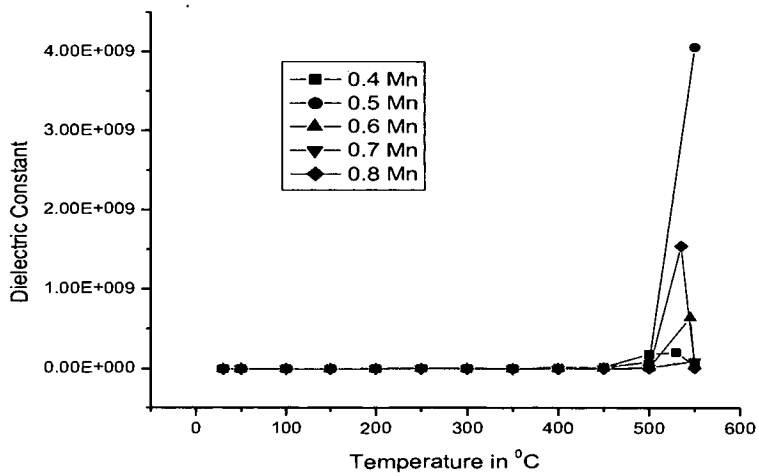
The dielectric constant values observed for the unsintered samples upto 550°C were in the range 5.0829×10^5 (for $\text{Mn}_{0.4}\text{Zn}_{0.6}\text{Fe}_2\text{O}_4$) to 1.4867×10^7 (for $\text{Mn}_{0.7}\text{Zn}_{0.3}\text{Fe}_2\text{O}_4$). The dielectric constant values for the samples sintered at 1100°C and 1300°C were in the range 1.36×10^6 - 4.4026×10^8 and 2.8613×10^7 - 4.5073×10^9 respectively. With the instrument employed for the measurements of the capacitance as a function of temperature, it was possible to obtain the transition temperature of only $\text{Mn}_{0.8}\text{Zn}_{0.2}\text{Fe}_2\text{O}_4$ ferrite sample sintered at 1300°C . The transition temperature of this sample was found to be 535°C .



(a)



(b)



(c)

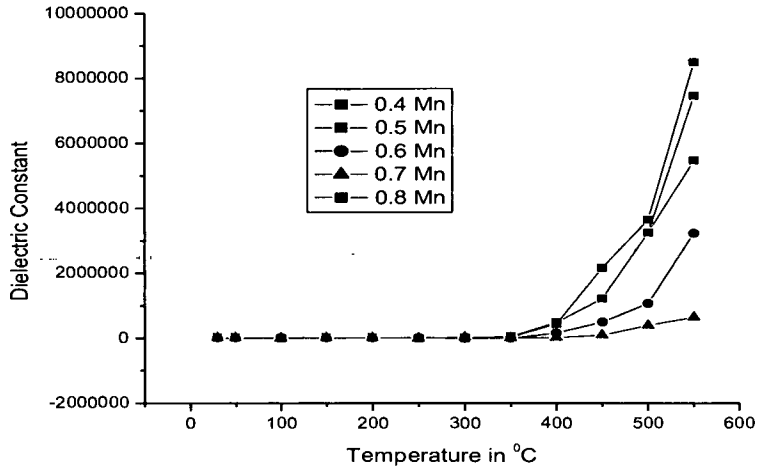
Fig.5.10. Variation of dielectric constant with temperature for various Mn-Zn ferrite (a) unsintered samples, sintered, at (b) 1100°C and (c) 1300°C obtained by the mechano-chemical method.

Ferrite samples prepared by wet chemical method:

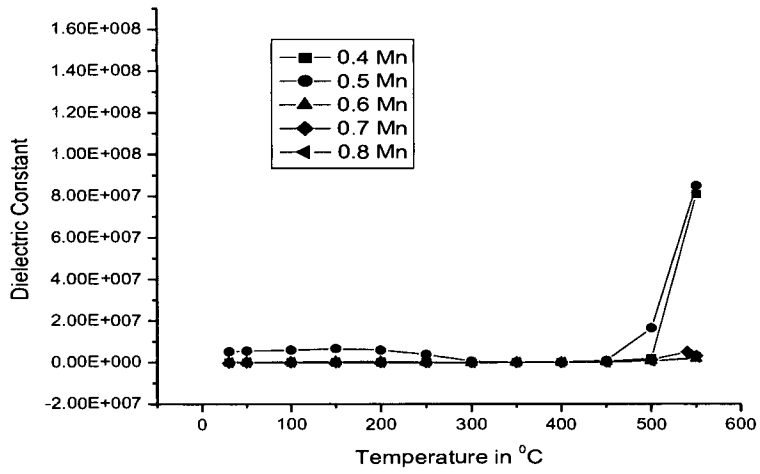
The variation of dielectric constant with temperature, at frequency of 20Hz, for the $Mn_xZn_{(1-x)}Fe_2O_4$ samples prepared by the wet chemical method is shown in Fig.5.11 (a),(b) and (c).

It can be seen from the figures that the Mn-Zn ferrite samples obtained by this method also follow the same pattern as seen in the case of the mechano-chemical method for all the samples that is the dielectric constant (ϵ') increases with increasing temperature. The values of dielectric constant for the unsintered samples were in the range 63682×10^5 - 8.4891×10^6 the lowest being for $Mn_{0.7}Zn_{0.3}Fe_2O_4$ and the highest for $Mn_{0.5}Zn_{0.5}Fe_2O_4$. Similarly, in the case of the samples sintered at $1100^\circ C$ and $1300^\circ C$, the values of dielectric constant were in the range of 2.3192×10^6 - 8.4934×10^7 and 2.3882×10^7 - 3.4278×10^8 respectively.

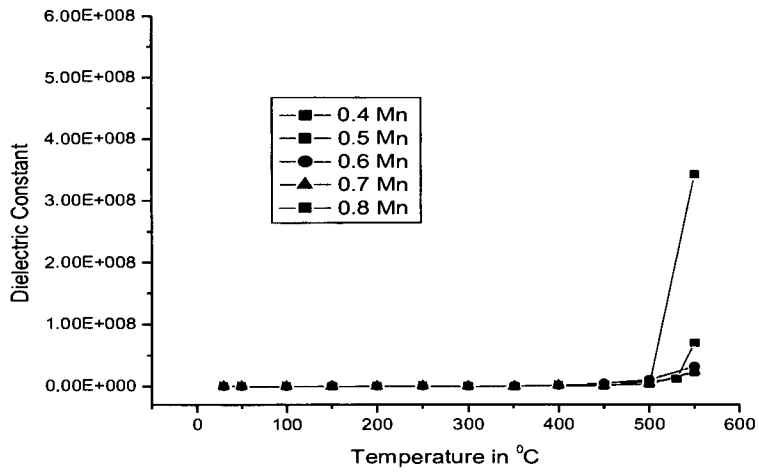
The dielectric constant values were lower for the wet chemical method as compared to the values obtained for the samples prepared by the mechano-chemical method, for the same composition. Better homogeneity, symmetry and the uniform smaller grains in the case of the samples obtained by the wet chemical method may be the reason for lower values of the dielectric constant.



(a)



(b)



(c)

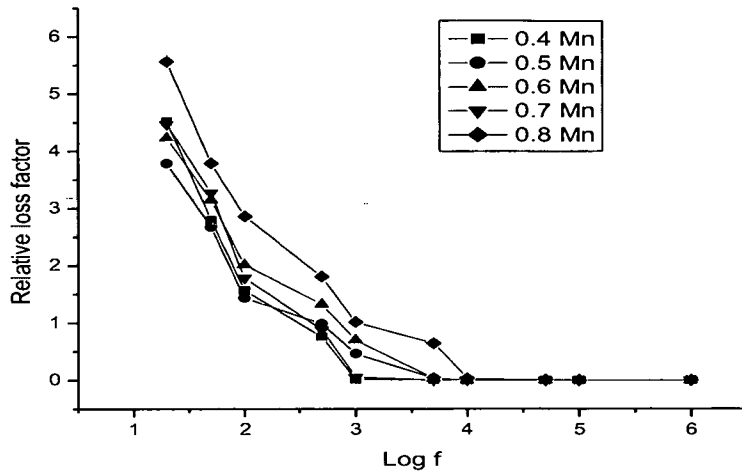
Fig.5.11. Variation of dielectric constant with temperature for various Mn-Zn ferrite (a) unsintered samples, sintered, at (b)1100°C and (c) 1300°C obtained by the wet chemical method.

The decrease in values of the dielectric constant with increase in the frequency and secondly, the increase in values of the dielectric constant with the increase in the temperature, observed in the present studies for the samples prepared by the novel methods, are in agreement with the theories well documented for ferrite materials.

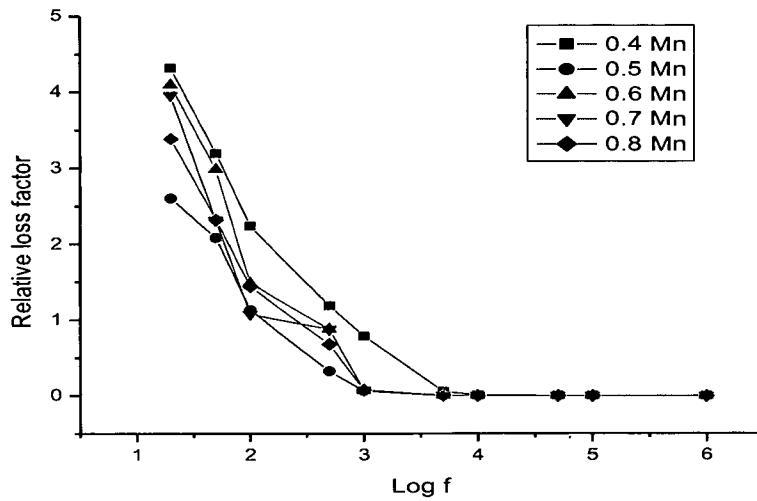
5.6.3.3 DIELECTRIC LOSS FACTOR:

Ferrite samples prepared by mechano-chemical method:

The variation of dielectric loss factor ($\tan \delta$) with the applied frequency for the ferrite samples is shown in Fig. 5.12. (a) and (b). It is observed that, for all the samples the value of $\tan \delta$ decreases as the frequency is increased and reaches a constant value at higher frequency (1MHz) for unsintered as well as for the sintered samples.



(a)



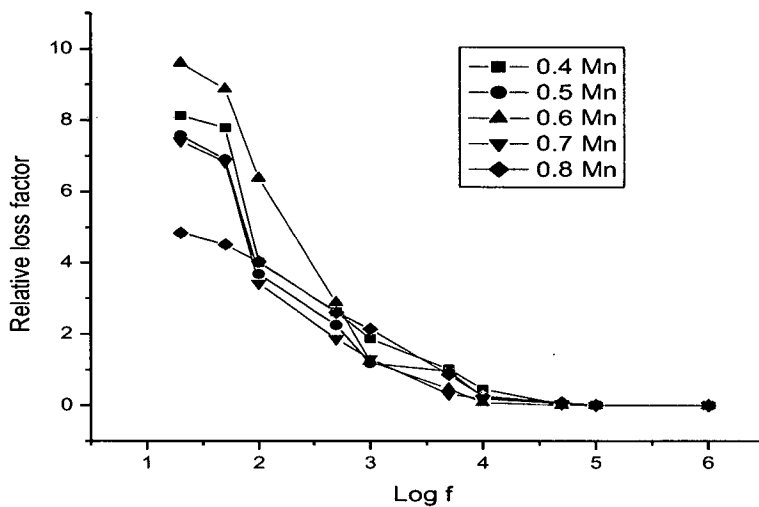
(b)

Fig.5.12. Variation of relative loss factor with log f for Mn-Zn ferrites (a) unsintered (b) sintered at 1300°C samples, obtained by the mechano- chemical method.

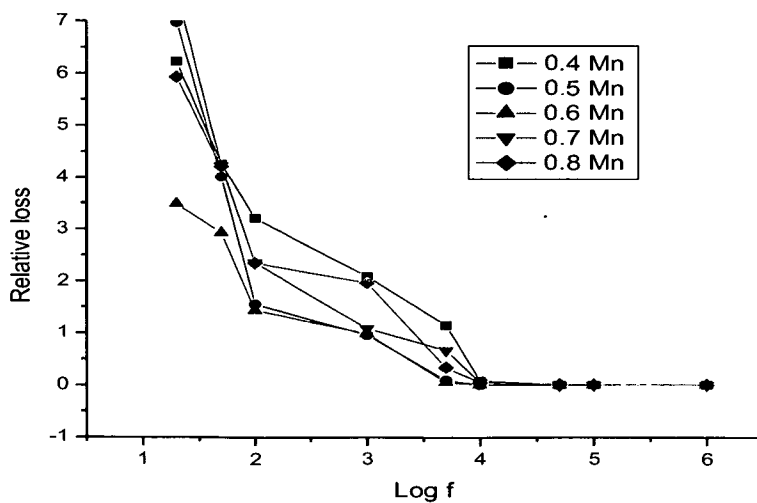
Ferrite samples prepared by wet chemical method:

Similarly, the variation of dielectric loss factor ($\tan \delta$) with the applied frequency, for the Mn-Zn samples prepared by the wet chemical method, is illustrated in Fig. 5.13. (a) and (b). It is clearly seen from the

figures, that for all the samples the $\tan \delta$ value decreases as the frequency is increased and reaches to a constant value at 1 MHz for the unsintered as well as for the sintered samples.



(a)



(b)

Fig.5.13. Variation of relative loss Factor with $\log f$ for various Mn-Zn ferrite (a) unsintered (b)sintered at 1200°C samples, obtained by the wet chemical method.

REFERENCES :

- [1] A. R. Von Hippel, 'Dielectric Materials and Applications', Chapman and Hall Ltd, London, (1954).
- [2] J. Peters, K. J. Standley, 'The Dielectric Behaviour of Mn- Mg Ferrite', Proc. Phys. Soc., 71 (1958) 131.
- [3] L.G. van Uitert, Proc. IRE., 44 (1956) 1294.
- [4] K. Iwauchi, Japan J. Appl. Phy., 10 (1971) 1520.
- [5] E. J.W. Verwey, J. Helman, Chem. Phy., 15 (1947) 174.
- [6] C. G. Koops, Phy. Rev., 83 (1951) 121.
- [7] C. Gillaud, R. Bertrand, J. Des. rese. Cont. Nat. Res. Scientific, 3 (1950) 73.
- [8] T. E. Bradburn, G. R. Rigby, Tras. Brit. Ceram. Soc., 52 (1953) 417.
- [9] M. Rosenberg, P. Nicolau, I. Bunget, Phys. Stat. Sol., 4 (1964) K 121.
- [10] S. A. Maizen, Phy. Stat. Solidi, (Germany), 70/1 (1982) k 71.
- [11] A. B. Naik, J. J. Powar, Indian J. Pure Appl. Phys., 23 (1985) 436.
- [12] A. A. Samokhvaloy, A. G. Rustamov, Sov. Phys. Sol. State, 6 (1964) 749.
- [13] A. A. Samokhvaloy, A. G. Rustamov, Sov. Phys. Sol. State, 9 (1965) 961.
- [14] A. J. Bosmann, C. C. Creve, Phys. Rev., 144 (1966) 763.
- [15] G. H. Jonker, J. Phys. Chem. Solids, 9 (1959), 165.

- [16] E. J.W. Verwey, J. H. de Boer, Reuil Ches Travaux chimques des Phys. Bas (Czeckh), 55(1936) 531.
- [17] Z. Sisma, J. Simsova, V. A. M. Borabers, Proc. 11th Int. Conf. on progr. Semiconductors, (Warsaw, Poland), 2 (1972) 1294.
- [18] N. Rezlescu, E. Rezlescu, Solid State commun., 14 (1974) 69.
- [19] E. J. W. Verwey, P. W. Haayman, F. C. Romeijn, G. W. Van Oosterhout, Philips Res. Rep., 5 (1950) 173.
- [20] G. H. Jonker, J. Phys. Chem. Solids, 9 (1959) 165.
- [21] J. Yamashita, T. Kurosawa, J. Phys. Chem. Solids, 5 (1958) 34.
- [22] T. Holstein, Ann.Phys., New York, 8 (1959), 343.
- [23] J. Appel, Solid state Phys., 18 (1969) 41.
- [24] I. G. Austin, N. F. Mott, Adv. Phys., 18 (1969).
- [25] B. Gillot, Mat. Res. Bull, 11 (1976) 848.
- [26] H. L. Tuller, A. S. Nowick; J. Phys. Chem. Solids, 38 (1977) 859.
- [27] G. Srinivasan, C. M. Srivastava, Phys. Stat. Solidi, 108 (1981) 665.
- [28] P. V. Reddy, T.S Rao. Phys. Sol. (a), 92 (1985)303-307.
- [29] V.R.K. Murthy, J. Sobhanadri, Phys. Stat. Sol. (a), 38 (1976) 647.
- [30] P. L. Morin, T.H. Gabelle, Phys. Rev., 99 (1955) 467.
- [31] M. K. Fayek, S. S. Ata-Allah, K. Roumailh, S. Ismail Mater. Lett., 61 (2009)1010-1012.
- [32] A. A. Sattar, H. M. El-Sayed, K. M. El-Shokrofy, M. M. El-Tabey, J. Mater. Sci., 42 (2007) 149–155.
- [33] S. Mandal, D. Banerjee, R. N. Bhattacharya, A. A. Ghosh, J. Phys. Condens. Matter, 8 (1996) 2865 - 2868.
- [34] G. Moltgen, Z. Angew, Phys., 4 (1952) 216.

- [35] F. Haaberey, *J. Appl. Phys.*, 40 (1969) 2835
- [36] K. Iwachi, *Japan J. Appl. Phys.*, 10 (1971) 1520.
- [37] C. Prakash, J. S. Baijal, *J. Less common Metals*, 107 (1985) 169.
- [38] V. P. Miroshkin, Y.I.Panovaand, V.V.Passynrov, *Phys. Stat. Sol. (a)*, 66 (1981) 779.
- [39] G. P. Kramer, J. Ya Ponava, V. V. Passynkov, *Phys. Stat. Sol. (a)* 86 (1993) 95.
- [40] O. S. Josyulu, J. Sopbhanadri, *Phys. Stat. Solidi A*, 59 (1980) 323.
- [41] P.V. Reddy, T. S. Rao, *J. Less common Metals*, 86 (1982) 255.
- [42] J. C. Maxwell, 'A Treatise on Electricity and Magnetism', Clarendon Press, Oxford,(1982) 328.
- [43] K. W. Wagner, *Ann. Physik*, 40 (1913) 817.
- [44] K. Iwachi, S.Yamato, Y. Baudo, *Japan J. Appl. Phys.*, 10 (1971) 1513.
- [45] K. Iwachi, S.Yamato ,Y.Chika, K. Naokaza, *J.Phys. Soc. Japan*, 49 (1980) 1328.
- [46] S. Chikazumi, S. Charap, 'Physics of Magnetism', John Wiley and Sons Inc., New York, (1964) .
- [47] K. Iwachi, *Japan. J. Appl. Phys.*, 10 (1971) 1520–1528.
- [48] M. I. Klinger, A. A. Samokhvalov, *Phys. Status Solidi B*, 79 (1977) 9.
- [49] M. Drogenik, A. Znidarsic, I. Zajc, *J. Appl. Phys.*, 82 (1) (1997) 333- 340.
- [50] E. M. M. Ibrahim, *J. Appl. Phys.*, A 89 (2007) 203–208.
- [51] B. Gillot, M. El Guendouzi, P. Perriat, *J. Mater. Sci.*, 26 (1991) 4808-4812.

- [52] T. Nakamura, Y. Okano, J. Appl. Phys., 79, (1996) 7129.
- [53] E. Otsuki, S. Yamada, T. Oysuka, K. Shoji, T. Sato, J. Appl. Phys., 69 (1996) 5942.
- [54] D. Ravinder, K. Latha, J. Appl. Phys., 75 (10) (1994) 6118.
- [55] D. Ravinder, B. Ravi Kumar, Mater. Chem. Phys., 82 (2003) 321–326.
- [56] D. Ravinder, K. Vijaya Kumar, Mater. Lett., 49(2001)57–62.
- [57] B. Ravi Kumar, D. Ravinder, Mater. Lett., 53 (2002) 441– 445
- [58] D. Ravinder, Phys. Status Solidi (a), 139 (1993) K 69.
- [59] R. Reddy, A. V. Ranga, G. Mohan, D. Ravinder, B. Boyanov, J. Mater. Sci., 34 (1999), 3169.
- [60] M. B. Reddy, P. V. Reddy, J. Appl. Phys.,(UK), 24 (1991) 975.
- [61] R. Raman, V. R. K. Murthy, B. Vishvanathan, J. Appl. Phys., 69 (7) (1991) 4053.
- [62] K. Latha, K. Sathya Mohan, D. Ravinder, Physica Status Solidi (a), 142 (1994) K 103.
- [63] L. I. Rabinkin, Z.I. Novikova, 'Ferrites', Minsk, (1960) 146
- [64] N. Rezlescu, E.Rezlescu, Phys. Status Solidi A, 23 (1974) 575.
- [65] K. L. Yadav, R.N.P. Chowdhary, Mater. Lett., 19 (1994) 61.
- [66] S. Bera, R.N.P. Chowdhary, Mater. Lett., 22 (1995) 197.
- [67] N.K. Misra, R. Sati, R.N.P. Chowdhary, Mater. Lett., 24 (1995) 313.

CHAPTER SIX

SUMMARY

6.1 CONCLUSIONS:

A systematic study was undertaken to develop and standardize a novel method of synthesis of Mn-Zn ferrite material. In this method, an attempt was made to combine the mechanical method with the chemical method to obtain the desired ferrite materials. The work was aimed at preparing a series of the ferrite materials with the general formula $Mn_{(x)}Zn_{(1-x)}Fe_2O_4$, where $x=0.40, 0.50, 0.60, 0.625, 0.65, 0.675, 0.70$ and 0.80 . Further, it was proposed to investigate the structural, the physical, the magnetic and the electrical properties of the ferrite products by using known methods.

In addition to the above, the synthesis of these ferrite materials was also carried out, with the same compositions, by using the wet chemical method. The various properties of the ferrite products, obtained by this route were studied and compared with those obtained by mechano-chemical method.

In both the methods, hydrazinium acetate was used as ligand for obtaining the precursors and a conventional mode of decomposition of the precursor was adopted.

The ferrite products obtained on decomposition of the precursors were found to yield the expected single phase Mn-Zn ferrite materials. This was confirmed from analysis of the compounds by different known methods of characterization like: the Atomic Absorption Spectroscopy (AAS), the Infrared Spectroscopy (IR), the X-ray Diffraction Spectroscopy (XRD) and the thermal analysis.

The relevant data has been presented in Chapter Three. The percentage composition of metals Mn, Zn and Fe in the ferrite products, obtained by the AAS, confirmed the formation of Mn-Zn ferrites by these novel methods. The IR spectra for the samples show typical metal-oxygen absorption bands for the ferrites. The XRD data obtained for the samples are in agreement with the reported d-values for Mn-Zn ferrites.

The particle size calculated by using the Scherer formula indicates the presence of nano sized particles in the oxide products. The calculated average crystallite sizes were in the range of 16.12 nm to 42.20 nm for the mechano-chemical method and 18.14 nm to 67.29 nm for the wet chemical method. The TEM micrographs of the samples further confirmed that these Mn-Zn ferrite materials contained nanometer sized particles. The particles were found to agglomerate due to their fine size.

Calculated lattice constant values for the Mn-Zn ferrite samples, obtained by both mechano-chemical as well as the wet chemical method are in the range (Table 3.8) of $8.4198 \text{ \AA}^0 - 8.4519 \text{ \AA}^0$ and $8.4529 \text{ \AA}^0 -$

8.4687 A⁰ respectively. These values are in agreement with the reported values for these types of ferrite materials. From the percentage porosity calculated by the known method, the samples prepared by the mechano-chemical and the wet chemical methods are found to have high porosity of 43.14 – 30.23% and 38.57-28.21% respectively (Table 3.12).

The saturation magnetization (M_s) studies for Mn-Zn ferrite samples prepared by the mechano-chemical method show (Table 4.1) the highest value of 50.91 emu/g for $Mn_{0.625}Zn_{0.375}Fe_2O_4$ among the unsintered samples; which increases to 68.59 emu/g for $Mn_{0.65}Zn_{0.35}Fe_2O_4$ (sintered at 1300⁰C) among the sintered samples. While for Mn-Zn ferrite samples prepared by the wet chemical method (Table 4.2), $Mn_{0.7}Zn_{0.3}Fe_2O_4$ was found to have $M_s=43.66$ emu/g, the highest among unsintered samples. The value increased to, 68.36 emu/g for $Mn_{0.625}Zn_{0.375}Fe_2O_4$, sintered at 1300⁰C, among sintered samples.

The magnetic permeability of $Mn_{(x)}Zn_{(1-x)}Fe_2O_4$ samples prepared by the mechano-chemical method were found to increase with the sintering temperature. The values were in the range of 1791 (for $Mn_{0.5}Zn_{0.5}Fe_2O_4$ sintered at 1000⁰C), being lowest, and 16183 (for $Mn_{0.6}Zn_{0.4}Fe_2O_4$ sintered at 1300⁰ C) being highest.

The relative loss factor was found to be low for all the samples sintered across all the temperatures.

The Curie temperature for a few unsintered samples was found to show superparamagnetic behavior with single domain, which gets converted to multi domain on sintering the samples above 1200⁰C.

The resistivity variation with temperature for all the samples was found to show the general semi-conductor behaviour. The resistivity decreases with increase in sintering temperature. This is due to the increase in their particle size as can be seen from the SEM micrograph of the sintered samples at various sintering temperatures.

The thermoelectric power (TEP) studies of the samples, obtained by both the methods, indicated that the ferrite samples show n – type semi conductor behaviour for all the compositions. The Seebeck coefficient values of the samples obtained by the mechano-chemical method were in the range -186 uV/K to - 452 uV/K. The samples prepared by the wet chemical method were found to show overall higher values of Seebeck coefficient as compared to mechano-chemical method. The values were from -285 uV/k to -782 uV/K.

The dielectric constant values for all the Mn-Zn ferrite samples were found to decrease with frequency and were found to increase with increasing temperature as reported for most of the ferrite samples. The transition dielectric temperature values were above 550⁰C for most of the samples.

The dielectric loss factor was found to be very low for the unsintered as well as the sintered samples.

In the present study, high values of M_s , the saturation magnetization, for the unsintered ferrite powder samples were observed compared to the most of the reported values for nanoparticle ferrite samples and the hysteresis losses for the samples were found to be lower. The highest value of M_s was obtained for the sample with $x=0.625$ and $x= 0.70$ in the case of the samples prepared by the mechano-chemical method and the wet chemical method, respectively.

For the samples synthesized by both the above methods, the Curie temperature values were also found to be higher than the reported values for such oxides. The lattice constant 'a', the particle size, the saturation magnetization, the Curie temperature and the hysteresis loss were found to depend on the Mn concentration in the Mn-Zn ferrite samples prepared during the studies.

All the above mentioned measurements were also carried out for the bulk samples obtained by sintering of the nanoparticle samples and similar results were obtained.

Further, the study also provided more information on the behavior of the bulk samples. It was also observed that the properties of the samples depended not only on the Mn concentration, but also on the microstructure

of the samples. The microstructure of the samples was found to change with sintering temperatures. Scanning electron micrographs of the samples sintered at elevated temperatures, 1000°C, 1100°C, 1200°C and 1300°C indicated an increase in the grain size as well as in the densification of the samples. The magnetic and the electrical properties study carried out for these samples confirmed that, apart from Mn concentration in the sample, the other factors affecting these properties are the microstructure and the sintering conditions of the sample. The samples exhibit high values for saturation magnetization, low loss as mentioned earlier, and also higher magnetic permeability, higher resistivity and the dielectric constant. The saturation magnetization (68.59 emu/g), the permeability value 16183 (for mechano-chemical method), low relative loss factor (10^2 to 10^{-6}), the room temperature resistivity (10^8 ohm-cm), and the Seebeck coefficient with negative thermo-emf indicated n-type semiconductor behaviour of these ferrites prepared by these novel methods. With hopping of electron between Fe^{2+} and Fe^{3+} as the mechanism of conduction in these ferrite materials, the high value of dielectric constant (10^8) and the extremely low loss are important parameters for Mn-Zn ferrite samples to exhibit enhanced performance.

Structural and magnetic studies of the Mn-Zn ferrite samples, prepared by employing two simple routes, revealed that the critical Mn proportion for high performance oxide material by these routes is about 0.65.

Thus, through the present study a novel mechano-chemical method of synthesis has been successfully tried and standardized. This new method yields Mn-Zn ferrite materials at lower temperatures thus minimizing the stoichiometric defects which are normally observed in high temperature synthesis. This method yields nanosized ferrite material exhibiting improved performances. Similar observations have been made for the Mn-Zn ferrite material obtained by the novel wet chemical method used for the synthesis. The bulk samples produced by sintering of this nanoparticle Mn-Zn ferrite material, prepared by both the methods, also exhibit enhanced and unique properties.

6.2. SCOPE FOR THE FUTURE WORK:

Research in science and its technological development are important for the future growth, for the benefit of the mankind. As there is always a scope for extension of research, useful work can be done on these materials, for their use in wider areas,

Further study can be undertaken in following areas;

1. The structural properties of the sintered samples for deeper understanding of the same.
2. The surface area measurement and adsorption studies of this ferrite materials for the catalytic applications and also as sensors,
3. Study of magnetite properties at low temperatures and low field by employing VSM and SQUID,

4. The investigation of superparamagnetism in unsintered nano size samples,
5. Study of permeability of the sintered samples prepared by the wet chemical method, and,
6. Any other relevant investigations on neutron diffraction, microwave absorption studies, etc can be carried out for a variety of applications of these materials.

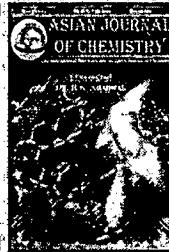
As these materials find use in high technological areas, one can always take up future studies on different properties of these materials.

PUBLICATIONS:

- V. J. Pissurlekar and J. S. Budkuley, "High porosity Mn-Zn ferrites obtained by using mechano-chemical and wet chemical method", *Asian Journal of Chemistry*, Vol. 23, No. 4 (2011), 1677-1679.

PAPERS PRESENTED DURING CONFERENCES:

- "*Synthesis and Magnetic Properties of Mn -Zn Ferrite Nanoparticles*", 3rd, International Symposium on Materials Chemistry, BARC Mumbai, 7- 11 Dec 2010.
- "*Synthesis and magnetic properties of ultrafine Mn - Zn ferrite materials obtained by photocatalytic decomposition of precursor*", National Seminar on Advanced Materials-2010, Department of Physics, Shivaji University , Kolhapur, 19 - 20 March 2010. [**This paper was awarded Third prize**].
- "*Synthesis and magnetic properties of $Mn_xZn_{(1-x)}Fe_2O_4$ nano particles*", National Conference on Recent Advances in Magnetic Materials and Applications Thiagarajar College of Engineering Madurai, 20 -21 Jan 2010.
- "*Mechano-chemical synthesis of ultra fine particle Mn-Zn mixed metals ferrites*", National Conference on Advances in Physical and Theoretical Chemistry Calicut University, 19-20 March 2009.
- "*Magnetic properties of nano particles Mn-Zn mixed metal ferrites synthesized by novel method*", National Seminar on Recent Trends in Nanoscience Nanotechnology and their Applications at Bhaurao Kakatkar College Belgaum, 20 - 21 Feb. 2009.
- "*Novel method of synthesis of ultrafine high performance magnetic material Mn-Zn mixed metal ferrites*", International Conference on Magnetic Materials and their Applications for 21st Century National Physical Laboratory New Delhi, 21 - 23 Oct. 2008.



High Porosity Mn-Zn Ferrites Obtained by Using Mechano-Chemical and Wet Chemical Method

VIKAS J. PISSURLEKAR^{1*} and JAYANT S. BUDKULEY²

¹Department of Chemistry, P.E.S.'s SRSN College of Arts and Science, Ponda, Goa-403 401, India

²Department of Chemistry, Goa University, Taleigao Plateau, Goa-403 206, India

*Corresponding author: Tel: +91 832 2221184; E-mail: vikjsp@yahoo.co.in

(Received: 2 July 2010)

Accepted: 11 December 2010

AJC-9386

Manganese-zinc ferrites are synthesized by two different methods namely mechano-chemical and wet chemical, using same ligand. XRD data is used to confirm formation of single phase of ferrites. Lattice constants, X-ray densities, mass densities of the ferrite samples are determined. Porosities calculated by densities method for the samples are found to have high values.

Key Words: Mechano-chemical, Lattice constants, Density, Porosity.

INTRODUCTION

Ferrites have been studied by many researchers for last several decades due to their wide applications as magnetic materials for electronic components like audio and video equipments, power transformers, telecommunications, etc¹. Ferrites are also known to exhibit catalytic properties². Manganese-zinc ferrites are characterized by high magnetic permeability, low core loss, high saturation magnetization and dielectric resistivity^{3,4}. Mn-Zn ferrites are found to show enhanced performance with reduced particle size. During the last two to three decades researchers have reported studies on basic physical and chemical mechanism governing performance of ferrites obtained from the ceramic method, but less attention has been given to evolution of properties and the microstructure.

Insight into the porosity of ferrite materials is very important especially when these substances are to be used as catalysts or sensors. Oxide materials having high porosity exhibit better catalytic property^{5,6} and are good sensors^{7,8}. Convenient, simple and reliable method^{9,10} of determining the porosity of materials involves using the values of lattice constants, X-ray densities and mass densities of these substances. In case of Mn-Zn ferrite it has been reported^{11,12} that the lattice constant 'a' increases with Mn content.

In the present study an attempt has been made to make use of the X-ray and mass densities to evaluate the porosity of Mn-Zn ferrites prepared by a mechano-chemical method and compare the same for samples obtained by using modified wet chemical method.

EXPERIMENTAL

Mn_xZn_(1-x)Fe₂O₄ (x = 0.4, 0.5, 0.6, 0.7 and 0.8) ferrite samples were synthesized by two different methods. In the first case, calculated amounts of pure 99.9 % MnO₂, ZnO and Fe₂O₃ were taken as starting materials and ball-milled with ball to material ratio of 10 at 80 rpm speed for 10 h in Acmas Technocracy Ball Mill (model Acm-82303) to obtain a powdered mixture. This mixture was then treated with predetermined amount of aqueous hydrazinium acetate and homogenized to a thick paste. The acetate hydrazinate precursor of mixed metals was slowly dried on sand bath using conventional method of heating. The dried paste was then ignited to obtain the desired product which was used for further investigations.

In wet chemical method, aqueous solution containing manganese acetate, zinc nitrate and ferric nitrate, having metal ions in stoichiometric proportion, was treated with hydrazinium acetate to obtain the precursor. The mixture was then dried and ignited to obtain fine particle product.

The samples so obtained were characterized by using X-ray diffraction method. The d-values were used to identify the phase and to confirm the formation of ferrites. The mass density was determined from the mass and volume of the sample by using pycnometric method. From X-ray density and mass density, the porosity in each sample was determined.

RESULTS AND DISCUSSION

The X-ray diffraction patterns of Mn_xZn_(1-x)Fe₂O₄ samples, obtained by two methods, show formation of single phase of

Mn-Zn ferrite (Figs. 1 and 2). However, from the angle of diffraction ' θ ' it is found that for the samples prepared by mechano-chemical method, the lattice constant values are in the range 8.4195 to 8.4519 Å while for those synthesized by wet chemical method 'a' values are on the higher side and are in the range 8.4529 to 8.4687 Å.

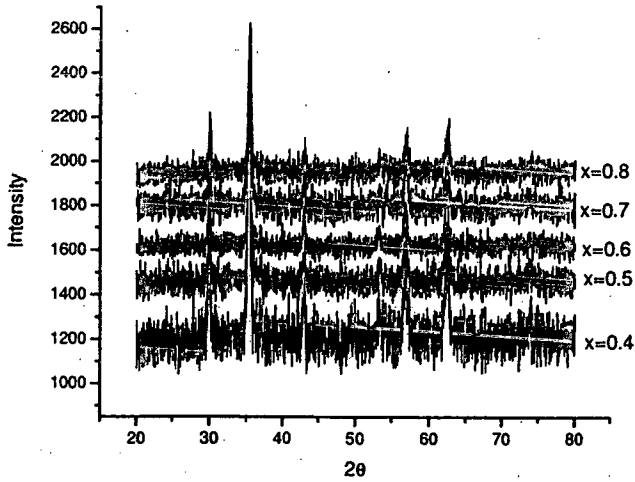


Fig. 1. XRD pattern of $Mn_xZn_{(1-x)}Fe_2O_4$ samples from mechano chemical method

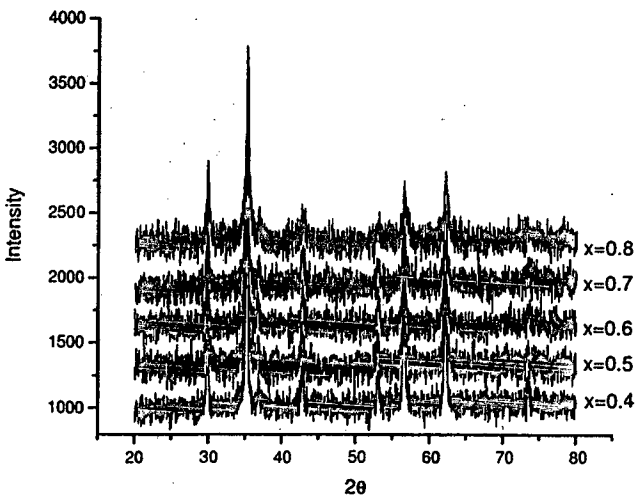


Fig. 2. XRD pattern of $Mn_xZn_{(1-x)}Fe_2O_4$ samples from wet chemical method

The lattice constants 'a' values, obtained¹³ from X-ray data, were subsequently used to calculate X-ray density by using the relation $\rho_x = 8M/Na^3$, where 8 is the number of atoms in a unit cell of spinel lattice, M the molecular weight of the ferrite, 'a' is the lattice constant and N is Avogadro's number. X-ray densities for the samples obtained from mechano-chemical method (Fig. 3) are found to be lower than those of samples prepared by wet chemical method (Fig. 4). The X-ray densities depend on molecular weight and lattice constant of the ferrite sample. As expected, in both the cases, the X-ray densities are found to decrease with increase in the value of lattice constant, since 'a' is inversely proportional to the X-ray density. Also, the X-ray density decreases with increase in Mn content. Lattice constant 'a' for the samples is directly proportional to Mn content in the samples as reported earlier^{11,12}.

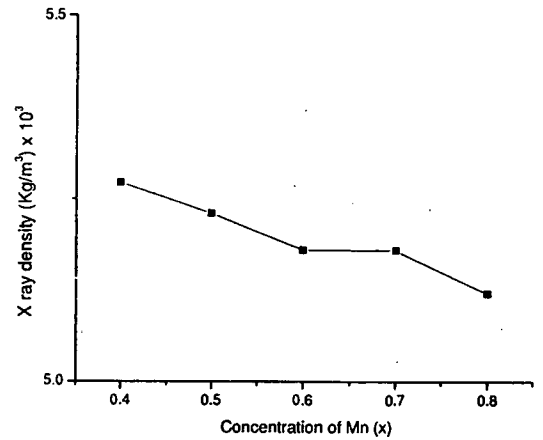


Fig. 3. X-ray density of $Mn_xZn_{(1-x)}Fe_2O_4$ samples from mechano chemical method

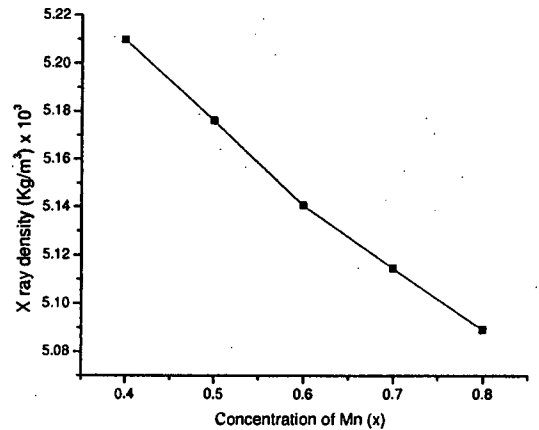


Fig. 4. X-ray density of $Mn_xZn_{(1-x)}Fe_2O_4$ of wet chemical method

The mass densities of ferrites are found to be lower for the samples prepared by the mechano-chemical method (Fig. 5) as compared to the samples obtained from wet chemical method (Fig. 6). Obviously it is due to the fact that in wet chemical method the formation of precursor occurs at ionic level and hence the compactness of the final ferrite material. This is not so in case of samples obtained from mechano-chemical method. The mass densities of ferrite samples increase with increase in Mn content which is due to the higher specific gravity of Mn (7.21 g/cm³) as compared¹⁴ to Zn (7.133 g/cm³).

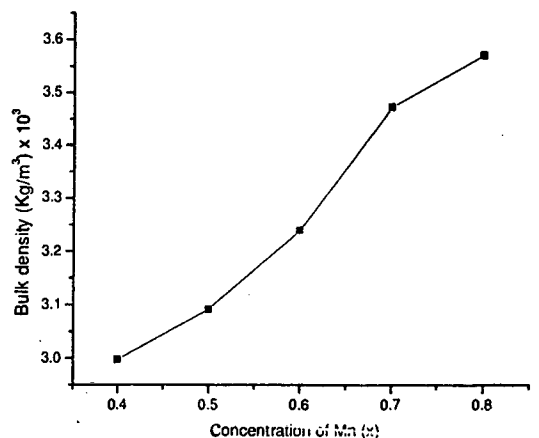


Fig. 5. Mass density of $Mn_xZn_{(1-x)}Fe_2O_4$ from mechano chemical method

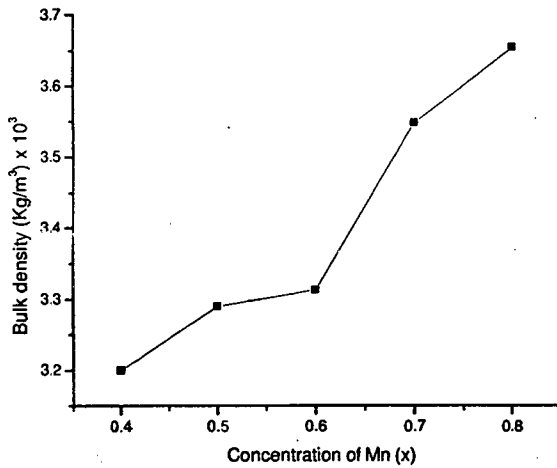


Fig. 6. Mass density of $Mn_xZn_{(1-x)}Fe_2O_4$ from wet chemical method

The particle size of the ferrite sample was calculated using Scherer's formula i.e. $t = 0.9 \lambda / B \cos \theta$. The values so obtained for the samples are in the range of 16.12 nm to 28.16 nm for mechano-chemical method, where as for the wet chemical method it is in the range 16.42 to 33.54 nm. In wet chemical method involving hydrazine based ligand, additional heat is generated during the thermal decomposition of the precursor due to self-sustained exothermic auto combustion resulting in nucleation of ferrite materials. Due to this, the particle size of ferrite samples in case of the wet chemical method is larger than that of samples prepared by the mechano-chemical method.

The percentage porosity (P) was calculated using the formula: $P = 1 - (\rho / \rho_x)$, where 'p' is bulk density and ' ρ_x ' is X-ray density¹². Samples obtained by both methods have high porosity values. Among the two methods, ferrites obtained from the mechano-chemical method show higher porosity values ranging from 43.14 to 30.23 % (Fig. 7). And the values are in the range of 38.57 to 28.21 % for the wet chemical method (Fig. 8). The porosity is found to decrease as the ratio (ρ / ρ_x) increases with increasing Mn content.

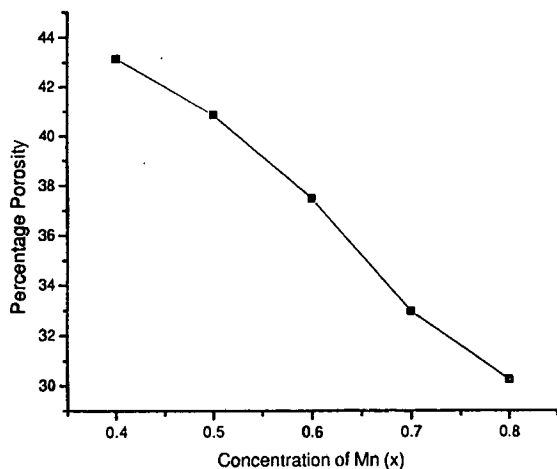


Fig. 7. Percentage porosity of $Mn_xZn_{(1-x)}Fe_2O_4$ samples prepared by mechano chemical method

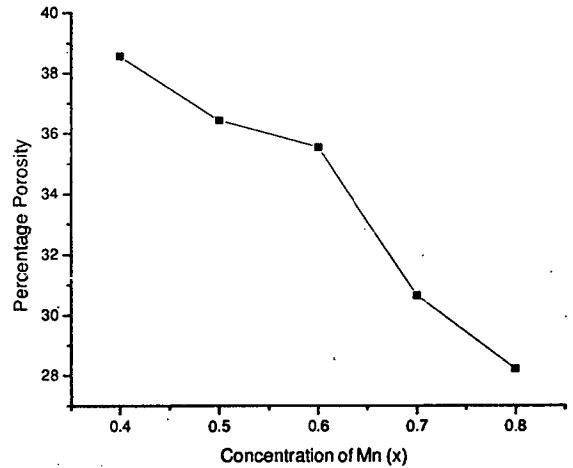


Fig. 8. Percentage porosity of $Mn_xZn_{(1-x)}Fe_2O_4$ samples prepared by wet chemical method

Conclusion

(a) The formation of single phase ferrite from precursor obtained with the same ligand in mechano-chemical method and wet chemical method. (b) Lattice constants obtained for mechano chemical method are lower as compared to wet chemical method. (c) Mass densities of ferrites obtained by the mechano-chemical method are also found to be lower in comparison to the wet chemical method. (d) Ferrites obtained by these methods have high porosity with slightly higher values in the case of mechano-chemical method.

REFERENCES

1. M.I. Rosales, A.M. Plata, M.E. Nicho, A. Brito and M.A. Ponce, *J. Mater. Sci.*, **30**, 4446 (1995).
2. T. Mimani, P. Ravindranathan and K.C. Patil, *Proc. Indian Acad. Sci. (Chem. Sci.)*, **99**, 209 (1987).
3. G. Ott, J. Wrha and R. Lucke, *J. Magn. Magn. Mater.*, **254-255**, 535 (2003).
4. Z.G. Zheng, X.C. Zhong, Y.H. Zhang, H.Y. Yu and D.C. Zeng, *J. Alloys Comp.*, **466**, 377 (2008).
5. C.S. Hwang and N.C. Wang, *Mater. Chem. Phys.*, **88**, 258 (2004).
6. L. Ma L. Chen, S. Chen, *Mater. Chem. Phys.*, **114**, 692 (2009).
7. N. Rezlescu, E. Rezlescu, F. Tudorache and P.D. Popa, *Roman. Rep. Phys.*, **61**, 223 (2009).
8. N. Bagum, M.A. Gafur, A.H. Bhuiyan and D.K. Saha, *Phys. Status Solidi A*, **207**, 986 (2010).
9. R.V. Mangalaraja, S. Ananthakumar, P. Manohar, F.D. Gnanam and M. Awano, *J. Mater. Lett.*, **58**, 1593 (2004).
10. E.C. Snelling, *Soft Ferrites, Properties and Applications*, Butter Worth and Co. (Publisher) Ltd., London, edn. 2 (1988).
11. E.V. Gopalan, I.A. Al-Omari, K.A. Malini, P.A. Joy, D.S. Kumar, Y. Yoshida and M.R. Anantharaman, *J. Magn. Magn. Mater.*, **321**, 1092 (2009).
12. S. Dasgupta, K.B. Kim, J. Ellrich, J. Eckert and I. Manna, *J. Alloys Comp.*, **424**, 13 (2006).
13. T.J. Shinde, A.B. Gadkari and P.N. Vasambekar, *J. Mater. Chem. Phys.*, **111**, 87 (2008).
14. D.R. Lide, *CRC Handbook of Chemistry and Physics*, CRC Press, London, edn. 7 (1995).